UNIVERSITÉ LAVAL

The Role of Glass Modifiers in The Solubility of Tm^{3+} Ions in As_2S_3 glasses

Thèse

Ani GALSTYAN

Doctorat en physique
Philosophiae doctor (Ph.D.)

Québec, Canada

The Role of Glass Modifiers in The Solubility of Tm^{3+} Ions in As_2S_3 glasses

Thèse

Ani GALSTYAN

Sous la direction de :

Younès MESSADDEQ, directeur de recherche
Tigran GALSTIAN, codirecteur de recherche

RÉSUMÉ

Au cours des années une variété des compositions de verre chalcogénure a été étudiée en tant qu'une matrice hôte pour les ions Terres Rares (TR). Pourtant, l'obtention d'une matrice de verre avec une haute solubilité des ions TR et la fabrication d'une fibre chalcogénure dopée au TR avec une bonne qualité optique reste toujours un grand défi. La présente thèse de doctorat se concentre sur l'étude de nouveaux systèmes vitreux comme des matrices hôtes pour le dopage des ions TR, ce qui a permis d'obtenir des fibres optiques dopées au TR qui sont transparents dans l'IR proche et moyenne. Les systèmes vitreux étudiés ont été basés sur le verre de sulfure d'arsenic (As_2S_3) co-dopé aux ions de Tm^{3+} et aux différents modificateurs du verre.

Premièrement, l'addition de Gallium (Ga), comme un co-dopant, a été examinée et son influence sur les propriétés d'émission des ions de Tm a été explorée. Avec l'incorporation de Ga, la matrice d'As_2S_3 dopée au Tm a montré trois bandes d'émission à 1.2 µm ($^1H_5 \rightarrow {}^3H_6$), 1.4 µm ($^3H_4 \rightarrow {}^3F_4$) et 1.8 µm ($^3F_4 \rightarrow {}^3H_6$), sous l'excitation des longueurs d'onde de 698 nm et 800 nm. Les concentrations de Tm et de Ga ont été optimisées afin d'obtenir le meilleur rendement possible de photoluminescence. À partir de la composition optimale, la fibre Ga-As-S dopée au Tm^{3+} a été étirée et ses propriétés de luminescence ont été étudiées. Un mécanisme de formation structurale a été proposé pour ce système vitreux par la caractérisation structurale des verres Ga-As-S dopés au Tm^{3+}, en utilisant la spectroscopie Raman et l'analyse de spectrométrie d'absorption des rayons X (EXAFS) à seuil K d'As, seuil K de Ga et seuil L_3 de Tm et il a été corrélé avec les caractéristiques de luminescence de Tm.

Dans la deuxième partie, la modification des verres As_2S_3 dopés au Tm^{3+}, avec l'incorporation d'halogénures (Iode (I_2)), a été étudiée en tant qu'une méthode pour l'adaptation des paramètres du procédé de purification afin d'obtenir une matrice de verre de haute pureté par distillation chimique. Les trois bandes d'émission susmentionnées ont été aussi bien observées pour ce système sous l'excitation à 800 nm. Les propriétés optiques, thermiques et structurelles de ces systèmes vitreux ont

été caractérisées expérimentalement en fonction de la concentration d'I_2 et de Tm dans le verre, où l'attention a été concentrée sur deux aspects principaux: l'influence de la concentration d'I_2 sur l'intensité d'émission de Tm et les mécanismes responsables pour l'augmentation de la solubilité des ions de Tm dans la matrice d'As_2S_3 avec l'addition I_2.

SUMMARY

Over the years a number of chalcogenide glass compositions have been studied as host matrices for Rare Earth (RE) ions. However, it still remains a great challenge to obtain a glass matrix with high solubility of RE ions and to fabricate a RE doped chalcogenide glass fiber with good optical quality. The present PhD thesis focuses on the study of new glassy systems as host matrices for doping of RE ions, which allowed to obtain RE doped optical fibers transparent in near and middle IR. Studied glassy systems were based on well-known arsenic sulphide (As_2S_3) glasses co-doped with Tm^{3+} ions and different glass modifiers.

Firstly, the addition of Gallium (Ga) ions as co-dopants was examined and their influence on the emission properties of Tm ions was explored. With the incorporation of Ga into the host, Tm doped As_2S_3 glasses display three strong emission bands at 1.2 μm ($^1H_5 \rightarrow {}^3H_6$), 1.4 μm ($^3H_4 \rightarrow {}^3F_4$) and 1.8 μm ($^3F_4 \rightarrow {}^3H_6$) under excitation wavelengths of 698 nm and 800 nm. Despite the very small glass forming region of the system Ga-As-S we could optimise the concentration ratio of Ga and Tm to achieve the highest possible photoluminescence efficiency. From the optimal composition, Tm^{3+} doped Ga-As-S fiber was drawn and its luminescence properties were studied. Through structural characterisation of Tm doped Ga-As-S glasses, using Raman spectroscopy and Extended X-ray Absorption Fine Structure (EXAFS) spectroscopy at As K-edge, Ga K-edge and Tm L_3-edge, a formation mechanism has been proposed for this glassy system and it was correlated with luminescence features of Tm ions.

In the second part, the modification of Tm^{3+} doped As_2S_3 glasses with the incorporation of halides (namely Iodine (I_2)) was investigated, as a method for tailoring the process parameters for purification, in order to obtain a high purity glass matrix via chemical distillation. All three of above mentioned emission bands were observed for this system as well, under the 800 nm of excitation wavelength. Optical, thermal and structural properties of these glassy systems were characterized experimentally depending on the concentration of I_2 and Tm in the glass, where the attention was concentrated on two principal aspects: the influence of the

concentration of I_2 on the intensity of emission of Tm and the mechanisms responsible for the increase of the solubility of Tm ions in As_2S_3 glass matrix with addition of I_2.

CONTENT

LIST OF TABLES

LIST OF FIGURES

LIST OF ABBREVIATIONS AND ACRONYMS

RE	Rare Earth
IR	Infrared
NIR	Near Infrared
MIR	Middle Infrared
Tm	Thulium
As	Arsenic
S	Sulphur
Ga	Gallium
I_2	Iodine
ChGs	Chalcogenide glasses
ChHGs	Chalco-halide glasses
SRO	Short Range Order
T_g	Glass transition temperature
T_x	Crystallisation onset temperature
T_c	Crystallisation temperature
T_s	Softening temperature
T_f	Beginning of melting temperature
T_m	Melting temperature
DSC	Differential Scanning Calorimetry
TMA	Thermo-mechanical Analysis
FTIR	Fourier Transform Infrared Spectroscopy
XRD	X-ray diffraction
EXAFS	Extended X-ray Absorption Fine Structure
ASE	Amplified Spontaneous Emission
EDX	Energy dispersive X-ray

ACKNOWLEDGMENTS

First of all I would like to express my sincere gratitude to my supervisor Prof. Younes Messaddeq who provided me the opportunity to work in Canada with the team at CERCP (Excellence Research Chair of Canada in Photonics). I am grateful to Prof. Messaddeq for making this research project possible, for his unconditional support and unceasing encouragement during my PhD studies.

In particular I would like to thank my co-supervisor Prof. Tigran Galstian, who met me in Quebec, personally introduced me to Laval University and guided my first steps, as well as, provided professional support and advices.

I am also extremely grateful to Sandra Helena Mesaddeq for her invaluable help in carefully planning and managing my research projects and guidance in all steps of my work. She has created a friendly space in which ideas could be explored.

I would like to express my measureless gratitude to Prof. Igor Skripachev for his support to accommodate me in a new laboratory environment, for creating experimental setups and for teaching and helping me to prepare chalcogenide glasses, which was the most difficult and important part of my research study.

Remarkably, I would like to thank the technical team of the COPL (Center for Optics Photonics and Lasers) for providing a high quality support in laboratories.

I thank the Canadian Excellence Research Chair program for their financial support.

Finally, and most of all, I am deeply grateful to my family and my friends who encouraged me and provided all the necessary help to make the decision to move to Canada and to start the PhD project.

Ani Galstyan

FOREWORD

The present thesis is based on three manuscripts of articles published in peer-reviewed journals (during my PhD project). I am the principal author in all of them.

My first article was realized in collaboration with the group of Prof. Réal Vallée from Center for Optics Photonics and Lasers

- A. Galstyan, S.H. Messaddeq, V. Fortin, I. Skripachev, R. Vallee, T. Galstian, Y. Messaddeq *"Tm^{3+} doped Ga–As–S chalcogenide glasses and fibers"* **Optical Materials** 47, pp. 518–523 **(2015).**

A small paragraph was added in this article (Chapter 4.3.3, page 62, Fig. 4.10) discussing thermal properties of Tm^{3+} doped Ga-As-S glasses that were not included in the published article.

My second article was realized in collaboration with Prof. Carlo Segre from Illinois Institute of Technology (IIT):

- A. Galstyan, S.H. Messaddeq, C.U. Segre, T. Galstian, Y. Messaddeq *"Structural analysis of Tm^{3+} doped As–S–Ga glasses by Raman and EXAFS spectroscopy"* **Journal of Non-Crystalline Solids** 432, pp. 487–492 **(2016).**

Finally, my third article was realized in collaboration with Prof. Igor Skripachev from Institute of Chemistry of High Purity Substances of the Russian Academy of Sciences:

- A. Galstyan, S.H. Messaddeq, I Skripachev, T. Galstian and Y. Messaddeq *"Role of iodine in the solubility of Tm^{3+} ions in As_2S_3 glasses"* **Optical Materials Express** Vol. 6, No. 1 **(2015).**

A chapter was added in the end of this article (Chapter 7.3.6, page 106, Fig. 7.11), discussing luminescence properties of Tm^{3+} doped I-As-S glass fibers. This chapter was not included in the published version of the article.

The roles of authors in these articles are the following: All the authors participated in the subject discussions. The subjects and experiment strategies were discussed with Prof. Y. Messaddeq and Prof. T. Galstian. The preparation of glass samples was realized by me and I Skripachev. Spectroscopic studies of glasses were principally performed by me. Structural studies of glass samples by EXAFS were realized by me and Prof. C. Segre. Structural studies by Raman spectroscopy was realized by me and S.H. Messaddeq. The experiment of luminescence measurements in doped chalcogenide glass fiber was discussed with Prof. Réal Vallée and realized by Vincent Fortin.

The writing of manuscripts was principally realized by me. After discussing the content and structure with S.H. Messaddeq, I provided my version of manuscript to all co-authors who revised, edited and completed it.

CO-AUTHORS:

Sandra Helena Messaddeq: Center for Optics, Photonics and Laser, Department of Physics, Engineering Physics and Optics, Laval University, Pav. d'Optique-Photonique, 2375 Rue de la Terrasse, Québec, G1V 0A6, Canada.
e-mail: sandra.messaddeq@copl.ulaval.ca

Igor Skripachev: Institute of Chemistry of High Purity Substances of the Russian Academy of Sciences, 49 Tropinin Str. Nizhniy Novgorod, 603950, Russia.
e-mail: brigsiq@yahoo.com

Vincent Fortin: Center for Optics, Photonics and Laser, Department of Physics, Engineering Physics and Optics, Laval University, Pav. d'Optique-Photonique, 2375 Rue de la Terrasse, Québec, G1V 0A6, Canada.
e-mail: vincent.fortin@copl.ulaval.ca

Carlo Segre: Illinois Institute of Technology, 3101 South Dearborn St., Chicago, IL 60616, USA.
e-mail: segre@iit.edu

Réal Vallée: Center for Optics, Photonics and Laser, Department of Physics, Engineering Physics and Optics, Laval University, Pav. d'Optique-Photonique, 2375 Rue de la Terrasse, Québec, G1V 0A6, Canada.
e-mail: real.vallee@copl.ulaval.ca

Tigran Galstian: Center for Optics, Photonics and Laser, Department of Physics, Engineering Physics and Optics, Laval University, Pav. d'Optique-Photonique, 2375 Rue de la Terrasse, Québec, G1V 0A6, Canada.
e-mail: tigran.galstian@phy.ulaval.ca

Younes Messaddeq: Center for Optics, Photonics and Laser, Department of Physics, Engineering Physics and Optics, Laval University, Pav. d'Optique-Photonique, 2375 Rue de la Terrasse, Québec, G1V 0A6, Canada.
e-mail: younes.messaddeq@copl.ulaval.ca

Ani Galstyan

CHAPTER 1
INTRODUCTION

1.1. MOTIVATION

The first demonstration of a laser was reported in 1961 by Sorokin et al. [1] in Sm^{3+} doped CaF_2 laser materials. In the same year Snitzer published his paper on laser oscillation in Nd^{3+} doped barium crown glass [2] and then on the possibility of fiber laser operation [3]. These important works led to further exploration and development of fiber lasers. A large number of materials have been investigated and laser action has been demonstrated over a wide wavelengths range from the ultraviolet to the mid-infrared (IR). Rare Earth (RE) doped lasers and amplifiers have found application in a number of different areas including telecommunication, material processing, medical diagnosis and treatment, printing and marking, environmental sensing, counter measures, etc.

Recently, the development of optical glass fibers has revolutionized the telecommunications industry, with fibers replacing copper wires and radically expanding our ability to transmit flaw-free data throughout the world. This relatively new technology has made significant contributions towards the advancement of our life. Presently our planet is covered with millions of kilometers of optical fiber based on silica (SiO_2) glasses, which gives us ability to communicate and to exchange information. Such optical fibers allow high bandwidth transmission of data over long distances. The optimum transmission windows for SiO_2 fiber are located at 1.3 μm and 1.55 μm, representing the second and third telecommunications windows. These windows, near the intrinsic loss minimum of the material, are separated by absorption due to water molecules. The presence of the hydroxyl (OH-) impurity in silica introduced overtone absorption around 1.4 μm [4,5] which effectively divided the region of lowest attenuation into two separate windows.

The invention of the erbium (Er) doped SiO_2 fiber amplifier in 1987 [6] was a major breakthrough in fiber optic technology, allowing long distance data transmission through SiO_2 fiber by means of the amplification of optical signals at the

coincident wavelength of 1.54 μm. This was a significant improvement on electronic repeaters which required the conversion between optical and electronic signals. However, the gain bandwidth of the Er doped fiber spans only a small fraction of this continuous low loss window. Doping with other REs could allow to use wavelengths that are not covered by the Er doped fiber, but problems associated with the vibrational structure of silica prevent its use as an amplifier medium when doped with ions such as praseodymium (Pr), thulium (Tm) and dysprosium (Dy) [7]. Silica glass is by a long way the most favourable material to use for long distance optical fiber telecommunications. However, there are aspects of the properties of silica, which make it unsuitable for certain applications. First of all the RE solubility of silica is low and the phonon energy is high (1100 cm^{-1}) [8], leading to non-radiative decay of many transitions of RE dopants. The non-linear refractive index of silica is relatively low ($2.5 \cdot 10^{-20}$ m^2W^{-1}) [9], which means that non-linear devices based on silica require relatively high intensities to operate. The transmission wavelength of silica is limited to 2 μm, which limits the applications beyond this wavelength.

The nature of the application determines the particular requirements for the laser source such as the laser wavelength, output power, beam quality, power consumption, size, fabrication and maintenance costs, etc. The fundamental parameter in this list is the laser wavelength which depends on the available radiative transitions between the energy levels of the RE ions, which in their turn depend on the host material. The main factors which limit the number of available laser transitions are the competing multiphonon transitions and the transparency of the host material. This motivates the search for new laser materials with low phonon energies and extended transparency as alternative hosts for RE doped devices, which could fill the gaps in the existing spectrum of laser wavelengths and extend the spectrum towards shorter and longer wavelengths.

The search for new non-oxide vitreous materials led to the development of fluoride and chalcogenide glasses (ChGs). Made from low phonon energy materials, with heavier ions and weaker bond strengths, these glasses provide transmission into the mid-far IR region [10,11]. The optical window for most fluoride glasses lies in the 0.25 – 4.0 μm range [10]. Halide compounds have played a key role in glass

formation (ZrF4, InF3, GaF3 and AlF3). These glass formers are normally combined with other halide compounds, which act as a network stabilizer or modifier. Probably the most significant of these fluoride glasses is known by its acronym ZBLAN (ZrF_4-BaF_2-LaF_3-AlF_3-NaF) [12]. Some glasses based on halides have been successfully demonstrated as fiber amplifiers with optical amplification in both the second and third telecommunications window (E and S). The development of the Pr^{3+}- doped fiber amplifier with signal gain at 1.3 μm [13] and Tm^{3+}-doped fiber amplifier with maximum gain at 1.47 μm [14] and 1.65 μm [15] has been realized. In recent years several papers have been published reporting a laser emission at 2.7μm [16], 2.8 μm [17] and 2.9 μm [18] in Er^{3+} doped fluoride glasses and glass fibers. In addition, two contributions of fluoride glass have included emission of blue up-converted light from a Tm^{3+}-doped fiber [19] and a Ho^{3+}-doped fiber laser emitting at 3.9 μm [20].

ChGs transmit to longer wavelengths in the IR than silica and fluoride glasses. ChGs based on sulphur, selenium and tellurium typically transmit up to 10 μm, 15 μm and 20 μm, respectively [21]. ChGs have a nonlinear refractive index around two orders of magnitude higher than silica [8]. This makes them suitable for ultra-fast switching in telecommunication systems [22]. Moreover, this long wavelength transparency enables ChGs to be used for several applications including thermal imaging, night vision, CO_2 laser power delivery, radiometry and remote chemical analysis [23]. In addition, some ChGs exhibit structural/optical change when irradiated with light resulting in a localized reversible or irreversible change in the refractive index [24]. This photosensitivity allows photo writing of waveguides [25,26] and design of micro-lenses [27]. ChGs often exhibit much lower phonon energy (360-425 cm^{-1}) [9], which allows the observation of certain transitions in RE dopants [28,29] that are not observed in silica. The low phonon energy of chalcogenides can be thought of as resulting from the relatively large mass of their constituent atoms and the relatively weak bonds between them. The enhanced mid-IR transmission in ChGs, with reduced maximum phonon energy leads to lower non-radiative decay rates and increased radiative quantum efficiency for electronic transitions of RE dopants introduced into the glasses [30]. However, most IR

materials suffer from thermo-mechanical degradation, poor resistance to air and moisture and are especially prone to crystallization [10,11,31-34].

One of the first and well known ChGs is the arsenic trisulphide (As_2S_3) glass. It had been known for long time that blending of arsenic and sulphur can form a dark red-coloured glass that is transparent well beyond 2 μm. Being an excellent glass former, As_2S_3 was a logical choice to be drawn into crude fiber using a simple fiber drawing technique. The fabrication of the first As_2S_3 fiber was reported in 1965 [35]. Since then, As_2S_3 glasses and fibers have maintained an important role in IR technology. Due to its transparency up to 7 μm, lack of crystallization and good thermal stability As_2S_3 has been considered as an alternative host matrix for RE ions. As_2S_3 glasses were initially used for hosts of several RE ions such as Nd^{3+}, Ho^{3+}, Er^{3+}, Dy^{3+} and Tm^{3+} [36]. As_2S_3 glasses doped with only 0.4 wt.% Nd^{3+} showed fluorescence at 1.09 μm and 1.38 μm, while glasses doped with 2.0 wt.% Dy^{3+} exhibited fluorescence at 2.98 μm and 4.40 μm. Further, doping of Ho^{3+} up to approximately 2.0 wt.% showed fluorescence at 2.01 μm. No emission of Tm^{3+} or Er^{3+} was observed in As_2S_3 glasses. As it was seen RE ions are not soluble in As_2S_3 glasses or the solubility is very low, which is the major drawback of As_2S_3 glasses as a host for RE ions. Even a slight increase of the amount of RE dopants in these glasses leads to the clustering of ions and brings the glass to the crystallization and the concentration quenching of the luminescence.

Much effort has been devoted to the development of glass compositions appropriate for RE doping. Several sulphur-based glassy systems have been studied as hosts for RE ions such as Ga_2S_3-La_2S_3 (GLS) [37], GeS_2-Ga_2S_3 (GGS) [38], GeS_2-As_2S_3-Ga_2S_3 (GAGs) [39-41], Ge-Ga-Sb-S [42], GeGaS-GSI [43]. It has been claimed that the Ga can dramatically increase the solubility of RE ions in ChGs. Addition of Ga to the host in a concentration ratio of at least 10:1 = [Ga]: [RE] can increase RE emission by an order of magnitude for the same level of RE-dopant [39]. However, the tendency to crystallization in all these systems is quite high unlike the As_2S_3, so the incorporation of Ga in the As_2S_3 glass matrix could compromise the thermo-optical properties of the glass with the solubility of RE ions.

1.2. PROJECT AIM

The main objective of this thesis was to increase the solubility of RE ions in As_2S_3 glass in order to obtain a high purity glass doped with RE ions, with higher thermal stability for fiber drawing. Two different aspects of the modification of As_2S_3 glass matrix are presented. Firstly, the addition of gallium (Ga) as co-dopant is examined and its potential for use as active optical materials is explored. The second technique employs the modification of As_2S_3 network through the incorporation of halogen elements (iodine). The addition of these network modifiers was expected to break the As-S bonds and replace them with less energetic bonds thus providing the RE ion with a lower local phonon energy environment. The spectroscopic measurements of the absorption and emission spectra, as well as, the fluorescence lifetimes of the modified As_2S_3 glasses doped with RE ions allowed the effectiveness of each network modifying element to be assessed. The increasing of RE solubility in As_2S_3 glass, while maintaining its environmental stability, lower phonon energy (360 cm^{-1}[8]) and its extended IR transparency and the potential to be pulled into a fiber form, could potentially offer a promising improvement to the existing doped fibers, with the possible extension to longer wavelengths.

The second objective of the thesis is to understand the mechanisms responsible for the increase of the solubility of RE ions in As_2S_3 glass with the incorporation of certain modifiers. This realized through systematic study of the effects of network modifiers on the structure of the fundamental glass matrix and on the local environment of RE ions.

Mid-IR fiber lasers, using relatively cheap commercially available NIR diode lasers as pump sources, could offer an inexpensive and compact alternative to currently available mid-IR sources. The success of this project depends mainly on the fabrication of low loss fiber of sufficient length and with reasonably small core diameters, assuming the spectroscopic properties of the RE ions are favourable for mid-IR laser emission.

1.3. THESIS SYNOPSIS

This thesis describes original research in the design, fabrication and characterization of Tm^{3+} doped ChGs and glass fibers based on As_2S_3 glassy system. The main body of this thesis is formed by a number of journal papers written by the author herself. These papers have been embedded in the chapters in the original form they were published.

The thesis contains eight chapters, including this introduction, chapter 1.

Chapter 2 provides a necessary background regarding ChGs and their spectroscopic features. It gives an introduction to ChGs and Chalco-halide glasses (ChHGs) and their fundamental properties. The basic theory for the understanding of the spectroscopic properties of the RE ions and the influence of the host material was introduced as well.

Chapter 3 details the experimental techniques used for fabrication and for characterization of studied glasses and glass fibers. The purification and synthesis technology used for the fabrication of RE doped ChGs were discussed, as well as, the procedure of the fabrication of glass fibers. The need for high purity powdered precursors and their impact on optical quality and thermal stability for fabricated glasses is also discussed. Also we included all of the spectroscopic techniques used in the analysis of optical, thermal and structural properties of these glasses.

Chapter 4 focuses on the study of the effect of Ga in the emission properties of Tm^{3+} in As_2S_3 glass matrix. It describes the fabrication and characterization of Tm^{3+} doped Ga-As-S glasses. The concentration ratio of Tm and Ga was optimized to achieve the highest photoluminescence efficiency in this system. Optical and thermal properties of this glassy system were studied depending on the concentration of Ga and Tm. The fiber, drawn from optimal composition, is presented, and the experimental set-up used for characterization of luminescence properties of Tm^{3+} doped Ga-As-S fiber is explained.

Chapter 5 deals with more fundamental problem, the investigation of the mechanisms responsible for the solubility of Tm^{3+} ions in Ga-As-S glasses. Raman and EXAFS spectroscopies were used to investigate structural features of this glassy system. The structural changes made by the incorporation of Ga and Tm in As_2S_3

glass matrix and with the variation of their concentrations were studied. The changes in the local environment of Tm^{3+} ions, upon the increasing its content in the glass, is illustrated as well.

A separate **Chapter 6** represents the continuation of the chapters 4 and 5. It describes the attempts of purification of Ga-As-S glasses and it is dedicated to explain the motivation and the strategy of replacement of gallium with iodine in As_2S_3 glass. The modifications made in Ga-As-S glassy system that could decrease the melting temperature of the glass matrix and allow the purification of multicomponent glass are discussed.

Chapter 7 discusses new ChHGs (I-As-S) as host matrix for Tm^{3+} ions. Optimization of suitable host composition and Tm^{3+} dopant concentration level in I-As-S glass system was performed. This chapter describes and compares the thermal, optical and structural properties of this system depending on the concentration of iodine and Tm. Some structural mechanisms are proposed to explain the solubility of Tm^{3+} ions in As_2S_3 glass with the incorporation of iodine.

Finally, **chapter 8** summarizes the current status of the project and suggests some future work.

CHAPTER 2
BACKGROUND

In this chapter, we will give the basic background information regarding glass formation conditions in general. We will explain the formation of a glass in two aspects: structural and kinetic. Than we will expose different families of glasses, particularly those based on heavy metals (fluoride, halide and chalcogenide). We will be more focused on chalcogenide glasses and mostly on the glassy system based on Arsenic and Sulphur. As we are interested in RE doped glasses we will present the basic spectroscopic theory of RE elements: electronic structure, radiative and non-radiative transitions. We will study Tm^{3+} ions and give the important characteristics of this element in different glass matrices.

2.1. GENERAL CONSIDERATION ON GLASSES

The first use of the glass by mankind seemed to start with natural glasses such as obsidian, a natural volcanic glass (alumina-silicate glasses), for tools and weapons. The method of manufacturing of artificial glasses, using sand (SiO_2) and salt (NaCl), which could yield soda-silicate glasses (SiO_2–Na_2O) in charcoal fires, was accidentally discovered at Mesopotamia [44] by approximately 4500 BC. Because of the presence of impurities (such as Fe_2O_3) the glasses were coloured at that era. However, around the first century (in the Roman age) transparent wine glasses became available and methods for preparation of controlled shape glasses were developed. Bottles were produced by winding glass ribbons around a mould of compacted sand and after cooling, the sand was scraped from inside the bottle, leaving a hollow container with rough, translucent walls. Further developments led to the invention of glass blowing (in Phoenicia around 50 BC), which allowed producing more transparent glasses. This eventually enabled the fabrication of windows. Later, in the 17th century, Galilei and Newton used transparent glasses as optical components like lenses and prisms. Many other optical instruments such as eyeglasses, microscopes and telescopes were devised as well.

In everyday language, the word ‘‘glass’’ denotes a transparent and fragile material. In scientific language, the glasses are considered as non-crystalline solids obtained by cooling of super-cooled liquids. However, the fast cooling of liquid is not the only method for obtaining non-crystalline solids. Basically, the non-crystalline solids can be obtained by three different ways [45]: maintaining the structural disorder of the liquid phase (by fast cooling), using the disordered nature of the gas phase (by evaporation) and by interrupting the order of a crystal phase (mechanical compression).

The non-crystalline solids are solid materials, that are lacking long range order in their structure. For being classified as a good non-crystalline former, material must meet two conditions:

1) the network structure must be topologically disordered [46], because these structures possess intrinsic resistance towards crystallization, which requires topological changes (bond breakage and reformation)

2) the short-range order (SRO) must be the same as in the corresponding crystal.

In fact, not all non-crystalline materials are necessarily glasses. They are divided into two categories: glasses and amorphous solids. The non-crystalline solid is a glass, if its SRO is the same as that in its molten state (SRO (glass) = SRO (melt)). This condition is clearly satisfied for glasses formed by melt-cooling because the structure of a melt is frozen during the transition from liquid to glass. Whether a non-crystalline solid is made by melt-cooling or by other methods (for example evaporation) it is called glass as long as it satisfies this condition. If conditions 1) and 2) are respected, but SRO (glass) ≠ SRO (melt) the material will be classified as an amorphous solid. In addition, amorphous solids and glasses are distinct thermodynamically [45]. The free energy of amorphous solids is less than that of super-cooled liquid and they do not show structural relaxation. The heating of these substances leads to rapid crystallization or decomposition of structure before their melting point is reached. Contrariwise, the glass passes progressively from a solid state to a liquid state with the successive increase of temperature. Such transition (from solid to molten state or the reverse one) followed by the radical changes of

mechanical properties of the material is called a glass transition. So, the glass may be defined as following: the glass is a non-crystalline solid exhibiting the glass transition temperature [45].

The conventional method for producing a glass is the very rapid cooling of the liquid, in order to prevent the crystallization. With the decrease of the temperature, the viscosity of the liquid increases rapidly, leading to the freezing of the liquid to the final solidification. The temperature decrease leads to the contraction of the substance and when the solidification point (T_f) is reached, two phenomena can occur (Fig. 2.1) - either the liquid crystallizes and a discontinuity of ΔV_f is introduced or crystallization is prevented and the liquid passes to the super-cooled state and starting from certain temperature (T_g) the slope of the curve decreases to become close to that of the crystalline solid. The jump in the curve shows the transition from the super-cooled state to the glassy state. T_g is called the glass transition temperature.

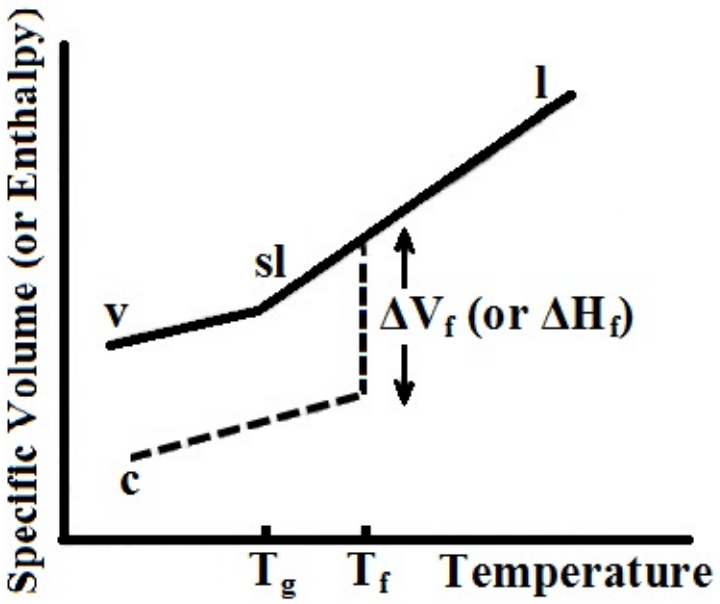

Fig. 2.1. Variation of the specific volume with temperature [45] (1 - liquid; s1 - Super-cooled liquid; c - crystal; v - glass).

2.1.2. CHALCOGENIDE GLASSES (ChGs)

The ChGs are glasses based on VI group elements (S, Se and Te) of the periodic table, combined with the elements of groups III (Al, Ga, In, Tl), IV (Si, Ge) and V (P, As, Sb, Bi). The history of ChGs is very different from that of oxides. As it is already mentioned the oxide glasses has a history longer than 5000 years, while the chalcogenides have only one and half-century history. The history of ChGs began in 1870 when Carl Schultz-Sellack reported experience on the transition radiation heat by the series of materials [47]. But the real interest and important studies on ChGs began in the 1950s in Russia and the United States. These glasses have been studied as semiconductor materials, ion conductors, IR transparent glasses and xerographic photoreceptor. Chalcogenides are studied by chemists as new glasses [48], by physicists as an amorphous semiconductors [49-50] and as photonic glasses by application-oriented researchers [51].

ChGs are very different in compositions and hence their classifications are also different [48,52]. ChGs can be classified as elemental, binary, ternary, etc. The alloys can be divided into stoichiometric (As_2S_3, $GeSe_2$) and non-stoichiometric compositions (S–Se, As–Se) as well.

Among three chalcogenide elements, only Se may exist in glassy state (thin films or glassy ingots) at room temperature [53]. S and Te are unstable at room temperature and crystallize immediately. Some molecular allotropes for S are known, but the most stable is the structure with the S_8 ring molecules. Glassy S can be obtained by quenching from ~160 °C (polymerization temperature) to temperatures below the T_g [54]. Te is much more metallic, having less directional chemical bonds. As a result, the material is likely to crystallize, and the bulk glass cannot be prepared [55].

The oldest and simplest chalcogenide binary alloys are the glasses based on arsenic and sulphide [56-59]. Arsenic trisulphide with the stoichiometric composition, $As_{40}S_{60}$ (As_2S_3 for short), has been intensively studied for years. In general, the stoichiometry of the As-S glasses can be changed dramatically within a broad glass-forming region. It is quite easy to increase, for example, the concentration of As and decrease the concentration of S in the glass to increase its refractive index

[60]. This is one of the reasons why these glasses are particularly good choices for fiber optic applications. As-S glasses have low T_g and they are quite stable against devitrification. The most thermally stable composition is obviously the stoichiometric As_2S_3 with the T_g of about 200 °C [48].

The structure of ChGs, however, cannot be described by means of a continuous random network which is isotropic in three dimensions, as in the case of amorphous silicon. The bonds in these vitreous compositions are essentially covalent [61] and the structure of ChGs can be locally layer-like (As_2S_3, As_2Se_3, GeS_2, and $GeSe_2$), or chain-like (pure S and Se). For all these materials, the structure is considerably flexible which is the result of the weak van der Waal's bonding between layers or chains [62], so the changes in the structure can be relatively easily accommodated. As_2S_3 glass has a polymeric structure composed of trigonal pyramids, where each center of As is linked with three sulphur centers (Fig. 2.2).

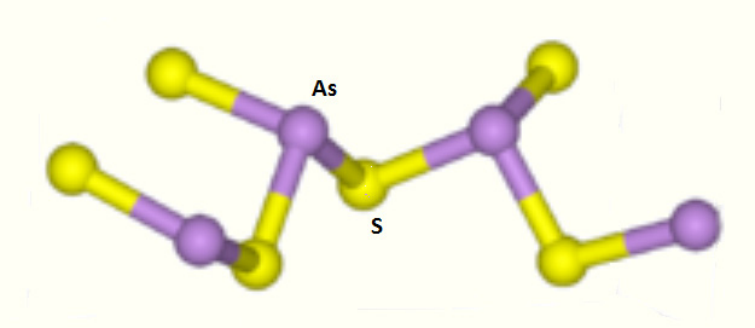

Fig. 2.2. Structural units of As_2S_3 glasses

Within above mentioned categories, one finds that the binary and ternary glasses are excellent choices for fiber drawing. Unlike the fluoride glasses, which normally include five or more components, most ChGs have only two or three elemental components. In general, these glasses have softening temperatures comparable to fluoride glass. The ChGs, however, are chemically more durable, especially against attack by moisture, than the fluoride glasses. A distinctive difference between these glasses and the other IR fiber glasses is that they do not transmit well in the visible region and their refractive indices are quite high.

The transmission range of chalcogenide fibers depends heavily on the mass of the constituent elements. The lighter-element glasses, such as As_2S_3, have a transmission range from 0.7 μm to ~7 μm [57]. Besides this glass, only Ge-S based

glasses and some phosphorous containing glasses are transparent in visible region [63]. Longer wavelength transmission becomes possible with the addition of heavier elements like Te and Se and this leads to the opacity in the visible region. A key feature of essentially all ChGs is the strong extrinsic absorption resulting from contaminants such as hydrogen, H_2O and OH^-. For example, there are invariably strong absorption peaks at 4.0 and 4.6 μm due to S-H or Se-H bonds, respectively, and at 2.78 μm and 6.3 μm due to OH^- and molecular water. As a result, typical chalcogenide loss spectra are normally replete with extrinsic absorption bands, which would seem at first sight to be sufficiently adverse for the applications of these fibers. However, many applications for these fibers are possible simply by working outside these extrinsic bands or by reduction of these bands by several cycles of purification of the raw material.

The exceptional transparency of these glasses in the IR explains their use in two categories: passive and active IR optics. In passive optics they were used as optical lens for IR cameras, planar waveguides for integrated optics or infrared sensors. In the field of active optics ChGs represent relevant materials for the use as optical amplifiers, which allow obtaining a substantial quantum yield of luminescence from RE ions, due to their low phonon energy (360 cm^{-1}).

Possessing all above mentioned features As_2S_3 glasses are very good candidates for the fabrication of RE doped fibers, but as it was already mentioned in chapter 1 the solubility of RE ions is very limited in this glass. So, in this thesis we describe the modification of the binary As_2S_3 by adding Ga in the network and the impact of structural changes, created by Ga, on the increase of the solubility of RE ions.

The glass formation in the Ga-As-S system was discovered in 1960 by Kolomiets, Goryunowa and Chilo [49]. The phase diagram in this system is presented in Fig. 2.3. As it can be seen the glass formation region is very small. In order to obtain a glass in Ga-As-S system high temperature of synthesis and very high cooling rate is required. The synthesis temperature is 900 °C and the glasses were quenched in ice water directly from 900 °C (cooling rate is about 200 ˚C / sec.) Under these conditions it was possible to enter only up to 3.5 at% of Ga in As_2S_3 glass.

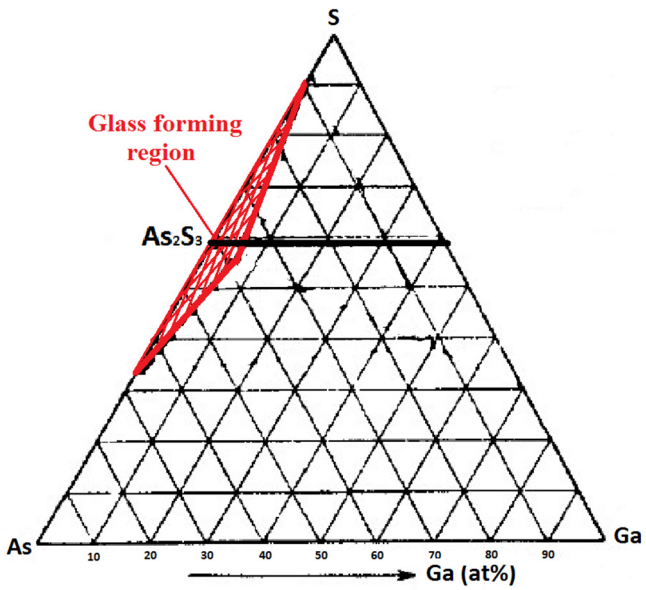

Fig. 2.3. Glass formation region in Ga-As-S system [49]

2.1.2. HALIDE GLASSES

The first halide glass was discovered in 1975 at the University of Rennes [64], which was based on zirconium fluoride. Generally, the T_g of typical fluoride glass is about four times lower than that of oxides and their thermal stability is considerably less. The most significant difference between oxide and fluoride glasses, however, is that metal fluorides do not form a glass as easily as metal oxides. This is in part due to the more ionic nature of the bonds in fluoride glass compared with greater covalent bonding in oxide glasses. Unlike oxide glasses, which form fourfold-coordinated and very stable tetrahedral structure and can be single component glass former, halide glasses are not fourfold coordinated and they are much less stable and therefore it is usually necessary to combine three or more halide compounds to obtain a stable glass. The only single component halide glass former is BeF_2, which has very little practical value, because of its toxicity and hygroscopicity.

However, varieties of different multicomponent halide glasses have been fabricated and explored [65,66], and some of them have been drawn into fiber (the most famous is the ZBLAN glass), despite their small working temperature range for fiber drawing. It is also important having a viscosity temperature relationship suitable

for fiber drawing, i.e. a small change in viscosity with changing temperature. The change in viscosity with temperature for halides is much steeper than for silica [65], which further complicates the fiber drawing process of these glasses.

Usually, fluoride glass fibers are drawn in a controlled atmosphere in order to minimize contamination by moisture or oxygen impurities, which can considerably affect the fiber quality. The reliability of fluoride glass fibers depends on protecting the fiber from moisture (UV acrylate or Teflon coating) and on pre-treatment of the preform to reduce surface crystallization. Halide glasses are normally kept free oxide (except of oxy-fluoride glasses), because it not only weaken the glass, but also can affect their transmission in the IR region.

However, the most principal advantage of halide glasses compared to oxides is their transparency in IR up to 6 μm and the possibility to increase the long wavelength transmission by substituting heavier cations for the lighter ions [67]. For example, the elimination of Zr from ZBLAN glass extends the transmission range by about 1 μm beyond the cut-off [68]. The other important feature of halide glasses is the sensibility of their refractive indexes to the composition. The refractive index of a glass can be easily displaced up or down and tailored it for the core or cladding of fiber, just with variation of the concentration of components. For example, AlF_3 can decrease the refractive index of the glass, while heavier PbF_2 increases it [69].

That is why very often halide glasses are mixed with oxide or chalcogenide glasses in order to achieve some specific thermal, optical or mechanical properties.

2.1.3. CHALCO-HALIDE GLASSES (ChHGs)

ChHGs are vitreous materials containing chalcogen and halogen elements. They could be considered as materials intermediate between halide glasses and ChGs. As a matter of fact, many of these compounds are considered not only substitution materials but also as glasses having their specific structural characteristics and thermal and optical properties. Each of these systems has its own advantages and inconveniences. For example, the relatively poor chemical durability and low thermal stability of halide glasses affect their practical applications [70]. On the other hand; chalcogenide glasses are well known [71] for their good chemical durability and

excellent transmittance in mid-IR. However, the multiphonon absorption of metal-chalcogen bonds affects the optical loss of the materials seriously and thereby results in an undesirably high attenuations loss at corresponding wavelengths [72].

The incorporation of halogen elements into ChGs is expected to produce changes in various properties of glasses. Optical properties are the most important ones to be considered. The addition of heavy halogen elements is expected to reduce the number of metal-chalcogen bonds, by forming metal-halogen bonds, and accordingly can reduce attenuation losses at the wavelength of practical interest. Obviously, it is expected to make a compromise between the improvement of optical properties and the possible degradation of thermal and chemical properties incurred by the formation of weak metal-halogen bonds. Moreover, the heavy atomic weight of halogens, which are neighbours to chalcogens in the periodic table, allows maintaining the low phonon character of the glassy matrix, therefore retaining the higher RE solubility and low rate of non-radiative decay. Halogen which is a non-bridging atom takes the role of terminal atom, by breaking metal-chalcogen-metal bonds, and form metal-halogen anionic complexes. These highly electronegative elements reduce the relocation of non-binding electrons of chalcogen, which has the consequence of increasing the bandgap of the material and exhibit better transmission in the UV-visible region. With the increasing of the transparency of a glasse in the visible region a greater number of energy levels of RE ions becomes available. The change in composition of the host matrix can affect the covalent nature of the network and therefore the properties of the RE. The addition of halogen not only assumes the pumping of more RE energy levels, but also the increase of the quantum yield and the lifetime of emission [73].

The first synthesis of ChHGs, in As-S-I ternary system, was reported by Flaschen in 1960 [74], followed by exploring other ChH glassy systems, such as Ge-Ch-H, As-Ch-H, M-Ch-H (Ch = S, Se, Te, H = Cl, Br, I, M = Sb, Si, Cs, Al, Ga) [75-77] and Te-H based glasses [78]. Fuxi [6] reported a variety of chalco-halide systems, allowing increasing the solubility of RE ions and none of them was based on Ga_2S_3, which claims that halogen element can increase the solubility of RE ions as well as the metals of III group (Ga, In, etc.)

In this thesis we studied the role of iodine in the solubility of RE ions in the As_2S_3 glasses as an alternative glass modifier for Ga. So, fig. 2.4 presents the glass forming region previously presented by Flaschen [74]. We must indicate that the glass formation region of this system is quite large and compositions containing up to 55 wt.% iodine (33 mol%) were successfully prepared.

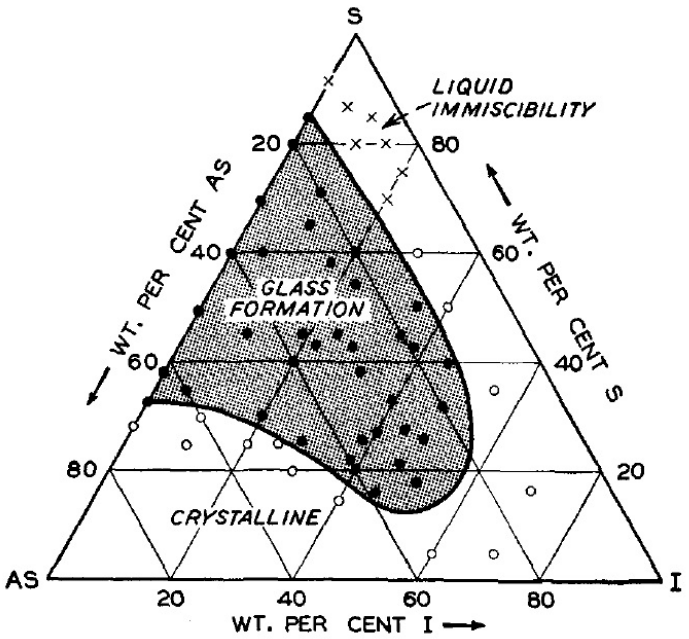

Fig. 2.4. Glass formation region in I-As-S system [74]

The temperature of synthesis was relatively low (500-600 °C) for these glasses and a minimum agitation was required for mixing due to the high fluidity of the melts.

2.2. SPECTROSCOPY OF RARE-EARTH IONS

RE ions have very important role in optical applications, especially in luminescent devices using single crystals, powders and glasses. RE ions have several special features that distinguish them from other optically active ions: they emit and absorb over narrow wavelength ranges, the most of emission and absorption wavelengths are relatively insensitive to host material, the lifetimes of metastable states are long and the quantum efficiencies tend to be high. All these properties

result from the nature of the states involved in these processes and lead to excellent performance of RE ions in many optical applications. Glassy hosts present special interest, because the versatility of glasses and the broader emission and absorption spectra, that they are able to provide, lead to the use of RE doped glasses in applications like lasers and amplifiers. Chalcogenide hosts are of particular interest, because they provide more metastable states and greater transparency at wavelengths beyond 2 μm. Moreover, the high intensities and long interaction lengths, obtained by fiber waveguides, make these devices vastly superior to their bulk glass counterparts in most applications.

2.1.2. ELECTRONIC STRUCTURE

The RE elements are categorised by a group of 15 elements known as the Lanthanides and are most stable in their triply ionised (3^+) form. The trivalent ionisation of these elements preferentially removes 6*s* and 5*d* electrons, and the electronic configuration of these ions becomes identical to xenon plus a certain number (1-14) of 4*f* electrons [79]. The remaining 4*f* electrons are therefore partially shielded by the outer $5s^2$ and $5p^6$ orbitals. Therefore, the influence of the host lattice on the optical transitions within the 4f-4f configuration is very small. These transitions are characterized with narrow, weak bands or sharp lines, and emission that can be highly efficient, unlike transition metals, which have much stronger interaction with the host and are characterized by broad, strong emission and absorption bands. In general, optical transitions of RE ions are inter-configurational and consist of two different types: $4f^n \rightarrow 4f^{n+1}$ (charge-transfer transition) and $4f \rightarrow 5^d$ [80]. Normally trivalent ions that tend to become divalent (Dy^{3+}, Ho^{3+}, Yb^{3+}, Er^{3+} Tm^{3+}) show charge-transfer absorption bands. Trivalent ions that have a tendency to become tetravalent (Ce^{3+}, Pr^{3+}, Tb^{3+}) show $4f \rightarrow 5^d$ transitions.

The 4*f* electrons interact only weakly with electrons on other ions, so the Hamiltonian of an individual RE ion can be written as follows [81]:

$$H(t) = H_{free\ ion} + V_{ion\text{-}static\ lattice} + V_{ion\text{-}dynamic\ \ lattice}\ (t) + V_{EM}(t) + V_{ion\text{-}ion}(t) \qquad (2.1)$$

where $H_{free\ ion}$ is the Hamiltonian of an ion in isolation, $V_{ion\text{-}static\ lattice}$ *and* $V_{ion\text{-}dynamic\ lattice}$ describe the static and dynamic interactions of ion with the host, respectively, $V_{EM}(t)$ treats the interaction of an ion with an electromagnetic field and $V_{ion\text{-}ion}(t)$ describes the interactions between RE ions. The interaction terms in Equation (2.1) are weak compared to the $H_{free\ ion}$ and can therefore be treated as perturbations. The first two terms are time independent and give rise to the electronic structure of a RE ion. The last three terms in Equation (2.1) are dynamic perturbations, which are time dependent and result in transitions between the states formed by the static interactions. A central field approximation is normally applied for treating $H_{free\ ion}$ [81], in which each electron is assumed to move independently in a spherically symmetric potential. So, the solutions can be constructed from two functions: radial and angular, where the radial function depends on the details of the potential, while the angular component is identical with that of a hydrogen atom and can be expressed as spherical harmonics. Because these solutions are constructed from hydrogenic states, total orbital angular momentum L (specified as S, P, D, F, …) and total spin S are the exact eigenvalues of the Hamiltonian [81]. The interaction of the 4*f* electrons with each other once the centrally symmetric contribution has been removed causes a splitting of the $4f^N$ electronic orbital state into a number of different states with different energies characterised by L and S. The *LS* coupling is most often used for the states of RE ions, where L and S are vectorially added and form the total angular momentum J (the states are labelled $^{2S+1}L_J$). L, S and J define the terms of the configuration, all of which are degenerate in the central-field approximation (Fig. 2.5). As it is shown in Fig. 2.5 the electrostatic interaction lifts the angular degeneracy and produces a spectrum of states the energies of which depend on L and S, but not J. Next is the spin–orbit interaction. Spin–orbit lifts the degeneracy in total angular momentum and splits the *LS* terms into J levels.

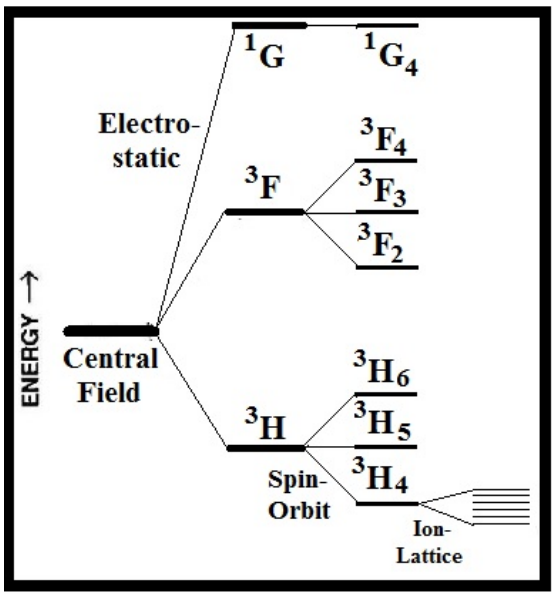

Fig. 2.5. Energy diagram illustrating the splitting of energy levels from electron–electron and electron–host interactions [81]

If only the diagonal matrix elements of the interaction are considered, different *LS* terms are not mixed and the states maintain their original values of *L* and *S*. In practice, the separation between *LS* terms is too small compared with the strength of the spin–orbit interaction, so in order to diagonalize the interaction matrix elements an intermediate coupling calculation is needed, which forms states that are linear combinations of different *LS* terms and, therefore, are eigenstates of *J*, but not of *L* or *S* [82]. Although both the electrostatic and spin–orbit interactions increase with increasing atomic number, spin–orbit increases more rapidly, and *LS* mixing becomes more significant for RE ions with high atomic number (Er^{3+}, Tm^{3+}, etc.).

The influence of the host on the electronic structure is very low and it changes the positions of these levels only slightly. The RE site symmetry in glasses is usually low enough to lift the degeneracy. The ion–lattice interaction can mix multiplets with different *J* values, although it normally remains a good quantum number. This admixture does not affect the positions of the energy levels, but it has a very important effect on the strengths of the optical transitions between levels [81].

2.2.2. RADIATIVE TRANSITIONS

As it was mentioned above the dynamic interaction terms in Eq. (2.1) are time-dependent and they result in transitions between the states established by the static interactions. For luminescent devices the most important term is V_{EM} (the interaction with the electromagnetic field), which gives rise to the absorption and emission of photons. Optical transitions from the infrared to the ultraviolet occur between states that belong to the $4f^N$ configuration. These states have the same parity, therefore electric–dipole processes are forbidden and transitions can occur only by the much weaker magnetic–dipole and electric–quadrupole processes. In solids, however, higher-lying states of opposite parity can be admixed into the $4f^N$ configuration (through ion–static lattice interaction), thereby introducing a degree of electric–dipole strength into the intra-*f*-shell transitions, the so called second-order electric–dipole contribution. This can happen only if the ion site lacks inversion symmetry, as it usually does in glasses. This is a very important effect because most visible and infrared RE transitions are dominated by these transitions.

The intensities and shapes of absorption and emission bands can be calculated if the $V_{\text{ion–static lattice}}$ is known. A semi-empirical technique for calculating the strength of RE transitions in solids was provided independently by Judd [83] and Ofelt [84] in 1962. Based on the assumption that the energy range occupied by the $4f^N$ multiplets as well as that spanned by the admixed opposite parity states are small compared with the separation between the states, the transition strength was written in the form [81]:

$$S_{a,b} = e^2 \sum_{t=2,4,6} \Omega_t \left| \left\langle b \left\| U^{(t)} \right\| a \right\rangle \right|^2 = 4\pi\varepsilon_0 \frac{3hcn(2J_a+1)}{8\pi^3 \bar{\nu}} \frac{1}{\chi} \int \sigma_{a,b}(\nu) d\nu \qquad (2.2)$$

where Ω_t are coefficients reflecting the effect of the crystal field, electronic wave-functions and the energy level separation, while $\left\langle b \left\| U^{(t)} \right\| a \right\rangle$ are doubly reduced matrix elements of the tensor operator $U^{(t)}$, which is a quantum mechanical operator for an electric dipole transition from state *b* to *a*. e is electron charge, ε_0 is the permittivity of vacuum, *h* is Planck's constant, *c* is the speed of light in vacuum, *n* is

the index of refraction of the host, $\bar{\nu}$ is the mean photon frequency and J_a is the J value of the initial state. The $\chi = \left(E_{loc} / E \right)^2$ is referred to as the local field correction and represents the enhancement of the electric field in the vicinity of the ion owing to the polarizability of the medium.

The matrix elements are virtually independent of the host material and have been tabulated by several authors [85-86]. The host dependence is contained in the three intensity parameters Ω_t (k = 2; 4; 6), known as Judd-Ofelt parameters. These parameters are usually determined empirically by performing a least squares fit of Eq. (2.2) to the integrated absorption bands obtained from a measured spectrum. Once the parameters have been determined, the strength of any radiative transition can be calculated for that dopant and host combination. Judd–Ofelt analysis is useful for obtaining strengths of transitions for which direct measurements are difficult or impossible. It should be noted that the accuracy of this analysis is limited to 10–15%.

2.2.3. NONRADIATIVE TRANSITIONS

Radiative return from the excited state to ground state is not the only possible transition. RE ions can undergo transitions caused by the interaction with vibrations of the host material. In crystals this corresponds to the emission and absorption of phonons. In glasses vibrational modes do not have a well-defined wave vector, because of the absence of translational invariance, but these excitations are still referred to phonons. If the electronic states are close enough that they can be bridged by one or two phonons, the non-radiative transitions will occur rapidly. In many cases the energy gap can be bridged by the simultaneous absorption or emission of several phonons. This process is known as multiphonon relaxation. Usually, the probability of multiphonon emission is many orders of magnitude less than the probability of emission or absorption of a single phonon, however, multiphonon processes can still be significant as the electron-phonon interaction is strong and phonons have a density of states that typically is 11 orders of magnitude larger than that of photons [87]. In general, if less than 5 phonons are required to bridge the energy gap, the rate of multiphonon emission is comparable with the radiative emission rates. One of the

simplest theoretical formulations used to describe multiphonon relaxation in crystals was developed by Kiel [87] and extended by Riseberg and Moos [88].

The multiphonon decay rate is inversely proportional to the exponential of the energy gap separating the two levels [89]:

$$w_{nr} = C\left[n(T)+1\right]^{p} e^{(-\alpha\Delta E)} \tag{2.3}$$

where C is an effective phonon frequency, α is host-dependent parameter, related to the coupling constant for the interaction. ΔE is the energy gap, p is the number of phonons required to bridge the gap, and $n(T)$ is the Bose–Einstein occupation number for the effective phonon mode. In practice, C, α, and p are considered as empirical parameters, which depend on the host, but are insensitive to RE ion and involved energy levels. They are obtained by fitting Eq. (2.3) to the non-radiative rates observed for many energy gaps using different levels and ions in the same host.

The large variation in vibrational spectra among materials makes the non-radiative relaxation rate extremely host-dependent. For example, oxides have larger non-radiative rates because their strong covalent bonds result in higher phonon frequencies. The weaker ionic bonds of chalcogenide and halide glasses lead to a much lower w_{nr} as well as higher transparency at MIR wavelengths. In general, glasses have much larger non-radiative rates than crystals of similar composition because of the larger effective phonon frequencies and stronger electron–phonon coupling (smaller α).

2.2.4. LINE-BROADENING MECHANISMS

For RE doped crystals, the absorption and emission transitions are usually observed at room temperature as discrete lines, while the transitions for glass hosts show broad absorption and emission bands in spectra. In general, two fundamental mechanisms are responsible for broadening the absorption/emission lines: homogeneous and inhomogeneous processes. For a homogeneously broadened transition a given wavelength will interact with all ions with equal probability, thus, any pump wavelength will produce the same gain spectrum and any signal

wavelength can saturate the entire band. In the case of inhomogeneous broadening, individual sections of the gain spectrum act independently and can be individually addressed by photons of different wavelengths.

For both crystals and glasses, the homogeneous broadening of transitions is caused by lifetime broadening, which occurs as a consequence of energy uncertainty principle, according to which the energy of a manifold with characteristic lifetime τ can only be within $\Delta E \geq \hbar/2\tau$ [90]. A large contribution to the homogeneous line width of an energy manifold comes from transitions which occur between levels in a single manifold. If the energy separation between levels is small (a few 100 cm^{-1}), energy can be absorbed from or emitted to vibrational modes of the host. These transitions usually involve a single mode of vibration and occur on a rapid time scale giving homogeneous line widths to the levels of 1- 300 cm^{-1}.

Inhomogeneous broadening occurs when the sites occupied by the RE ions are not identical. RE ions normally occupy almost identical sites, so in crystals inhomogeneous broadening may be observed only if imperfections exist in the crystal structure. In contrast, in glasses, inhomogeneous broadening is the dominant broadening mechanism. The disordered nature of glass exposes the RE ions to a distribution of possible environments, each with a characteristic set of field parameters. The distribution of fields at individual sites can be large and the energy manifolds of the ions may show considerable differences to their crystalline counterpart [59].

2.2.5. ION–ION INTERACTIONS

The radiative and non-radiative processes described above have concerned only isolated ions. When the concentration of RE ions is low, they are evenly distributed throughout the glass matrix and the large interionic distance prevents any ion-ion interactions. However, when the concentration of RE ion is increased, the distance between ions is reduced and interactions between ions become more likely. The interaction between RE ions is treated by $V_{\text{ion–ion}}$, the last term in Eq. (2.1). These interactions involve the transferring or sharing of energy between ions. The most

probable forms of ion-ion interaction, that can be manifested, are energy transfer, cross relaxation and concentration quenching.

Energy transfer: The energy exchange may occur among RE ions, and it may be radiative or non-radiative. Radiative energy transfer involves one ion emitting a photon, which is then reabsorbed by another ion. This process can distort the emission spectrum and cause radiation trapping. In most situations, it does not result in a transfer of significant amount of energy, however, and the more important processes involve excitation transfer between closely spaced ions without the exchange of real photons. Energy transfer can take place between two different species of ions as well, where the optically excited ion (donor) transfers the excitation to neighbouring ion (acceptor). This process can occur in a single step in which the particular donor ion that absorbs the photon transfers its energy to a nearby acceptor. If the donor concentration is high enough, another mechanism that can occur is the migration of the excitation among the strongly coupled donor ions (donor–donor transfer). If the acceptor is a trap or if the donor has a cooperative relaxation mechanism [81], other than transfer to the desired acceptor, energy transfer is a non-radiative process and results in the loss of excitation.

Cross-relaxation: Cross-relaxation is a process where an ion in an excited state transfers part of its excitation to a neighbouring ion, promoting the acceptor ion to a higher energy state, while demoting the donor to a lower state. In order this phenomenon to occur the energy levels of interacting ions must be approximately in the same energy gap. Because the energy gaps to the lower-lying states are small, both ions quickly decay non-radiatively to the ground state.

The cross relaxation process can be considered as not only detrimental but also beneficial, if one desires the ions to be in the excited states that result from the interaction. The process can be favourable since in some cases every excited donor ion results in two excited ions in an intermediate energy manifold. Cross relaxation can involve a single type of RE ion if the ion has two pairs of equally spaced energy levels. If the energy gaps are matched the energy transfer is called resonant. If an energy mismatch exists between the energy gaps, it may be compensated by the absorption and emission of phonons.

Concentration Quenching: Concentration quenching is a process where the quantum efficiency of an ion is reduced with increasing concentration of that ion. It can occur through any of the foregoing energy transfer processes and results in the loss of excitation. In this case the energy is transferred from donor to acceptor but the latter does not fluoresce and relaxes non-radiatively. In this process, the acceptor acts as energy hole and is sometimes called the deactivator.

2.2.6. THULIUM

Thulium is the thirteenth lanthanide element and has 12 electrons in its 4*f* shell. Due to its electronic features, Tm^{3+} has useful emission in a silica host as well as several additional transitions when it is doped in chalcogenide glasses. Much of the interest in Tm^{3+} is related to its emission that occurs in the gaps between the emission bands of Er^{3+} and Nd^{3+} (1400–2700 nm). A typical absorption spectrum of Tm^{3+} ions in GeGaSbS chalcogenide glasses is illustrated in Fig. 2.6. The absorption spectrum is nearly identical to that of silica glass except that the ultraviolet edge of the latter is shifted to longer wavelengths. Ground state absorption wavelengths of Tm^{3+} are normally 700 nm and 800 nm for chalcogenide glassy hosts. Energy level diagram of Tm^{3+} is illustrated in Fig. 2.6.

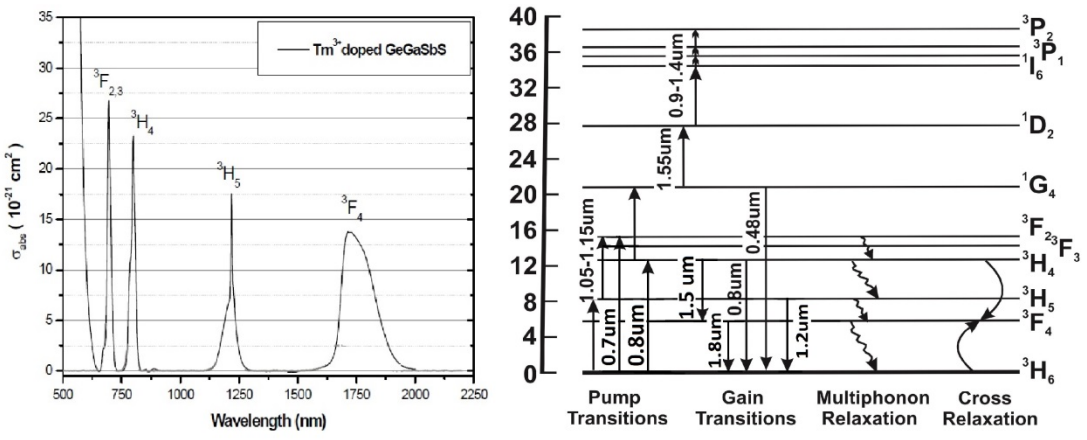

Fig. 2.6. Absorption cross-section of Tm^{3+} in GeGaSbS [91] and Tm^{3+} energy diagram

Tm^{3+} stat	Energy gap (cm^{-1})
$^3F_4$	5400
$^3H_5$	2250
$^3H_4$	4150
$^3F_{2,3}$	550, 1750

Table 2.1. Energy gap to next lower level for states of Tm^{3+} [81]

As it was already mentioned, effective energy gap separating neighbouring levels and effective phonon frequency are the parameters that control the non-radiative relaxation rate. Table 2.1 lists the first five excited states for Tm^{3+} together with an effective energy gap separating each level from the one just below it. The important $^3H_5$, $^3H_4$ and $^3F_4$ states of Tm^{3+}, responsible for emission at 1.22 um, 1.46 um and 1.82 um, respectively, are seen to have energy gaps small enough to render their quantum efficiency very sensitive to host glass composition. Therefore, non radiative decay of several transitions is much higher in silica glasses (phonon energy 1100 cm^{-1}) [8], while in chalcogenides, with much lower phonon energy (360-425 cm^{-1}) [9], these transitions become possible. The energy gaps below the $^3H_5$, $^3F_3$, and $^3F_2$ levels are so small (Fig. 2.6) that multiphonon emission causes them to have extremely short lifetimes, and it is unlikely that a population inversion can be achieved for any of these states regardless of host.

CHAPTER 3
METHODOLOGY AND TECHNIQUES

This chapter reviews the experimental techniques used to fabricate and characterise the RE doped chalcogenide glasses and fibers based on As_2S_3. The first part of this chapter details the procedures for the purification and the fabrication of chalcogenide glasses and the technics used for impurity analysis as well as, the details regarding the fabrication of optical fiber using double crucible technique. The second part is focused on spectroscopic techniques used in the analysis of optical, thermal and structural properties of prepared glasses. A brief introduction to each spectroscopic technique is given as well.

3.1. FABRICATION OF ChGs AND FIBERS

3.1.1. PURIFICATION AND PRODUCTION OF ChGs

Production of high purity ChGs and investigation of their properties is an actively developed domain of optical materials science. Raw materials, used in various optical or semiconductor applications, are purified in a controlled manner. For high optical quality materials the purification process represents a key challenge. The most important properties of ChGs useful for fabrication of optical devices are very sensitive to impurities, such as transparency, mechanical strength and laser damage resistance. The impurities embedded into the glass network or the dissolved impurities are observed in transmission spectra of ChGs as selective absorption bands and the position of each is determined by the nature of the impurity. The Table 3.1 gives the list of impurities found in ChGs and the positions of impurity maxima of absorption bands in the transmission spectra of ChGs. Their dependence on glass composition is normally weak. The main limiting impurities in the transparency range of ChGs are oxygen, hydrogen, carbon and silicon connected with each other or with components of glass matrix.

Component leading to absorption	Position of the maximum of absorption band (μm)
OH^-	2.92
S-H	4.01; 3.65; 3.11; 2.05
Se-H	7.8; 4.57; 4.12; 3.53; 2.32
As-H	5.02
H_2O	6.31; 2.86; 2.79
CO_2	4.33; 4.31; 15.0
COS	4.95
CSe_2	7.8
CS_2	6.68; 4.65
As-O (different forms)	15.4; 12.7; 9.5; 10; 8.9; 7.9; 7.5
Se-O	10.67; 11.06
Si-O	9.1-9.6
Non identifies bands	4.65; 5.17; 5.56; 6.0

Table 3.1. Positions of maxima of absorption impurity bands in ChGs [92]

There are three main sources of impurities in ChGs:

1. The first source of impurities comes from the initial components used for synthesis of the glass. Commercially available As, Ge and chalcogens are prepared for semiconductor applications and the attention is paid only to electrically active impurities (metal impurities are only 0.1-0.01 ppm wt.), meanwhile the concentration of the oxygen, hydrogen, carbon and silica impurities are still higher (1-100 ppm wt.) in raw materials.
2. The second source of impurities is the container used for the preparation of glasses. Silica ampoules are the main containers that used for the synthesis of ChGs. Hydrogen and silicon dioxide impurities are always present in the walls of silica ampoules and therefore during the synthesis of glass-forming melt they enter into the chalcogenide melt. Moreover, at higher temperatures, a thin layer of reaction products is formed on the surface of the walls of silica ampoule, because of the chemical interaction of chalcogenides with silica glass, which can

separate from silica and enter the melt in the form of hetero-phase inclusions [93].

3. The third source of impurities is environmental and residual vacuum gasses during the synthesis. At higher temperatures Arsenic and chalcogens are inclined to oxidation. Normally, the equilibrium partial pressure of oxygen during dissociation of oxides (As or chalcogens) is about 10^{-5}-10^{-7} Torr at 750°C [94], so to prevent the oxidation of these elements the synthesis is normally realized in vacuum sealed ampoules.

A general scheme for production of ChGs for fiber optics comprises the preparation of initial high-purity substances and mixing them together. The initial charge of ChGs with the given composition is melted in evacuated sealed silica ampoule in order to conserve the attained purity of substances. During the melting of elements, the optimum temperature and time of melting are selected, which are dissimilar for different glass systems, as well as the melt mixing conditions (providing homogeneity of micro-composition) and minimization of the contamination effect of the reactor walls. The melt solidification is carried out at time-temperature modes preventing crystallization of micro-compositions. Being individual for each system, these conditions are additionally governed by the mass of mixture, as well as, glass and melt stability to crystallization. Generally, the ChGs crystallize very easily, so to transform the melt into the vitreous state they must be cooled very quickly (1-200 ˚C/sec).

The simplest and the most developed techniques for preparation of high-purity ChGs is the synthesis of the mixture of glass-forming compounds by melting of the mixture under the vacuum. The elimination of impurities by this method is the most popular for As_2S_3 glasses. This method is the most efficient for relatively high-purity substances. The extraction of impurities from initial elements can be derived trough the multiple cycles of sublimation of As and the distillation of S under high vacuum. The problem connected with the separate purification of As or S is that these elements are oxidized very easily in normal environment, even at room temperature. Hence, in order to avoid the recontamination of purified elements they are maintained either in ampoules sealed under vacuum or in glove boxes under the nitrogen. The

scheme of the fabrication of ChGs with this system is presented in Fig. 3.1. High-purity As and S were loaded into the reactor of synthesis by evaporation from intermediate ampoules in an evacuated system (10^{-5} Torr). The elements are slowly evaporated at 250 °C, while the reactor is maintained at 120 °C. The vapour pressure of sulphur is high therefore, it is necessary to contain the high temperature mixture in the reactor that will not explode during glass mixing. Before connecting to the pump the system is attached to a trap, filled with liquid nitrogen, where the extracted impurities condense.

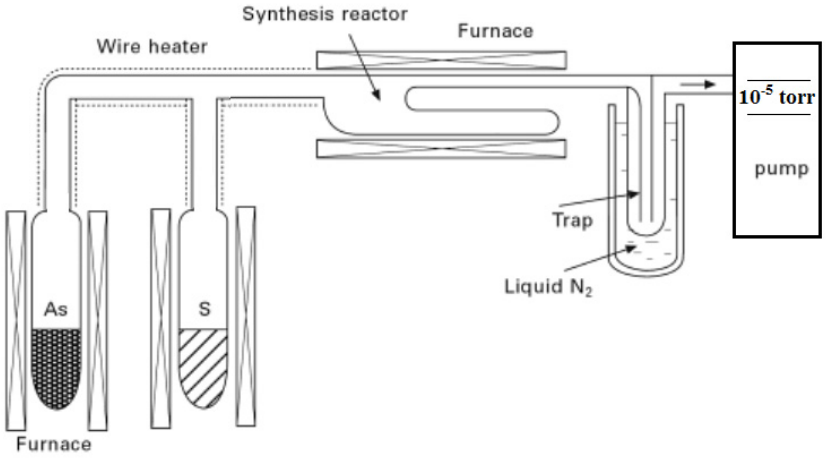

Fig. 3.1. Schematic set-up for purification of As_2S_3 glasses from initial high-purity elements [94].

After loading all elements in the reactor it is sealed under the vacuum and the melt homogenized in the rocking furnace at 750 °C for 8-12 hours. Solidification of the melt carries out at the rate of about 200 ˚C/sec, through a quenching in the water or with a flux of air.

Another well-developed method for the purification of high-purity ChGs includes the incorporation of oxygen or hydrogen getters (Al, Mg) in the system. These getters bind the oxygen (or hydrogen) containing impurities and promote the formation of low-volatile impurities which are not evaporated during the multiple distillation cycles of the glass and leads to the decrease of the content of impurities by 3-10 times, depending on the evaporation rate and the melt viscosity. This technique is discussed in more details in ref [94].

In addition to external sources of impurities, selective absorption bands in the transmission range of ChGs can be provoked by the presence of homo-bonds in the glasses as well. Metal-metal or chalcogen-chalcogen bonds are formed in the main structure of ChGs easily, due to relatively close formation energies of homo- and hetero-bonds. For example in As_2S_3 glasses the absorption bands at 5.1 and 5.5 μm can appear, which come from combined vibration S-S bonds [94].

3.1.2. PRODUCTION OF ChG FIBER

One of the best known methods of the fabrication of core/cladding optical fibers is the double crucible method. ChG fibers are obtained by drawing from the melt of preform. The schematic setup used for fiber drawing in presented in Fig. 3.2. The core and clad glass preforms (with required difference in refractive index) are placed in silica crucibles and heated up to the plastic state.

Normally, for ChGs the glass softening temperature range varies from 250-280 °C. Simultaneously, a pressure is applied over the preform to facilitate the extrusion of the melts. The melt is supplied from crucibles into a double drawing nozzle and at the output of the nozzle a conical part is formed, which is pulled forming a double-layered optical fiber. After that the fiber passes through the drawing nozzle for application of protective coating (acrylate coating is normally used) and through the furnace for polymer drying. Finally, the fiber is stowed on the reel. The drawing rate and the diameter of the fiber is determined by the rotation rate of the pulling mechanism and by the pressure applied over the preform melt. The core and cladding diameter ratio is determined by the ratio in diameter of circular and annular channels of the drawing nozzle and by the volumetric flow rate of the core and cladding melts.

Drawing from crucibles provides a high-quality surface and as a result the higher mechanical strength of optical fibers. This method was applied for drawing optical fibers from different chalcogenide glassy systems such as As-S, Ge-S, Ge-Se-Sb, As-Se-Te, As-S-Ga, As-S-I etc. Studies of time-stability of ChG fibers showed that from the point of view of their application, the optical and mechanical properties of such fibers with glassy cladding and protected surface are sufficiently stable in

time [95]. For example, As_2S_3 glass fiber has been stable in term of mechanical strength and optical losses for 3 years of storage at normal atmospheric condition.

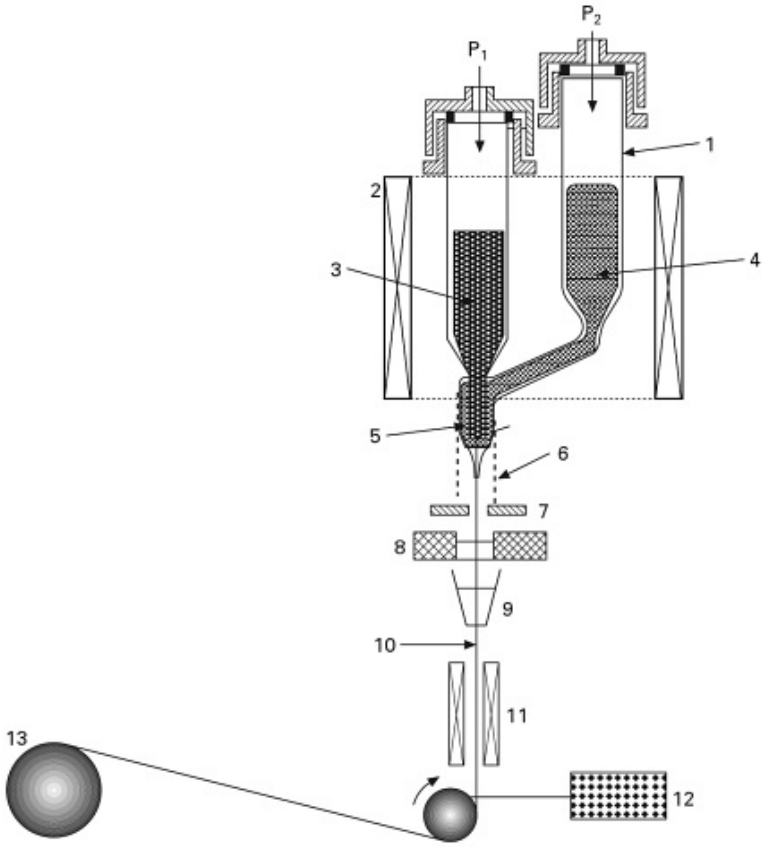

Fig. 3.2. Schematic set-up for fiber drawing by the double crucible method [94]: 1. double crucible; 2. thermostat; 3. core glass; 4. cladding glass; 5. drawing nozzle; 6. furnace; 7. pulling mechanism; 8. meter of the diameter; 9. drawing nozzle for application of polymer coating; 10. optical fiber; 11. furnace for polymer drying; 12. tension meter; 13. take-up reel.

3.2. CHARACTERISATION OF CHGS

3.2.1. THERMAL CHARACTERISATION

Thermal analysis is one of the most important set of measurement techniques in glass science. It gives information about the stability of glasses against devitrification, the kinetic of reaction and the characteristic temperatures. This chapter presents some basic principles of thermal analysis, such as differential

scanning calorimetry (DCS), thermo-mechanical analysis (TMA) and viscometric measurements.

Differential Scanning Calorimetry (DSC) is a thermal analysis technique that measures the flow of heat into the sample or out of it as a function of temperature. This technique is used for the detection of glass transition, crystallization and melting temperatures of a glass sample. The glass sample of 10-20 mg is inserted in an aluminium pan and placed on the pan supporter next to an identical, empty, reference pan. Both pans are heated with controlled temperature-time program (normally 10 °C/min) and the heat flow of the glass sample is compared with the reference. The heating is often accompanied by volatilization of chalcogenide components, thus the measurement is made in hermetically sealed container. Phase transitions are detected through the differential in heat flow supplied to the sample and reference pan. The first order phase transition of crystallization is an exothermic event, i.e. less flow is required from the heater to supply to the sample for maintaining the same temperature of sample and reference. So, the difference of heat flow between sample and reference will be maximal at the phase change (from amorphous to crystalline).

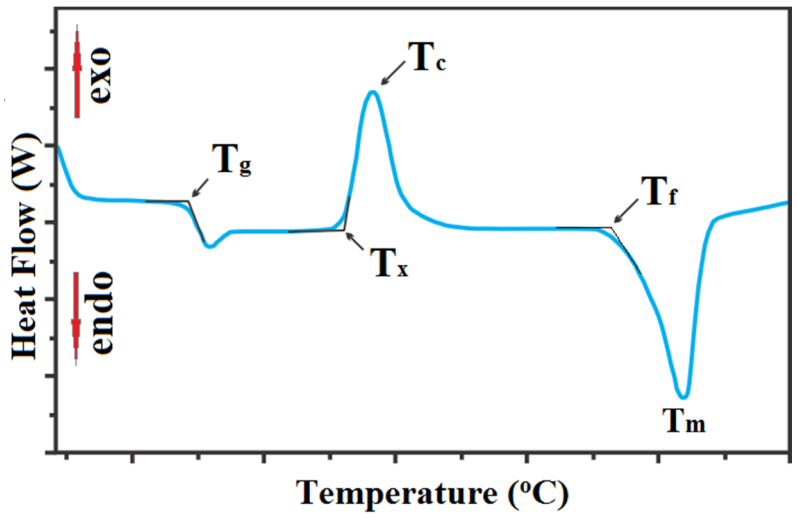

Fig. 3.3. Typical DSC curve for glasses

For glass samples the typical DSC curve looks like it is presented in the fig. 3.3. From this curve the glass transition temperature (T_g), the crystallization onset (T_x),

the crystallization peak (T_c), the beginning of melting temperature (T_f) and the melting peak (T_m) of the glass can be calculated. In the curve the glass transition is visible as slight endotherm and the T_g is defined as the intersection between two extrapolated tangents of the first endothermic peak of the curve. The T_x obtained from the intersection of the curves extrapolated from the inflection point of the exothermic peak. Similarly, the T_f can be found from the second endothermic peak. Being a first-order thermodynamic transition event, crystallization and melting are visible as much larger exo- and endotherms, respectively. They correspond to the first peak of maximum and the first peak of minimum on the curve.

For optical applications the T_x is more important value than T_c, as the crystalline phases begin to form at T_x and can lead to large scattering losses in optical systems.

Thermo-mechanical analysis (TMA) is another thermal analysis technique, which provides information on the mechanical response of a glass to an applied thermal load. This technique allows measuring the thermal expansion of a glass. The technique of measurement is as follows: A glass sample is placed on the measuring platform and placed in contact with silica pushrod. The sample is heated with temperature-time controlled heating program (5 °C/min) and the displacement of the pushrod is measured with a linear variable differential transformer. The representative TMA curve of a glass is presented in the Fig. 3.4.

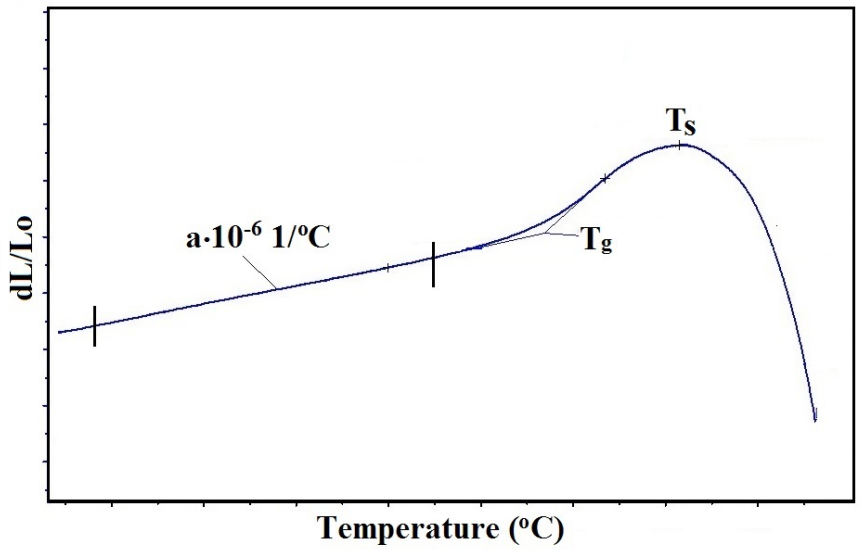

Fig. 3.4. Typical TMA curve for glasses

The average expansion coefficient for the given temperature interval can be calculated from this curve using the equation

$$\alpha = \frac{1}{L_0}\frac{dL}{dT} \qquad (3.1)$$

where α is the linear coefficient of thermal expansion, L_0 is the length of the sample at room temperature, dL is the change in length and the dT is the change in temperature. The expansion is an aggregative change in interatomic bonding distance [96] and there is no contribution from bonding change or conformation in materials, since the coefficient of thermal expansion is normally measured below the glass transition temperature. With the further increase of the temperature the dL/Lo increases more sharply up to certain value, which is followed by the drop of the curve (fig. 3.4). This allows measuring the glass transition temperature (T_g) and the softening temperature (T_s) of the glass sample.

Viscometry: The viscosity is one of the most significant parameters in the preparation and processing of glasses. A wide variety of viscometric techniques are used in academic and industrial glass science. The difference of measurement techniques depend on the measured viscosity region. For example the viscosity of ChGs changes over 10 orders of magnitude in less than 250 °C. An general overview of viscometric techniques is presented in ref. [94]. The viscoelastic behaviour of the glass is critical in hot-forming processes, such as fiber drawing, as it dictates the needed time temperature scale during the fiber fabrication. The best known technique for the measurement of the viscosity in glass softening region is the so called parallel plate viscometry. The principle of parallel-plate viscometry is the following [97-100]: a disk of glass, with specific parameters (6-12 mm diameter and 4-6 mm high) is sandwiched between two parallel silica plates inside a well-insulated furnace (Fig. 3.5). A compressive load is applied on the upper pedestal (load rod) and the sample is heated with time- temperature controlled program. The heating rate is normally maintained higher than 1 °C/min, in order to avoid the crystallization of the glasses during measurement which can lead to incorrect viscosity results. The rate of the thickness change of the sample is recorded as a function of time through a linearly variable differential transformer (LVDT).

Assuming that the viscous sample is incompressible and the flow is Newtonian, the glass viscosity may be calculated from the compression rate through the following equation [100]:

$$\eta = 2\pi \frac{Mgh^5}{30V(dh/dt)(2\pi h^5 + V)(1+\alpha T)} \qquad (3.2)$$

where η is the glass viscosity in Poise, M is the applied load, g is the gravity acceleration, h is the sample height at time t, V is the sample volume; dh/dt is the compression rate, α is the termal expansion of the glass.

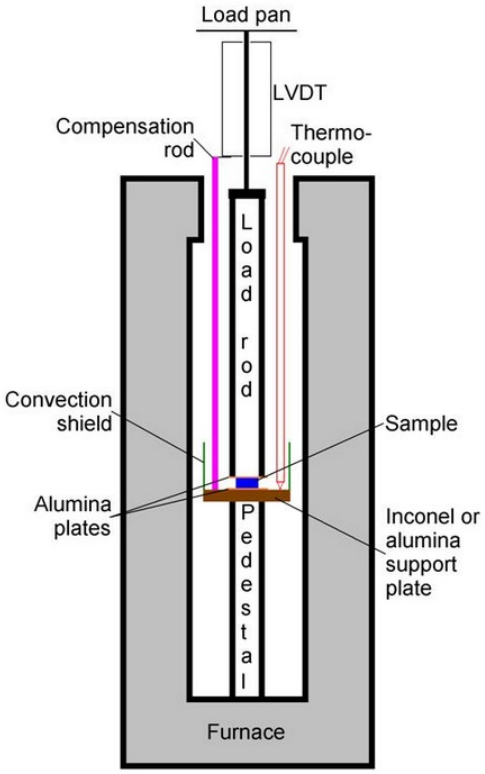

Fig. 3.5. Scheme of the parallel plate viscometer [101]

In order to soften a preform of ChG to form a fiber the temperature of bulk must be raised to 100 °C or more above its T_g, in order the glass to flow easily. Typical viscosity of the glass, at which the fiber is drawn, is $10^{6.5}$-$10^{5.5}$ Poises. However, the volatilization temperature of some ChGs is approximately 100°C higher than T_g, so special attention is needed in the variation of temperature range during fiber fabrication to prevent out-gassing of the glass, which could lead to the

changes in composition and the structure of the glass. Moreover, the viscosity-temperature curves of ChGs are much steeper than that of oxides and therefore the temperature range where the glass viscosity is about 10^6 Poises is much smaller, thus precise temperature control is critical for the drawing of ChG fibers.

3.2.2. OPTICAL CHARACTERISATION

As it was already mentioned ChGs are of great interest thanks to their exceptional optical features i.e. transparency in the IR region, high refractive index and low phonon energy leading to higher luminescence efficiency of RE ions. Therefore, the detailed knowledge of these properties will make possible to accurately predict the performance of ChGs in different optical applications. This chapter presents basic principles and techniques used for optical characterization of glasses, such as Fourier Transform Infrared spectrometry, refractive index and the luminescence measurement.

Fourier Transform Infrared spectrometry (FTIR) technique is the most preferred method of IR spectroscopy, which allows identifying unknown materials and determining the quality or consistency of a sample and the amount of components in a mixture. The term originates from the fact that a Fourier transform is required to convert the raw data into the actual spectrum. It is based on the absorption of IR radiation by the sample. IR radiation is passed through a sample, some of which is absorbed by the sample and some of it is transmitted. The resulting spectrum represents the molecular absorption and transmission, creating a structural image of the sample. The instrumental process is following: IR energy is emitted from air-cooled, pre-aligned tungsten halogen source, which passes through an aperture, which controls the amount of energy reaches to the sample (and to the detector). The beam enters the interferometer, where the spectral encoding takes place and the resulting interferogram signal exits as it is schematically presented in the Fig. 3.6. When the beam passes through the sample, specific frequencies of energy, which are uniquely characteristic of the sample, are absorbed. The beam finally passes to the detector for final measurement. The measured signal is digitized, sent to the computer where the

Fourier transformation takes place and the final IR spectrum is displayed. With this technique it is possible to measure the transmission spectra of glasses from 1.5 µm up to 25 µm.

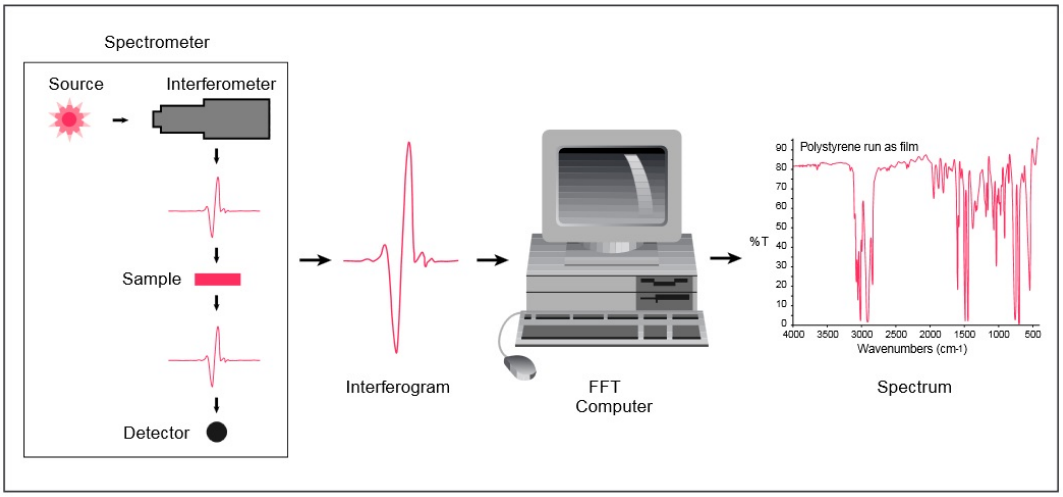

Fig. 3.6. Schematic representation of FTIR spectroscopy [102]

An IR spectrum represents a fingerprint of a sample with absorption peaks which correspond to the frequencies of vibrations between the bonds of the atoms making up the material. As it already discussed the presence of impurities has a major influence on optical properties of the glass, so this technique served as a good tool for the detection of undesirable structural units in the glass. In addition, the size of the peaks in the spectrum is a direct indication of the amount of material present in the glass.

Refractive index measurements: There are a number of ways to measure the refractive index of materials [103-104], but the most accurate method for unknown dielectric materials is through prism coupling. The principle of measurement is schematically shown in the Fig. 3.7. The sample is brought into contact with the base of a prism by means of a pneumatically-operated coupling head. A laser beam strikes the base of the prism and is normally totally reflected at the prism base onto a photo-detector. At certain critical value of the incident angle (θ_c), photons can tunnel into the bulk and enter into a guided optical propagation mode, causing a sharp drop in the intensity (Fig. 3.7 right) of light reaching the detector. Angular location of this mode determines the refractive index on the bulk. With commercially available Metricon 2010/M prism coupler (used for refractive index measurement in this thesis) the

refractive index can be measured for 5 different wavelengths (520 nm, 633 nm, 972 nm, 1308 nm and 1538 nm). The use of different coupling prisms (with different refractive index regions) allows measuring the dispersion across a wide wavelength range (from Vis to MIR).

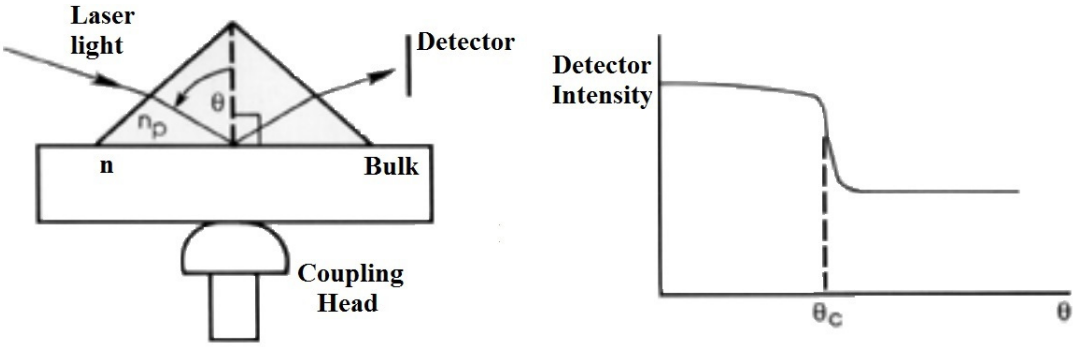

Fig. 3.7. Refractive index measurement principle for bulk glasses [105]

Luminescence measurements: The characteristics of luminescent devices follow from the optical properties of the ion–host combinations used: if one has the relevant information, it is possible to accurately predict the performance of the laser, amplifier or other luminescent source. One of the most powerful tools for obtaining the necessary information is optical spectroscopy, based on a specific excitation and emission processes of RE ions in glass matrix. One of the most appropriate devices for measuring the fluorescence of RE ions in materials is commercially available Horiba Jobin Yvon NanoLog 3-22-TRIAX spectrofluorometer, which was used for measuring the luminescence spectra of RE doped glasses in this thesis. The principle of measurement is following: the sample is excited with the 450 W continuous xenon lamp. Before the light beam reaches the sample, it passes through the excitation monochromator (Fig. 3.8), which transmits a wavelength specific to the excitation spectrum and blocking other wavelengths. The incident angle of the beam can be modified by rotating the stand of the sample. The light with the desired wavelength excites the sample and reflects from it. Following excitation, the RE ions relax and emit a light at an emission with characteristic wavelengths, normally longer than the excitation wavelength. The emitted light passes through the emission monochromator positioned at a right angle to the excitation light, which minimizes light scatter and

screens the emission light before it reaches the detector (Symphony II CCD detector operating in 1000-2200 nm.).

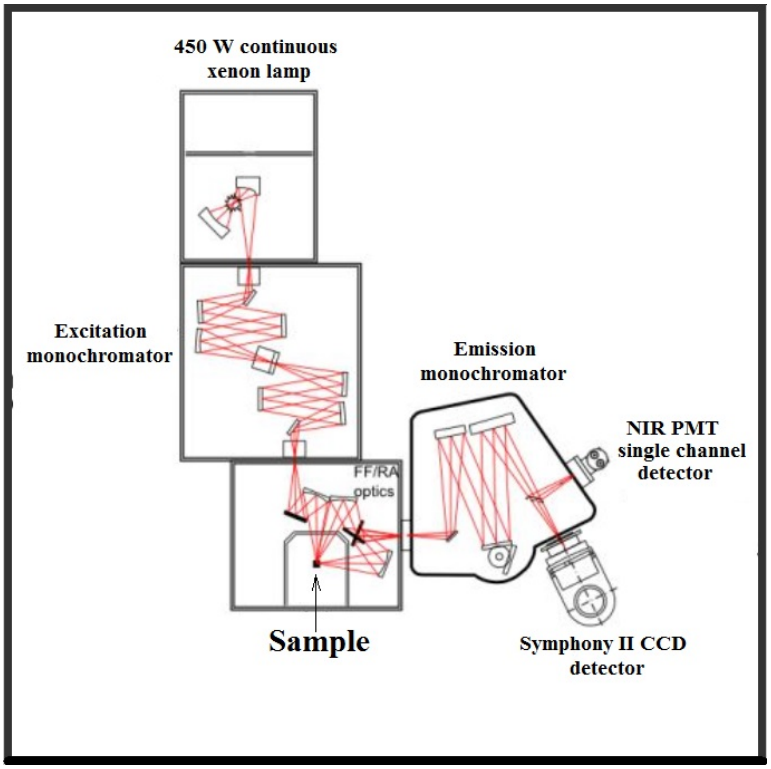

Fig. 3.8 Schematic presentation of Horiba Jobin Yvon NanoLog 3-22-TRIAX spectrofluorometer [106]

The detector measures the emitted light, displays the fluorescence value and produces the fluorescence signature of the RE ion. The intensity of fluorescence is proportional to the concentration level of the RE ions in the sample.

With the same device, the emission lifetime can be measured as well, using NIR PMT single channel detector (Fig. 3.8), operating in 1000-1700 nm wavelength region. In order to measure the emission lifetime the sample is excited with pulsed light at desired wavelength. Following this, emission was recorded at appropriate emission wavelength. Time per channel can vary from several hundred nanoseconds to milliseconds. Then, measurements were carried out until the peak channel reached 10000 counts. The decay curves are than fitted with a first-order exponential decay to extract the emission lifetimes. The decay in fluorescence can be measured over a wide time range: from picoseconds to milliseconds.

3.2.3. STRUCTURAL CHARACTERISATION

As it is already discussed in the chapter 2, ChGs lack a long range periodic ordering of the constituent atoms. Chemical ordering has a significant effect on the control of the atomic correlation in these glassy solids. The chemical bonding between atoms, which result in the short-range order, is responsible for most of the properties of glassy materials. Hence, by knowing the structure of a glass we can explain the mechanism responsible for particular properties and therefore control the phenomena occurring in these materials. The atomic structure and related properties in ChGs depend on preparation methods and history after preparation as well [107]. Various experimental techniques like X-ray diffraction (XRD), Electron diffraction, Molecular vibrational (IR and Raman) spectroscopy, Electron Spin Resonance (ESR), Nuclear Magnetic Resonance (NMR) and Extended X-ray Absorption Fine Structure (EXAFS) are used to probe the microscopic structures of ChG. Some of these techniques are discussed in this chapter.

X-ray diffraction (XRD) is one of the fundamental analyses used for the investigation of non-crystalline structure of glasses. This technique is based on observing the scattered intensity of an X-ray beam hitting a sample as a function of incident and scattered angle, polarization, and wavelength or energy. X-ray diffraction peaks are produced by constructive interference of a monochromatic x-ray beam scattered at specific angles from each set of lattice planes in a sample. The peak intensities are determined by the distribution of atoms within the lattice. Consequently, the x-ray diffraction pattern is the fingerprint of periodic atomic arrangements in a given material. A search of the ICDD standard database of x-ray diffraction patterns enables quick phase identification for a large variety of crystalline samples.

During the irradiation of sample with an X-ray beam, the detector revolves around the sample and measures the intensities of diffracted X-rays. The directions of constructive interference are found by Bragg formula: $2 \cdot d \cdot \sin\theta = n\lambda$, where d is the interlayer distance, θ the incident angle, n the refractive index and λ the wavelength. XRD spectra are obtained by varying the deviation angle (angle between incident

beam and direction of detector). Unlike crystalline solids, which have strong X-ray scattering, that is concentrated into a few sharp peaks, the scattering of glasses spread throughout reciprocal space and therefore typical XRD curve represents 2 or 3 large humps without any well distinguished peak.

Raman spectroscopy is a technique based on the inelastic scattering of monochromatic light, which allows observing vibrational, rotational, and other low-frequency modes in a system. During absorption and reemission of light by the sample, the frequency of photons undergoes some changes. Thus, these changes provide information about the vibration, rotation and other low frequency changes in the molecules. The effect of Raman scattering occurs when electromagnetic radiation faces the molecule and interacts with the bonds of the molecule. The photon with a specific wavelength excites the molecule either in the ground state or in an excited state. This leads the molecule to be in some virtual energy level for a short period of time before relaxation. When the molecule relaxes, it emits a photon and returns to a different rotational or vibrational state. The energy difference between the initial state and the new state leads to a frequency shift of the emitted photon. This phenomenon is schematically presented in Fig. 3.9. If the final state of vibration of the molecule is more energetic than the initial state, the emitted photon is shifted to a lower frequency (Stokes shift), so the total energy of the system remains constant. If the final vibrational state is less energetic than the initial state, the emitted photon is shifted to a higher frequency (anti-Stokes shift).

As a result, Raman spectroscopy provides an invaluable analytical tool for molecular finger printing as well as monitoring changes in molecular bond. Each molecule has a different set of vibrational energy levels, and the emitted photons have unique wavelength shifts. Vibrational spectroscopy involves collecting and examining these wavelength shifts and using them to identify structural units formed in a sample. Different peaks in the spectrum correspond to different Raman excitations. Moreover, the polarization of the Raman scattered light can provide information on the symmetry and the deformations of the molecule.

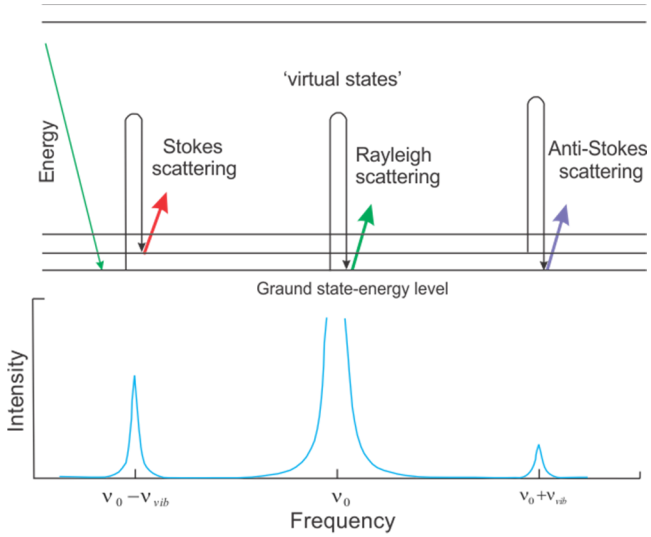

Fig. 3.9. Energy level diagram showing the states involved in the Raman signal

Extended X-ray Absorption Fine Structure (EXAFS) spectroscopy is a technique of analysis of X-ray absorption spectrometry using synchrotron radiation. It provides structural information about a sample by means of the analysis of X-ray absorption spectrum. It allows determining the chemical environment of a selected atom in terms of the number and type of its neighbours, inter-atomic distances and structural disorders. EXAFS is a powerful technique for the analysis of glasses, because it does not require a long-range order.

Theoretical description: The X-ray absorption coefficient (μ) for an atom is directly proportional to the probability of absorption of one photon and is a monotone decreasing function of energy [108]. The edge energy is characteristic of each atom. The incident x-ray beam is able to extract a core electron from atom if the energy of photon is equal to or greater than the edge energy. The ejected electron is called photoelectron and it has the characteristics of both a particle and a wave. Its kinetic energy is given by: $E = E_x - E_0$, where E_x is the energy of the X-ray photon and the E_0 is the energy of edge. If the absorbing atom is isolated in space, the photoelectrons propagate as unperturbed isotropic wave, but in most cases, there are many other atoms around the absorber, which become scattering centers for the photoelectron wave. The final state of the photoelectron can be described by the sum of the original and scattered waves [109]. This leads to an interference phenomenon that modifies

the interaction probability between core electrons and incident photons. A typical EXAFS spectrum is shown in Figure 3.10. The region near the maximum absorption is called XANES and it characterises the electronic state of the atom of interest. After the threshold of absorption, oscillations are observed, corresponding to the region of the EXAFS. These oscillations provide information on the distance between the excited atom and its nearest neighbours in the sample, as well as the nature of those neighbours.

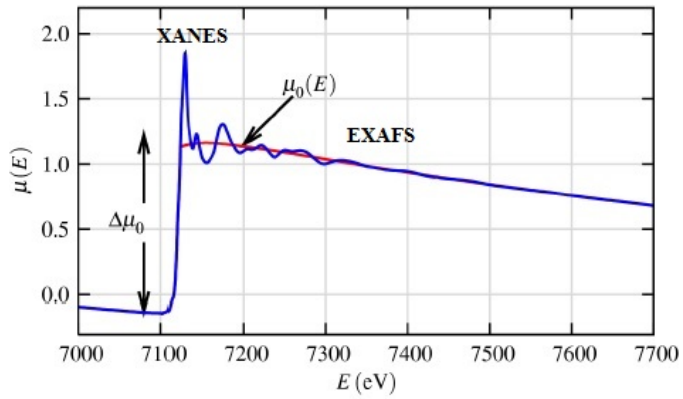

Fig. 3.10. Typical EXAFS spectrum [109]

For the EXAFS, only the oscillations well above the absorption edge are considered, and define the EXAFS fine-structure function χ(E), as [109]

$$\chi(E) = \frac{\mu(E) - \mu_0(E)}{\Delta\mu_0(E)} \tag{3.3}$$

where $\mu(E)$ is the experimental absorption coefficient and $\mu_0(E)$ is the intrinsic atomic absorption coefficient, $\Delta\mu_0(E)$ is the jump in the measured absorption $\mu(E)$ at energy threshold E_0. Such definition means that $\chi(k)$ contains only the oscillatory part of the absorption coefficient.

To connect χ to structural parameters of the system, it is necessary to convert the energy E to the wave number (k) of photoelectron, which is defined as:

$$k = \sqrt{\frac{2m(E - E_0)}{\hbar^2}} \tag{3.4}$$

where m is the electron mass. This transformation is called EXAFS equation [109]:

$$\chi(k) = \sum_j \frac{N_j f_j(k) e^{-2k^2\sigma_j^2}}{kR_j^2} \sin[2kR_j + \delta_j(k)] \qquad (3.5)$$

where N is the number of neighbouring atoms, R is the distance to the neighbouring atom, σ^2 is the Debye-Waller factor (disorder in the neighbour distance). $f(k)$ and $\delta(k)$ are scattering properties of the neighbouring atoms, i.e. a scattering amplitude function and a phase function, respectively. They depend on the Z of the neighbouring atom. The different frequencies apparent in the oscillations in $\chi(k)$ correspond to different near-neighbour coordination shells.

EXAFS measurements: For x-ray source it is typically used a synchrotron, which provides a full range of x-ray wavelengths, and a monochromator made from silicon to select a particular energy. There are two modes of measurements of EXAFS spectra: transmission and fluorescence.

The most common EXAFS beam-line works in transmission. It collects data measuring the decrease of the beam intensity as it passes through the sample while scanning energy using a crystal monochromator. This method works well for concentrated samples, i.e. samples with higher concentration of the element of interest (> 10%). For thick samples or lower concentrations, monitoring the x-ray fluorescence is the preferred technique. In a fluorescence XAFS measurement, the x-rays emitted from the sample include the fluorescence line of interest, fluorescence lines from other elements in the sample, and both elastically and inelastically scattered x-rays [109].

Experimental spectra are usually recorded by scanning energy from about 200 eV below the explored edge to 1000 eV above it. Energy steps are varied between 0.05–2.0 eV, depending on the energy interval and the experimental setup. A spectrum recording takes from 15 minutes up to three hours.

Data reduction: The first step in data analysis is the redaction of raw data. The software used for the signal extraction, by background removing, is called Athena (FEFFIT software package). This delicate operation can be divided into following steps:

1. Conversion of measured intensities to $\mu(E)$.
2. Subtraction of a smooth pre-edge functions from $\mu(E)$ to get rid of any instrumental background and absorption from other edges.
3. Identification of the threshold energy E_0 (the energy of the maximum derivative of $\mu(E)$).
4. Normalisation of $\mu(E)$ to 1.
5. Removing of a smooth post-edge background function to approximate $\mu_0(E)$.
6. Isolation of the XAFS $\chi(k)$.
7. Weighting by k the XAFS $\chi(k)$ and Fourier transformation into R-space (see figures 5.4-5.6).

Data modeling: After obtaining of EXAFS spectra in R-space, the data are exported into a program called Artemis (FEFFIT software package), where the experimental signal is simulated. Experimental functions are extracted from proper reference samples whose structure is already known. These can be used due to the phase and amplitude transferability principle, which claims that phases and amplitudes are insensitive enough to chemical environment in order to be extracted from a well-known sample and transferred to an unknown sample containing the same absorber-scatter pair at a similar distance [108]. Once these theoretical scattering factors are calculated, they are used in the EXAFS equation (Eq. (3.5)) to refine structural parameters from the data, i.e. the calculated functions $f(k)$ and $\delta(k)$ are used in the EXAFS equation to predict and modify the structural parameters N, R and σ^2. We allow E_0 to change until we get the best-fit to the $\chi(k)$.

The accuracy of the structural parameters estimated with EXAFS spectroscopy heavily depends on the data and the quality of the analysis. Errors are generally about 0.01 to 0.02 Å interatomic distances, and 5-15% for coordination numbers.

CHAPTER 4
Tm^{3+} DOPED Ga-As-S CHALCOGENIDE GLASSES AND FIBERS

As it is already mentioned, among all chalcogenide systems, As_2S_3 glasses were the most extensively studied because of their high thermal stability, broad transparency window and easy fiber fabrication. However, the utilisation of these glasses in the active applications is limited, because of the low solubility of RE ions in this glass matrix. So, the primary focus of this work is to improve the solubility of Tm^{3+} ions in As_2S_3 glass.

The present chapter is based on an article manuscript that discusses the role of Ga in the solubility of Tm^{3+} ions in the As_2S_3 matrix. For this research the network modifier Ga was co-doped with Tm in As_2S_3 glass, in an effort to modify the local environment of the Tm^{3+} ions. The effects of co-doping are examined by studying the spectroscopic properties of the Tm^{3+} ion in the different compositions of glass host environments using standard spectroscopic techniques. The main aim of this work was the achievement of the highest possible intensity of luminescence of Tm in As-S-Ga system by varying the concentrations of Ga and Tm in the glass. Optical and thermal properties of this system were studied, as well, in order to achieve the optimal composition of glass preform for fiber drawing. Luminescence properties of Tm^{3+} doped Ga-As-S fiber were also explored.

RÉSUMÉ DE L'ARTICLE INSÉRÉ

Verres et fibres Ga-As-S dopés au Tm^{3+}

Ce travail est consacré à l'étude d'une nouvelle famille de verres chalcogénures comme une matrice hôte pour le dopage des ions terres rares (TR). L'effet de Ga sur la solubilité des ions TR dans la matrice d'As_2S_3 a été exploré. Les propriétés d'émission de Tm^{3+} dans le verre Ga-As-S ont été étudiées par des mesures de photoluminescence. Trois bandes d'émission à 1.2 μm ($^1H_5 \rightarrow {}^3H_6$), 1.4 μm ($^3H_4 \rightarrow {}^3F_4$) et 1.8 μm ($^3F_4 \rightarrow {}^3H_6$) ont été obtenues sous l'excitation d'une lampe à 698 nm et 800 nm. Les propriétés optiques et thermiques des verres As-S-Ga dopés au Tm ont été analysées pour les différentes concentrations de Ga ainsi que de Tm, afin d'obtenir les paramètres optimaux pour la préforme du verre convenable pour la production d'une fibre optique. Une fibre Ga-As-S dopée au Tm^{3+} a également été fabriqué et les trois bandes d'émission obtenues dans le verre ont été aussi bien observées dans la fibre.

Optical Materials 47 (2015) pp. 518-523

Article history:
Received 13 April 2015
Received in revised form 2 June 2015
Accepted 16 June 2015
Available online 19 June 2015

Tm^{3+} doped Ga-As-S chalcogenide glasses and fibers

A. Galstyan, S.H. Messaddeq, V. Fortin, I. Skripachev, R. Vallée, T. Galstian, Y. Messaddeq*

The Center for Optics, Photonics and Lasers (COPL), Laval University, 2375, rue de la Terrasse Quebec, QC, G1V 0A6, Canada

ani.galstyan.1@ulaval.ca

ABSTRACT

Tm^{3+} doped Ga-As-S chalcogenide glass samples were produced using As_2S_3 pure glass as starting materials. Their photoluminescence properties were characterized and strong emission bands were observed at 1.2 μm ($^1H_5 \rightarrow {}^3H_6$), 1.4 μm ($^3H_4 \rightarrow {}^3F_4$) and 1.8 μm ($^3F_4 \rightarrow {}^3H_6$) under excitation wavelengths of 698 nm and 800 nm. The thulium and gallium concentrations were optimized to achieve the highest photoluminescence efficiency. From the optimal composition, a Tm^{3+} doped Ga-As-S fiber was drawn and its optical properties were studied.

Keywords: Ga-As-S glasses, Tm^{3+} doped chalcogenide glasses, rare-earth doped fibers.

4.1. INTRODUCTION

Chalcogenide glasses show great potential for laser applications in the IR region because of their low phonon energy (i.e. 400–450 cm^{-1} for sulphides), and consequently low non-radiative decay rates [110], compared to other glass systems. Since these glasses also possess a high refractive index (n > 2), it results in a strong local electric field around the ions which induces high emission and absorption cross-sections [111]. A variety of chalcogenide systems were considered as host glasses for RE ions, namely Ge-S [112], Ge-Ga(As)-S [41,113-116], Ge-Sb-S [117], Ga-Ge-Sb-S [42,91,118,119] and Ga-La-S [33,120-122]. However, the majority of doped chalcogenide glasses were prone to crystallization, making the fiber drawing process very difficult. As_2S_3 glasses were the most extensively studied because they present a high thermal stability, a broad transparency window up to 7 μm and they can be easily drawn into fibers [60]. There have been several demonstrations of As_2S_3 glasses doped with RE ions such as Nd^{3+}, Ho^{3+}, Er^{3+} and Dy^{3+}. However, the solubility of RE ions in the glass matrix was limited and induced crystallization [36]. According to previous reports, the solubility of RE ions in chalcogenide glasses can be improved dramatically by adding gallium (Ga) in the host matrix [2,20,21]. Such solubility increase has been reported to be associated with the formation of GaS_4 tetrahedra in the vitreous network [22-24]. The increased solubility of REs in presence of gallium would actually come from the formation of chemical bonds between Ga and RE ions which compensate for the free S_2-ions negative charge. Kolomiets et al. first reported the incorporation of Ga in As_2S_3 glasses in 1960 [127]. It was shown that the glass formation region in the Ga-As-S system was very small: a maximum Ga concentration of 3.5 at% could be incorporated.

In this paper, we studied the Ga-As-S ternary system as a new host matrix for Tm^{3+} ions. Tm^{3+} doped chalcogenide glasses are very attractive laser gain media that can not only emit light at 1.2 μm and 1.8 μm, but also near 1.45 μm, 2.3 μm and 3.4 μm (unlike silicate glasses) using readily available and cheap laser diodes pumps in the near infrared. We optimized the concentration ratio of Ga and Tm^{3+} in Ga-As-S glasses to achieve optimal physical and optical properties, i.e. obtain a transparent and homogeneous glass with high luminescence efficiency. A distillation process of

the starting compounds under high vacuum was first performed to produce a high purity glass based on As_2S_3. Afterwards, the Ga and Tm^{3+} were added to produce the adequate glass composition in the Ga-As-S system

4.2. EXPERIMENT

4.2.1. BULK GLASS PREPARATION AND CHARACTERIZATION

The Ga-As-S glasses were prepared by melting Ga_2S_3 crystalline compound (99.999%) and pre-purified As_2S_3 glass based on a new purification procedure developed at the COPL (pending Patent). Glasses were synthesized in silica ampoules sealed under high vacuum (10^{-5} Torr). The ampoule was placed in a rocking furnace and heated at a rate of 1°C/ min up to 900°C. After being rocked for 12 hours, the homogenized glass was successively quenched in water at room temperature for a few seconds and annealed at 160°C for 6 hours to remove the thermal stress. The glass rods were then cut into disks and polished with an abrasive silicon carbide disc to obtain flat and transparent bulk glasses.

The emission spectra of Tm^{3+} doped Ga-As-S glasses were collected with a Horiba Jobin Yvon NanoLog 3-22-TRIAX spectrofluorometer. The samples were excited with a 450 W continuous xenon lamp connected to a computer controlled monochromator. Excitation wavelengths of 698 nm and 800 nm were selected, i.e. near the absorption peaks of the doped glasses. The luminescence spectra were measured with a Symphony II CCD detector operating in the infrared region from 1000 to 2200 nm. Fluorescence lifetime measurements were also performed with a NIR PMT single channel detector with 1000 - 1700 nm wavelength range. The fluorescence decay curves were fitted with a first-order exponential decay to extract the emission lifetimes.

The X-ray diffraction (XRD) spectra of the powdered samples were obtained with a Siemens D5000 X-ray diffractometer. The X-ray source was made of a Cu anode and emitted at a wavelength of 1.54 Å. XRD data were collected in reflection mode with Theta-Theta configuration (2Theta step = 0.02°, time step = 1.2 s) using a

NaI scintillation counter detector. It was processed with the JADE 2.1 software based on the JCPDS database of ICDD (International Centre for Diffraction Data).

The IR transmission spectra from 1 to 20 μm were measured with a PerkinElmer Frontier FT-IR/FIR Spectrometer using the factory-supplied MIR source and MIR TGS detector combination.

The glass transition temperature (T_g) was measured with a Netzsch 404 F3 Pegasus differential scanning calorimeter (DSC). A 20 mg glass sample was placed in the aluminum crucible and heated up to 400 °C (10°C/min ramp) and the heat flow was compared with that of an empty crucible.

The density was measured with an Electronic Densitometer MD-300S based on Archimedes' principle.

The refractive index was measured with a Metricon 2010/M prism coupler for 1308 nm and 1538 nm wavelengths. A prism with index range 2.35 - 3.10 was used for these measurements.

4.2.2. FIBER PREPARATION AND CHARACTERIZATION

The chalcogenide glass fiber was drawn using the double crucible method, with Tm^{3+} doped Ga-As-S glass as the core and As_2S_3 glass as the cladding. The core and cladding diameters are 11 μm and 210 μm, respectively (Fig. 4.1). The numerical aperture (core/cladding) is about 0.52 for wavelengths in the 1.3 - 1.5 μm range. The cladding can also serve as a multimode guide due to its large refractive index compared to the acrylate polymer jacket.

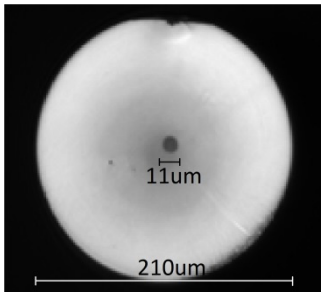

Fig.4.1. Image of the Tm^{3+} doped Ga-As-S glass fiber.

We measured the amplified spontaneous emission (ASE) spectrum generated by this fiber. The setup used for this experiment is shown in Fig. 4.2. A 789 nm

multimode laser pump providing output power up to about 1 W is delivered in a 250 µm coreless silica fiber. This silica fiber is then butt-coupled to a 16 cm segment of our Tm^{3+} doped Ga-As-S fiber using precision alignment mounts. The residual pump power is then filtered out from the output signal with an homemade dielectric stack long pass filter (T ≈ 0.01 % at λ= 789 nm, T > 75 % at λ > 1200 nm) and the ASE signal is collected by a multimode silica fiber having a 220 µm diameter core (242 µm diameter cladding) and a numerical aperture of 0.22. The output spectrum is measured with two commercial fiber-coupled optical spectrum analysers OSA (Yokogawa AQ6370D and Yokogawa 6375) covering the short wavelengths from 0.6 to 1.7 µm and the longer wavelengths from 1.2 to 2.4 µm respectively.

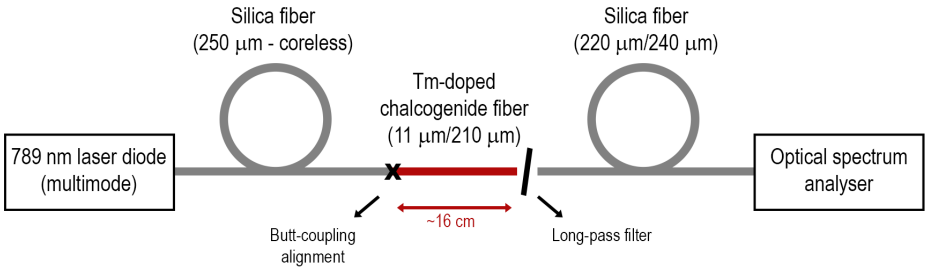

Fig. 4.2. Experimental setup used to measure the ASE spectrum of the Tm^{3+} doped Ga-As-S glass fiber.

The ASE spectrum was measured for an incident pump power of 430 mW. Considering a Fresnel reflection of about 17% and the slight mismatch between the Ga-As-S fiber and the coreless silica fiber diameters, the estimated launched pump power is at least 250 mW (in the cladding of the fiber).

4.3. RESULTS AND DISCUSSION

4.3.1. EFFECT OF Ga CONCENTRATION ON Tm^{3+} DOPED Ga-As-S GLASSES

Systematic studies were performed to quantify the effect of Ga in the optical and thermal properties of Tm^{3+} doped Ga-As-S glasses. For this section, the concentration of Tm^{3+} was fixed to 0.2 at% and the Ga concentration was varied from

0 to 4 at% based on a previous study by Kolomiets et al. [127]. The infrared transmission spectra are shown in Fig. 4.3. A red shift in the UV-visible region and a decrease in the maximum transmission are observed with increasing concentrations of Ga in the stoichiometric matrix. The difference of unoccupied energy levels between the molecular orbitals of As-S and Ga-S is not substantial; therefore the red shift could be related to structural defects (e.g. Ga-Ga homo-bonds). The decrease of the maximum transmission could be explained by inhomogeneities in the glass. For comparison, we have included the transmission spectra of the pure As_2S_3 sample which shows some residual oxygen but is free of impurities such as S-H and H_2O. The addition of Ga and Tm^{3+} during the preparation process introduces other impurities as can be observed in the transmission spectra. The absorption bands in the Ga-As-S glass spectra are attributed to traces of oxygen and hydrogen (i.e. S-H, H_2O and As-O bonds) [92].

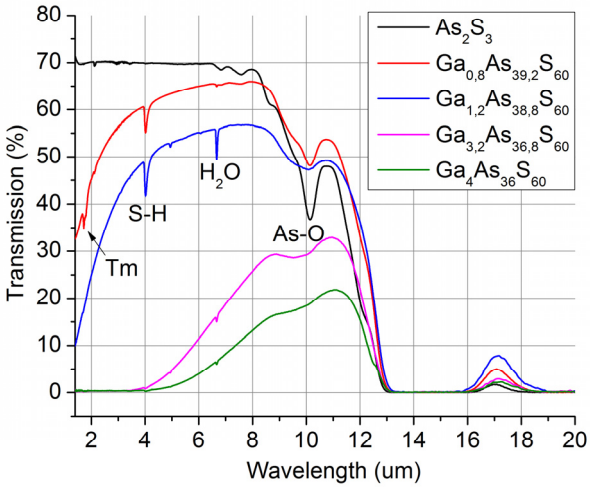

Fig. 4.3. IR transmission spectra of 0.2% Tm^{3+} doped Ga-As-S glasses (thickness is 2.5 mm). The spectra of an undoped As_2S_3 glass sample are shown for comparison.

Table 4.1 shows the glass transition temperature (T_g), the density and the refractive index of Ga-As-S glasses doped with 0.2 % Tm^{3+}. The glass transition temperature typically depends on the bonding strength and on the coordination number (N) per atom [128]. Since the bonding strength of Ga-S is higher compared to As-S and since the coordination number is 4 for Ga while it is only 3 for As, an

increase of T_g is expected when replacing As_2S_3 by Ga_2S_3. However, the opposite behaviour occurs experimentally: the addition of Ga in the As_2S_3 matrix lowers T_g by approximately 10 °C. The lower T_g could be explained by the formation of metal-metal bonds which are weaker than hetero-bonds (e.g. bonding strength is 265 cm^{-1} for S_3Ga-GaS_3 and 335 cm^{-1} for Ga-S [129]). Note that T_g stays constant with further increase of Ga because of its lower solubility in the As_2S_3 glass network. The refractive index of the glass increases by 0.055 with the incorporation of Ga but further increase of the Ga content does not lead to significant changes.

The variation of the density is related to the change in the atomic weight and the atomic volume of the elements in the system. Since the atomic weight of Ga is slightly lower than that of As, the replacement of As by Ga caused a slight decrease in density: from 3.43 to 3.20g/cm^3.

	T_g (˚C) (±2˚C)	**Refractive index** (±0.003)		**Density (g/cm^3)** (±0.05)
		1308nm	**1538nm**	
As_2S_3	200	2.400	2.390	3.43
$Ga_{0.8}As_{39.2}S_{60}$	193	2.455	2.445	3.22
$Ga_{1.2}As_{38.8}S_{60}$	188	2.452	2.441	3.20
$Ga_{1.6}As_{38.4}S_{60}$	192	2.451	2.439	3.25
$Ga_{2.4}As_{37.6}S_{60}$	190	2.447	2.437	3.23
$Ga_{3.2}As_{36.8}S_{60}$	190	2.446	2.435	3.19
$Ga_4As_{36}S_{60}$	190	2.447	2.436	3.22

Table 4.1: Characteristics of 0.2 % Tm3+ doped Ga-As-S glasses

The XRD patterns recorded for 0.2 % Tm^{3+} doped Ga-As-S glasses are presented in Fig. 4.4. The patterns associated to samples with Ga = 0.8 and Ga = 1.2 at.% indicate an amorphous character while samples with concentrations of Ga ≥ 1.6 at.% show diffraction peaks superimposed to the broad amorphous profile. The intensity of these diffraction peaks increases with further increase of Ga content,

revealing the formation of a crystalline phase that can be assigned to Ga_2S_3 (JCPDS card No. 14-0401).

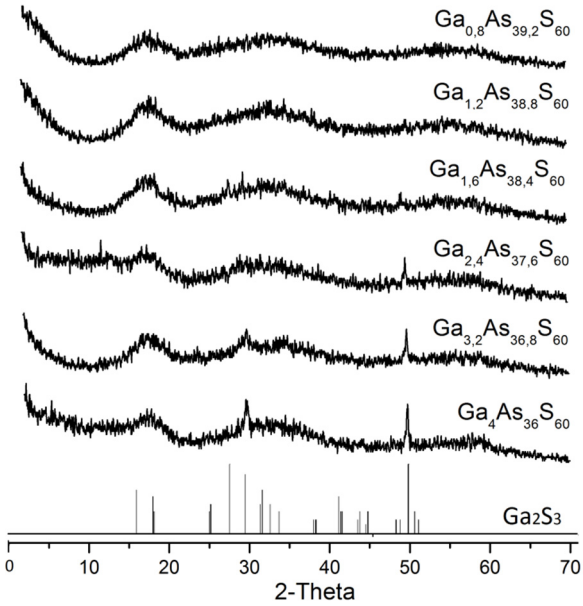

Fig. 4.4. X-ray diffraction of 0.2 % Tm^{3+} doped Ga-As-S glasses.

The emission spectra of 0.2 % Tm^{3+} Ga-As-S glasses were measured for Ga concentrations varying from 0.8 to 4 at%, excited at either 698 or 800 nm (Fig. 4.5). The excitation wavelengths 698 nm and 800 nm are near the absorption peaks of Tm in glasses. Lower absorption wavelengths were not used because the optical band-gap of these glasses is in the region of 600 nm. Thus, pumping at lower wavelengths would induce photo-darkening and reduce the luminescent intensity with exposure time.

No emission was observed for the Tm^{3+} doped As_2S_3 glass sample. However, the incorporation of Ga in the As_2S_3 vitreous network allowed the solubility of Tm^{3+} ions and its corresponding emission bands were observed. Three strong emission bands centered at 1.22 μm, 1.46 μm and 1.82 μm are shown in these spectra, corresponding to the optical transitions $^3H_5 \rightarrow {}^3H_6$, $^3H_4 \rightarrow {}^3F_4$ and $^3F_4 \rightarrow {}^3H_6$ respectively (Fig. 4.5c). With increasing Ga concentrations from 0.8 to 3.2 %, all emission bands are enhanced and their central wavelength is unaltered. However, the emission intensity decreases at Ga concentrations larger than 3.2 %, where the density of Ga_2S_3 crystallites is higher. The fluorescence spectra were measured for two different

excitation wavelengths (698 nm and 800 nm). The intensity of both 1.22 µm and 1.82 µm emission bands is significantly higher when using an excitation wavelength of 698 nm (as compared to 800 nm) whereas the 1.46 µm band has a similar intensity for both excitation wavelengths. This is related to the fact that at 698 nm, the levels $^3H_5$ and $^3F_4$ were populated more efficiently due to the cross-relaxation process $^3F_3$, $^3H_6 \rightarrow {}^3F_4$, $^3H_5$ [8,29].

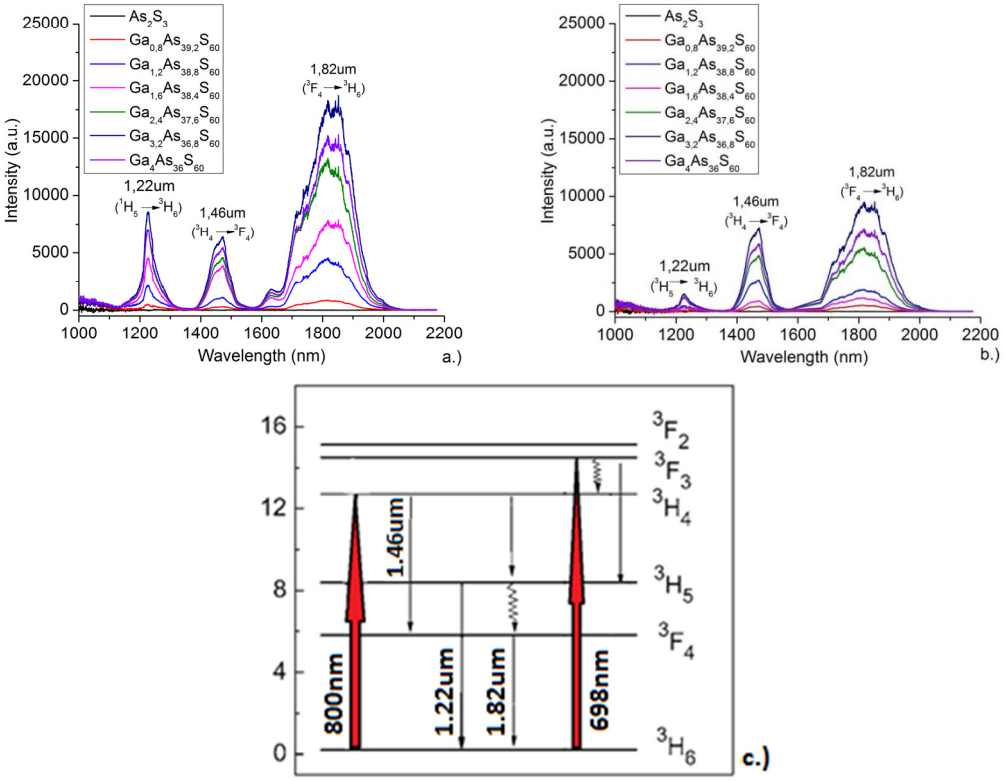

Fig. 4.5. Emission spectra of 0.2 % Tm^{3+} doped Ga-As-S glasses (a. excitation at 698 nm, b. excitation at 800 nm, c. energy diagram of Tm^{3+}).

Figure 4.6 shows the fluorescence effective lifetime of 0.2 % Tm^{3+} doped glasses as a function of the Ga content for an excitation wavelength of 800 nm. The fluorescence lifetime of the 1.22 µm emission band rises gradually with increasing Ga concentrations up to $6.84*10^{-4}$ s. As for the 1.46 µm emission band, its fluorescence lifetime is nearly constant around $1.25*10^{-4}$ s.

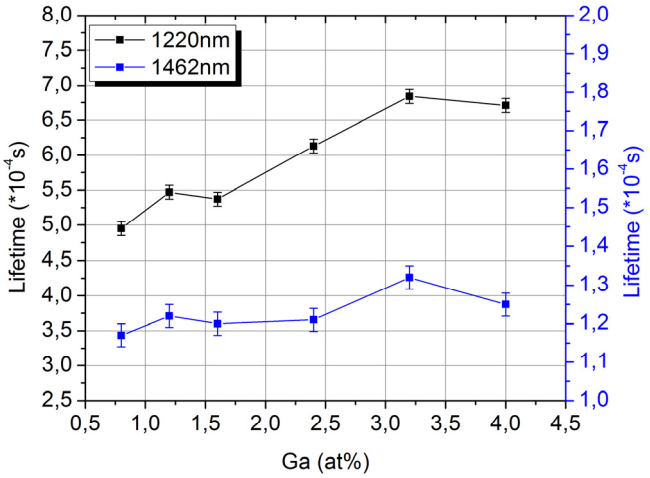

Fig. 4.6. Fluorescence effective lifetime vs Ga concentration in 0.2 % Tm^{3+} doped Ga-As-S glasses (excitation at 800 nm).

The increase of Ga in the As_2S_3 matrix enhances the solubility of Tm^{3+} ions allowing a stronger emission and longer lifetimes for glass samples up to 3.2at% of Ga. Above this value, the formation of a new Ga_2S_3 crystalline phase takes place (fig. 4.4), which contributes to the diminution of luminescence intensities and lifetimes, possibly due to a change in the degree of symmetry of Tm^{3+} ions local environment. In summary, the intensity of luminescence reaches its highest value at a Ga concentration of 3.2% (Fig. 4.5), but the crystalline phase begins to form for samples containing ≥2.4% of Ga (Fig. 4.4). In addition, the transmission of the glass falls as the Ga concentration is increased beyond 0.8 % (Fig. 4.3). We therefore selected the $Ga_{0.8}As_{39.2}S_{60}$ glass as the optimal composition for investigating the effect of Tm^{+3} dopant concentration on luminescence.

4.3.2. EFFECT OF Tm^{3+} DOPANT CONCENTRATION IN $Ga_{0.8}As_{39.2}S_{60}$ GLASSES

This section presents the characteristics of $Ga_{0.8}As_{39.2}S_{60}$ glasses with different Tm^{3+} concentrations. The luminescence spectra are presented in Fig. 4.7 for both excitation wavelengths (698 nm and 800 nm). The emission intensity initially increases and reaches its maximum for samples with 2 % Tm^{3+}. The intensity substantially decreases for higher Tm^{3+} concentrations.

The effective lifetime of Tm^{3+} doped $Ga_{0.8}As_{39.2}S_{60}$ glass is presented in Fig. 4.8. As expected, the lifetime is also maximal at 2 % Tm^{3+} and is reduced above this concentration. These values are comparable to the lifetimes reported with other chalcogenide glass systems such as Ge-Ga(As)-S [4,30] and Ga-La-S [33].

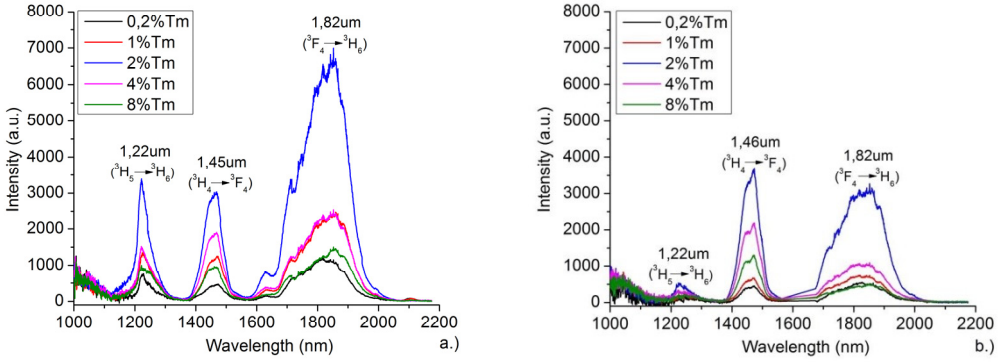

Fig.4.7. Emission spectra of Tm^{3+} doped $Ga_{0.8}As_{39.2}S_{60}$ glasses (a. excitation at 698nm, b. excitation at 800nm).

Samples having 2% Tm^{3+} are completely amorphous (no apparent crystallization). As the Tm^{3+} concentration is increased to 4%, a partial crystallisation is observed which can be assigned to the Tm_2S_3 crystalline phase (JCPDS card No. 44-1157 and 71-0089).

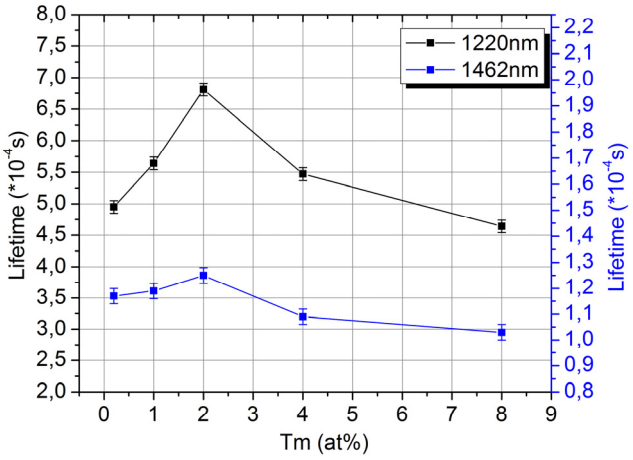

Fig. 4.8. Fluorescence effective lifetime vs Tm^{3+} concentration in $Ga_{0.8}As_{39.2}S_{60}$ glasses (excitation at 800 nm).

With further increase of the Tm^{3+} concentration (> 4 %), the peaks associated with the Ga_2S_3 crystalline phase start to appear along those of Tm_2S_3. These results provide evidence in favour of an inhomogenous distribution or clustering.

The lifetime of an excited state is governed by a combination of probabilities for all possible radiative and non-radiative transitions, i.e. radiative lifetime, non-radiative relaxation due to multiphonon relaxation and energy transfers to neighbouring ions. The increase of emission lifetimes with increasing Tm concentration up to 2at% is related to the multi-phonon relaxation due to a decrease of phonon energy of the glass matrix, responsible for longer fluorescence lifetime [20]. By further increasing the concentration of Tm^{3+} ions, the mean distance between ions in the lattice becomes small enough so the transfer of excitation energy to neighbouring ions becomes possible, which depopulates the excited states. Additionally, at higher Tm concentrations (4%), the crystalline phases of Tm_2S_3 and Ga_2S_3 begin to form in the glass matrix (fig. 4.9), which can also affect the degree of symmetry of Tm^{3+} local environment.

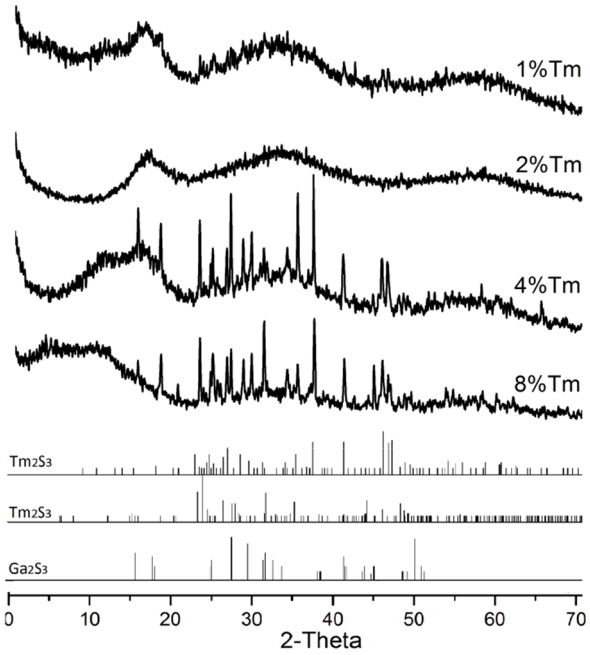

Fig. 4.9. X-ray spectra of Tm^{3+} doped $Ga_{0.8}As_{39.2}S_{60}$ glasses.

4.3.3. EMISSION PROPERTIES OF Tm^{3+} DOPED Ga-As-S GLASS FIBER

Based on the previous results (high thermal stability and amorphous phase), we initially selected both the 1%Tm^{3+} and 2%Tm^{3+} doped $Ga_{0.8}As_{39.2}S_{60}$ glass compositions as good candidates for the fabrication of preforms to produce optical fibers. However, the 1% Tm^{3+} doped $Ga_{0.8}As_{39.2}S_{60}$ glass composition was chosen to draw the fiber, since it was completely homogenous and transparent comparing to glass sample obtained with 2% of Tm^{3+}.

In order to find the appropriate temperature region for fiber drawing, the viscosity of $Ga_{0.8}As_{39.2}S_{60}$:1%Tm^{3+} (core of the fiber) and As_2S_3 (cladding of the fiber) glasses was measured in the glass softening range. The viscosity-temperature curves are presented in Fig. 4.10. As it can be seen with the incorporation of Ga the viscosity curve of As_2S_3 shifted to a lower temperature. From these data it follows that at equal temperatures the viscosity of Ga based glass is considerably less than that of As_2S_3

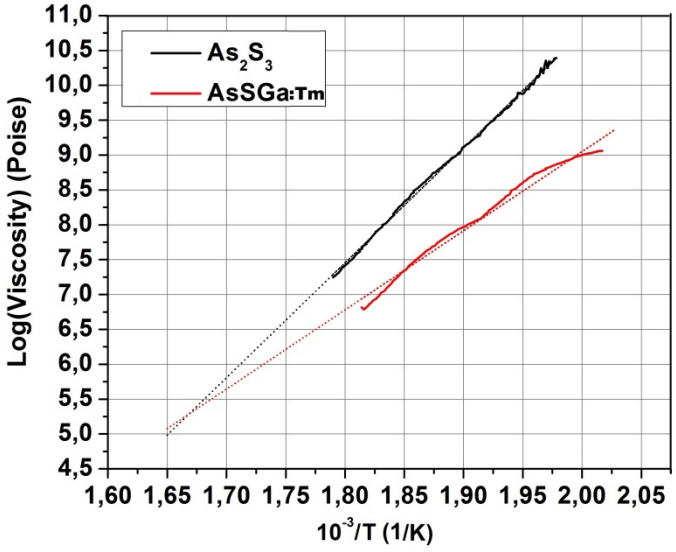

Fig.4.10. Viscosity vs. inverse of absolute temperature for $Ga_{0.8}As_{39.2}S_{60}$:1%Tm^{3+} and As_2S_3 glasses in the glass softening range

As it is generally established, the suitable viscosity range for fiber drawing is in the range of $10^{6.5}$-$10^{5.5}$ Poises, thus to find the temperature of fiber drawing for this system, the viscosity curves were extrapolated into the range up to 10^5 Poise (Fig. 10). It revealed that the fiber drawing temperature of $Ga_{0.8}As_{39.2}S_{60}$:1%Tm^{3+} is lower

comparing to that of As_2S_3, but they are almost in the same region (300-315 °C for the cladding and 285-310 °C for the core).

The coefficients of thermal expansion for both preforms were measured as well and it showed that with the incorporation of Ga (and Tm) it increased from $21.4 \cdot 10^{-6}$ to $22.8 \cdot 10^{-6}$ (1/°C). Hence, the fiber was drawn at ~300 °C.

The emission spectrum of the fiber is presented in Fig. 4.11. It was recorded at a spectral resolution of 2 nm and was averaged over 5 independent measurements. Three emission bands are clearly seen ($^3H_5 \rightarrow {}^3H_6$ around 1.2 μm, $^3H_4 \rightarrow {}^3F_4$ around 1.4 μm and $^3F_4 \rightarrow {}^3H_6$ around 1.8 μm) which is consistent with the fluorescence observed in the bulk samples with an excitation wavelength near 800 nm. Note that the peak, centered at 1578 nm, is caused by the residual pump power diffracted to higher orders by the spectrometer grating.

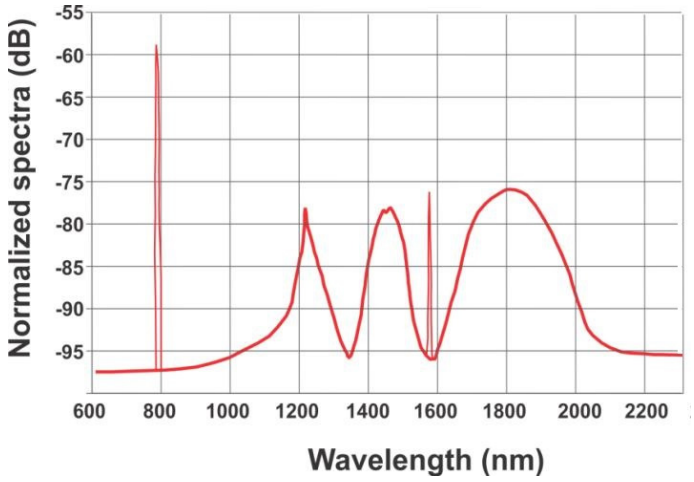

Fig. 4.11. Emission (ASE) spectra of the Tm^{3+} doped $Ga_{0.8}As_{39.2}S_{60}$ fiber (excitation at 789 nm)

Few papers have been reported on the literature regarding the luminescence of RE ions in Ga doped chalcogenide glass fibers [17, 31]. First, Cole et al reported the incorporation of Pr^{3+} in the glass composition based on GeAsGaSe [132]. He showed the IR emission in the 4-5 μm which corresponds to the transitions of Pr^{3+} ions between $^3F_4$ and $^3H_4$ energy levels. Later, West et al presented Gallium Lanthanum Sulphide (GLS) glass fiber having potential application in practical and efficient

1.3μm optical fiber amplifier [33]. In our work, this is the first time that three emission bands of Tm^{3+} ions were observed in the Ga based chalcogenide glass fiber. Tm^{3+} doped Ga-As-S glass fibers can be good candidates for the fabrication of amplifiers and infrared fiber lasers operating at 1.2, 1.4 or 1.8 μm wavelengths. Additionally, we can think about the possibility of the production of glass matrix with large emission band covering from 1.2 to 1.8 μm by using adequate co-dopants as Pr^{3+} for the emission at 1.3μm and Er^{3+} for the 1.55μm.

4.4. CONCLUSION

We have shown that the incorporation of Ga_2S_3 compound in the network of As_2S_3 glasses enables RE solubility. Tm^{3+} doped Ga-As-S glass samples were characterized and three strong emission bands at wavelengths around 1.2 μm ($^3H_5 \rightarrow {}^3H_6$), 1.4 μm ($^3H_4 \rightarrow {}^3F_4$) and 1.8 μm ($^3F_4 \rightarrow {}^3H_6$) were observed under the excitation of a lamp at 698 nm and 800 nm. Different samples having various concentrations of gallium and thulium were studied and the 1 % Tm^{3+} doped $Ga_{0.8}As_{39.2}S_{60}$ glass was identified as the optimal composition for the fiber preform. As we observed in the bulk samples, the doped fiber displayed all three emission bands.

These results indicate that Tm^{3+} doped Ga-As-S glass fibers are good candidates for the fabrication of fiber lasers operating at 1.22, 1.46 or 1.82 μm wavelengths.

ACKNOWLEDGEMENTS

The authors would like to thank the Canadian Excellence Research Chair program (CERC) on Enabling Photonic Innovations for Information and Communication for their financial support. The Natural Sciences and Engineering Research Council of Canada (NSERC) and the Canada Foundation for Innovation (CFI) agencies are also acknowledged.

CHAPTER 5

STRUCTURAL ANALYSIS OF Tm^{3+} DOPED As-S-Ga GLASSES BY RAMAN AND EXAFS SPECTROSCOPY

In order to be able to control the luminescence properties of the system it is important to know the crucial features and the critical factors of the system responsible for the emission of RE ions in the glass matrix. The subject of the present chapter is to understand the mechanisms that are responsible for the increase of the solubility of Tm ions in As_2S_3 glass with the incorporation of Ga. For this purpose we explored the molecular structure of Tm doped Ga-As-S glasses and correlated it to the luminescence properties of this system.

This chapter is based on a manuscript of a published article, which investigates structural properties of Tm doped Ga-As-S glasses depending on the concentration of Ga and Tm in the matrix. Raman spectroscopy and Extended X-ray Absorption Fine Structure (EXAFS) spectroscopy were used to explore the structural modifications of Tm^{3+} doped As_2S_3 glasses induced by the addition of Ga, as well as, the changes in the local environment of Tm^{3+} depending on its own concentration.

RÉSUMÉ DE L'ARTICLE INSÉRÉ

Analyse structurale des verres As-S-Ga dopés au Tm^{3+} par la spectroscopie Raman et EXAFS

Le sujet de ce travail est l'étude des mécanismes responsables de l'augmentation de la solubilité des ions de Tm^{3+} dans le verre As_2S_3 avec l'incorporation de Ga. A cet effet, nous avons exploré les propriétés structurales des verres Ga-As-S dopés aux ions de Tm en utilisant deux technique d'analyse structurale : spectroscopie Raman et EXAFS. Nous avons examiné les modifications de la structure moléculaire du verre As-S-Ga dopé au Tm, induites par la variation de la concentration de Ga et de Tm dans la matrice. Les changements dans l'environnement local de Tm en fonction de sa propre concentration dans le verre ont également été étudiés et corrélés à des propriétés de luminescence de ce système.

Journal of Non-Crystalline Solids 432 (2016) pp. 487–492
Article history:
Received 16 September 2015
Received in revised form 6 November 2015
Accepted 7 November 2015
Available online 1 December 2015

Structural Analysis of Tm^{3+} Doped As-S-Ga Glasses by Raman and EXAFS spectroscopy

A.Galstyan[1], S.H. Messaddeq[1], C.U. Segre[2], T. Galstian[1], Y. Messaddeq[1]
1. *COPL, Laval University, 2375, rue de la Terrasse, Quebec, QC, G1V 0A6, Canada*
2. *Illinois Institute of Technology, 3101 South Dearborn St., Chicago, IL, 60616, USA*
ani.galstyan.1@ulaval.ca

ABSTRACT

Structural properties of Tm^{3+} doped As-S-Ga glasses were investigated using Raman spectroscopy and Extended X-ray Absorption Fine Structure (EXAFS) spectroscopy at As K-edge, Ga K-edge and Tm L_3-edge. The Raman spectra are interpreted on the basis of comparison with the well-known Raman spectra of As_2S_3 glasses the structure of which mainly consists of pyramidal [$AsS_{3/2}$] units interconnected by S–S chains. Incorporation of Ga_2S_3 in As_2S_3 glass matrix induced the dissociation of S-S chains in behalf of the formation of tetrahedra [GaS_4]. Moreover, introduction of Tm into As-S-Ga glasses forms Tm-S bonds through the further dissociation of [$AsS_{3/2}$] pyramidal units. The deficiency of S in the glasses is compensated with the formation of As_4S_4 structural units. The EXAFS results indicate that Ga-S bond distance in the tetrahedra [GaS_4] decreases from 2.29Å to 2.26Å with the increase of Tm concentration in the glass. Meanwhile, Tm-S bond distance increases from 2.66Å to 2.71Å approaching to that of crystalline Tm_2S_3 and simultaneously, the coordination number of Tm gradually decreases from 7 to 4.

Keywords: Raman spectra of As-S-Ga glasses, EXAFS study of Tm^{3+} doped chalcogenide glasses, As K-edge, Ga K-edge, Tm L_3-edge.

5.1. INTRODUCTION

Sulphides based chalcogenide glasses attract considerable interest thanks to their low phonon energy, high refractive index, good chemical durability and good glass-forming ability. A variety of sulphide glass systems has been studied based on gallium, germanium, arsenic sulphides and combinations of them [1,6,113,114,131,133]. Among all these systems the arsenic trisulphide (As_2S_3) is the best known and the most explored system from the point of view of thermo-optical features and molecular structure [60]. When doped with rare earth (RE) ions [31,132,135], chalcogenide glasses open up the possibility of new transitions and significantly increased pumping efficiencies for fiber-optic amplifiers and infrared lasers. However, As_2S_3 glasses suffer from poor RE solubility [36], resulting the clustering of rare earth ions, which limits their applications as practical amplifiers or lasers.

According to previous reports, the solubility of RE ions can be increased dramatically with the addition of gallium (Ga) to the host [38,111,123] due to the presence of edge-sharing [GaS_4] tetrahedra which appear with the addition of Ga_2S_3 [124]. The increased solubility of RE is due to the fact that the incorporation of Ga provides compensation for the negative charge of free S^{2-} ions by forming chemical bonds with RE ions.

In our previous work, we explored different compositions of As-S-Ga glasses as host matrix for Tm^{3+} ions [136]. The luminescence properties of As-S-Ga:Tm glasses depending of Ga and Tm concentration were studied, as well as, their thermal and optical properties. It was found that the incorporation of Ga_2S_3 compound in the network of As_2S_3 glasses improved their RE solubility. Infrared emission spectra were recorded and strong emission bands at wavelengths around 1.2μm ($^1H_5 \rightarrow {}^3H_6$), 1.4μm ($^3H_4 \rightarrow {}^3F_4$) and 1.8 μm ($^3F_4 \rightarrow {}^3H_6$) were obtained under the excitation of a xenon lamp at 698nm and 800nm. A Tm^{3+} doped As-S-Ga glass fiber was also fabricated where all three emission bands were observed as in bulk samples.

The present work deals with better understanding of the structural changes created in the As_2S_3 glass matrix with the incorporation of Ga and Tm. A systematic structural study is performed in the As-S-Ga by varying the amount of Tm from 1 to

8%. To obtain structural information about the local environment in these glasses, Extended X-ray Absorption Fine Structure (EXAFS) analysis was performed at the As K-edge, Ga K-edge and Tm L_3-edge. Structural information was also obtained through Raman analysis as a function of glass composition for different concentrations of Ga and Tm.

5.2. EXPERIMENT

The Tm^{3+} doped As-S-Ga glasses were prepared by melting Ga_2S_3 crystalline compound (99.999%), metallic Tm^{3+} and the pre-purified As_2S_3 glass. The glasses were synthesized in silica ampoules sealed under high vacuum (10^{-5} Torr). The ampoule is placed in a rocking furnace and heated at a rate of 1°C/ min up to 900°C. After being rocked for 12 hours (for homogenization), the glass is quenched in the water at room temperature for few seconds and annealed at 160°C for 6 hours to remove the thermal stress.

The Raman scattering spectra were collected with a confocal Renishaw inVia spectrometer coupled to a Leica DM2700 microscope. A back-scattering geometry was used in the frequency range of 100-600cm^{-1}. The excitation light source was a 17 mW vertically polarized 633 nm (He-Ne) laser. The laser beam was focused with a 50X long working distance objective, generating a sub-micron spot size containing a total power at the sample of approximately 5-10mW. The frequency uncertainty was estimated to be ± 2 cm^{-1}. The deconvolution of Raman spectra were performed using curve fit function of Wire 4.1 software.

EXAFS measurements were carried out at the Sector 10-BM-B (MRCAT) beamline at the Advanced Photon Source [137] (Argonne National Laboratory, Chicago). All measurements were performed using powdered samples at room temperature. The EXAFS spectra were collected at the As K-edge (11867eV), Ga K-edge (10367eV) and Tm L_3-edge (8648eV). The Ga and Tm edges were measured in fluorescence mode using a 4 Element Vortex Silicon Drift detector. The As edge was measured in transmission mode, using Nitrogen (incident beam) and Argon (transmitted beam) filled ionization chamber detectors. The positions of the

monochromator for As, Ga and Tm edges were calibrated using Au, Ta and Cu metal foils, respectively.

Structural parameters including coordination number (N), interatomic distance (r) and the Debye-Waller factor (σ) were obtained from least squares fitting in k-space, using theoretical phase and amplitude functions using the IFEFFIT-based software [138] packages Athena and Artemis [139].

5.3. RESULTS AND DISCUSION

5.3.1. RAMAN SPECTROSCOPY

Figure 5.1 shows the Raman spectra of 0.2%Tm^{3+} doped $Ga_xAs_{40-x}S_{60}$ ($0<x<4$) glasses as a function of Ga concentration as well as the Raman spectra of As_2S_3 glass as reference. The structure of As_2S_3 glasses has been extensively studied by several authors using Raman spectroscopy [140-143]. It is generally accepted that the three dimensional network of As_2S_3 glass is built of trigonal pyramidal units [$AsS_{3/2}$], which are interconnected through S_2AsS-$SAsS_2$ bridges [20,23,24], which give rise to two main bands centered at 342 cm^{-1} and 495 cm^{-1}. Such bands can be observed in the Raman spectra of As_2S_3 glass in figure 5.1a.

The addition of Ga_2S_3 to As_2S_3 glass matrix gives rise to two bands centered at 189 cm^{-1} and 233 cm^{-1}, which are ascribed to the presence of As-As homo-polar bonds [145] in As_4S_4 realgar molecules and to Ga-S-Ga bend [146] in [GaS_4] tetrahedra, respectively. Besides, there are additional shoulders at approximately 365 cm^{-1} and 390 cm^{-1} (Fig. 5.1a) which have been associated to As_4S_4 cage-like nanocluster units [20,21,27] and to the symmetrical stretching vibration of [GaS_4] tetrahedra [15,28], respectively. Moreover, the band at 495cm^{-1} disappears with the incorporation of Ga (0.8 at%).

In order to better understand the role of the addition of gallium on the structural changes of the matrix of arsenic sulphide, the Raman spectra of studied glasses were deconvoluted with Gaussian peaks using least squares approach. A preliminary subtraction and a polynomial baseline were performed in the collected Raman spectra followed by the normalization at 342 cm^{-1}. The intensity of each band was calculated

by integrating the surface of the corresponding peak for all Raman modes present in the spectra, which allowed us to quantify the contribution of the molecular constituents to Raman spectra. The resulting structural trends for each assigned structural units depending on Ga contents are presented in the figure 5.1b.

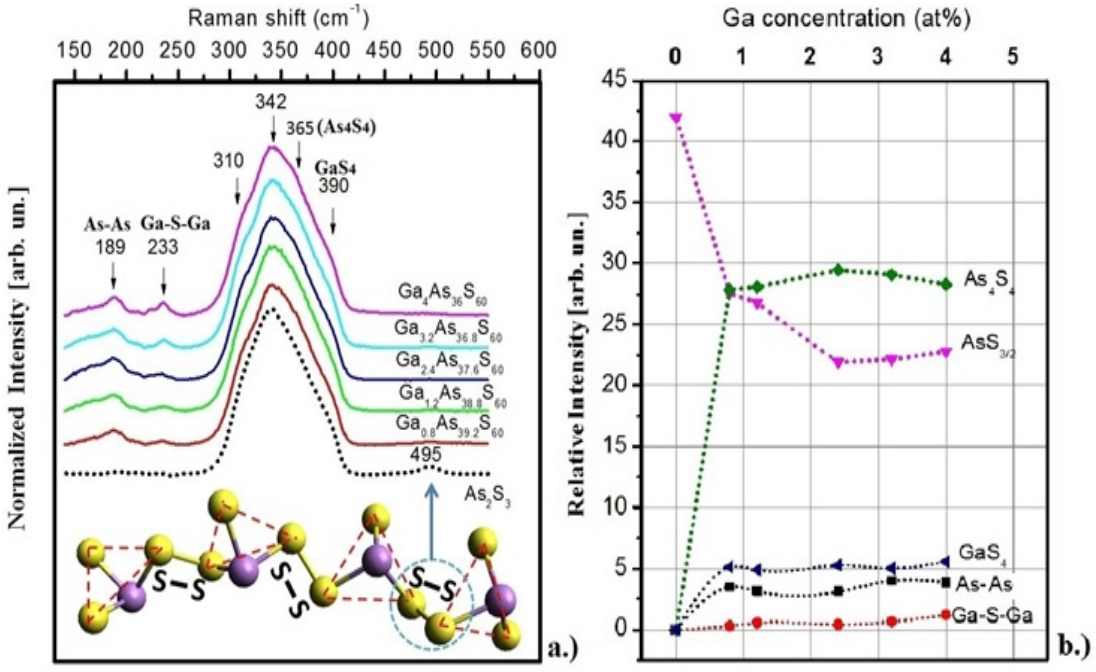

Fig. 5.1. a.) Normalized Raman spectra of 0.2%Tm^{3+} doped $Ga_xAs_{40-x}S_{60}$ glasses. The inset represents the schematic structure of As_2S_3 glasses. b) Relative intensities of Raman bands for different structural units as a function of Ga content.

It can be seen that the band associated with symmetric stretching of [$AsS_{3/2}$] pyramids (342cm^{-1}) decreases with the incorporation of Ga in the matrix, whereas the band assigned to As_4S_4 structural units (365cm^{-1}) increases in amplitude. A slight increasing of [GaS_4] tetrahedral units (390cm^{-1}), Ga-S-Ga bonds (233cm^{-1}) and As-As homo-polar bonds (189cm^{-1}) is observed as well. Further increasing the Ga concentration did not show any significant changes in the band amplitudes, which is probably related to the fact that the glass formation region in this system is very small and up to 3.5at% of Ga can be incorporated in the glass [127]. This limits the observation of significant structural changes in the glass upon the increasing of Ga content.

Based on the above results, one can suppose that the sulphur, originally connecting [$AsS_{3/2}$] pyramids, was removed to provide extra sulphur needed for the formation of [GaS_4] tetrahedra. This trend is observed through the disappearance of the band centered at 495 cm^{-1} and the increase of the shoulder at 390cm^{-1} (Fig. 5.1b). It is well know that the formation of [GaS_4] tetrahedra from Ga_2S_3 results in a deficiency of sulphur in the glasses since the S/Ga ratio of Ga_2S_3 is 1.5 which is less than the 2 required to form tetrahedra [149]. Therefore, as we increase the amount of Ga_2S_3 in the glass matrix, [$AsS_{3/2}$] pyramidal units started to be dissociated creating non-bridging sulphurs for Ga, which is visualised by the decrease of the 342 cm^{-1} band. Simultaneously, the migration of sulphur from [$AsS_{3/2}$] pyramids to [GaS_4] tetrahedra results in the formation of metal-metal (As-As) bonds in the glass (forming As_4S_4 units).

Therefore, we can consider that the molecular structure of our As-S-Ga glass matrix consists of [GaS_4] tetrahedra and [AsS_3] pyramids randomly linked by shared sulphur atoms surrounded by realgar-like As_4S_4 molecules (fig. 5.2).

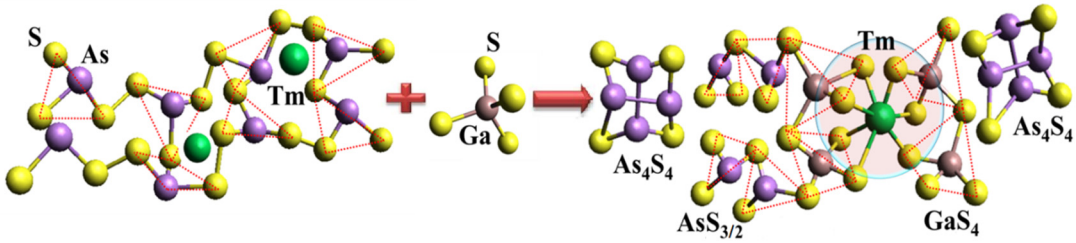

Fig. 5.2. Schematic representation of structural units formed in As_2S_3 glass with incorporation of Ga and hypothetical local structure model around Tm ions in As-S-Ga glasses

In our previous work [136] we observed that the incorporation of Ga in the As_2S_3 vitreous network allowed the solubility of Tm^{3+} ions and its corresponding emission bands were observed. Prior to addtion of Ga, the Tm^{3+} ions are described as clustered [150] and no emission was observed in As_2S_3 glasses. This behaviour may instead be due to a lack of solubility and random precipitation which avoid the luminescence [111]. With the introduction of Gallium, Ga complexes the RE-ion in the presence of chalcogen forming [RE^{3+}-S-Ga^{III}] type species as already confirmed by Aitken et al. [151] in the sulphide glasses. We can suppose that the originally Tm

cluster are dissolved into Ga site rather than in As regions and then become fully spread until proportions of such Ga regions reach a certain critical value (in our case, Ga=3.2 at% [136]). So, [GaS_4] tetrahedra form a shell around the Tm ions (Fig.5. 2), and the resultant complex is readily incoporated into the As_2S_3 glass with the same analogy as in silica glasses co-doped with Al_2O_3 to dissolve the rare earth element in the glass matrix [152].

As follows, we choose the sample already doped with Ga_2S_3 (namely $Ga_{0.8}As_{39.2}S_{60}$ glasses) where the process of As_2S_3 pyramidal units breakage already has taken place, and we mesure the Raman spectra of this matrix with different Tm^{3+} concentrations (1-8 at.%). Results are presented in Figure 5.3. Raman spectrum of c-Tm_2S_3 is added as a reference. As we can see from the spectra, with the incorporation of Tm a new band appears at 224 cm^{-1}, which is associated to Tm-S bonds [153] and with the increase of Tm concentration the intensity of this band increases slightly. The bands at 233 cm^{-1} (Ga-S-Ga) and 390 cm^{-1} ([GaS4] tetrahedral) stay almost constant upon the variation of Tm content in the glass (fig. 3b). On the other hand, the band at 365 cm^{-1} (As_4S_4) continues to increase. Simultaneously, the band at 342 cm^{-1} ([AsS_3]) decreases in amplitude. A slight increase of the band at 189 cm^{-1} (As-As) is observed as well.

This behaviour could indicate that the introduction of Tm into As-S-Ga matrix results in the formation of Tm-S bonds by breaking the As–S bond in [AsS_3] pyramidal units, which increases the concentration of homo-polar (As–As) bonds due to the deficiency of sulphur. This would suggest that the formation of more As_4S_4 units is favoured, which is associated with the increase of the band at 365 cm^{-1}. So, we could confirm that even a very small concentration of Ga atoms is able to facilitate the solubility of Tm^{3+} ions and enhance their fluorescence properties [136]. Despite the fact that with the increase of Tm concentration up to 8at% the band at 342cm^{-1} ($AsS_{3/2}$) gradually decreases and the band at 224 cm^{-1} (Tm-S) continues to increase, the intensity of emission of Tm^{3+} ions decreases at ≥4at% [136], which could indicate that at higher concentrations, even if more Tm-S bonds are formed, the environment of Tm is no more favourable for the solubility of ions, and this leads to the decrease of luminescence.

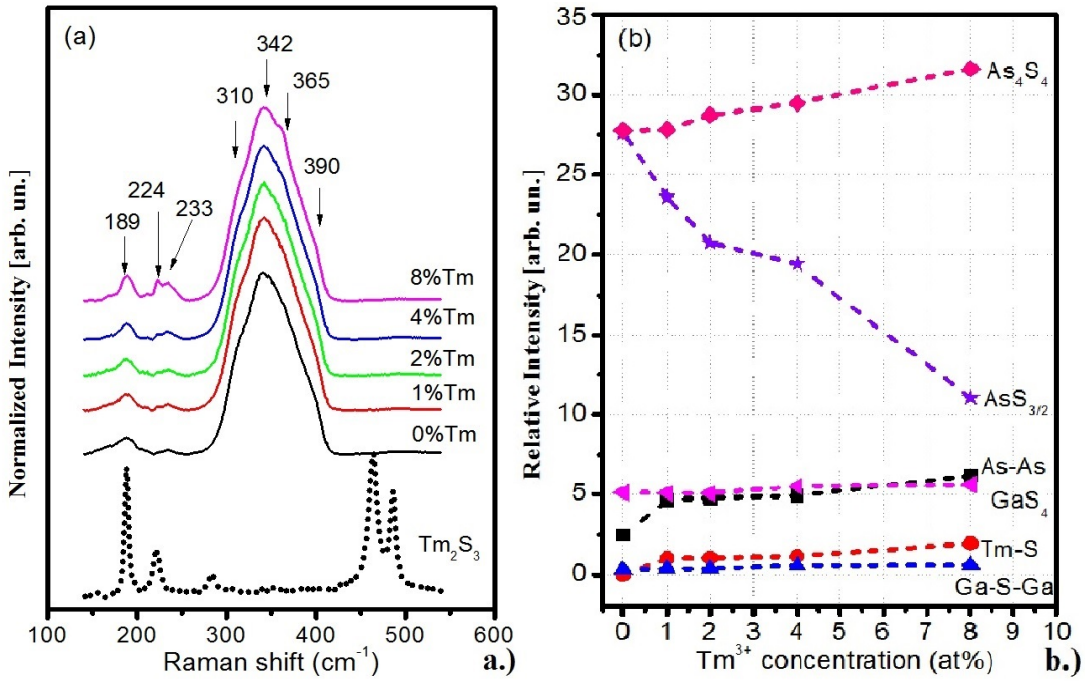

Fig. 5.3 a.) Normalized Raman spectra of Tm doped $Ga_{0.8}As_{39.2}S_{60}$ glasses. b.) Relative intensities of Raman bands for different structural units as a function of Tm content $Ga_{0.8}As_{39.2}S_{60}$ glasses.

These structural changes suggest that Tm ions act as a modifier in the As_2S_3 glass matrix. A similar mechanism was proposed by Pisarski et al. [154] based on visible and infrared spectroscopy data on Tm^{3+} ions in lead borate glass system.

5.3.2. EXAFS

In order to further investigate the structural modifications imported by Tm^{3+} ions in the $Ga_xAs_{40-x}S_{60}$ glasses, EXAFS analysis at As K-edge, Ga K-edge and Tm L_3-edge was performed. EXAFS spectra of As K-edge of As_2S_3 glass and Ga K-edge of Ga_2S_3 crystalline compound were also collected as references. The range of the Fourier Transform for As and Ga was 2-15$Å^{-1}$, and for Tm it was 2-10$Å^{-1}$. The range of the R-space fit was 1-3Å for all three elements.

As K-edge

The k^3-weighted $\chi(k)$ experimental EXAFS spectra of As *K*-edge, the corresponding Fourier transforms and their theoretical fits are shown in Fig. 5.4. The

nominal compositions of glasses, studied with EXAFS spectroscopy, and the structural parameters for the first coordination shell are presented in Table 5.1.

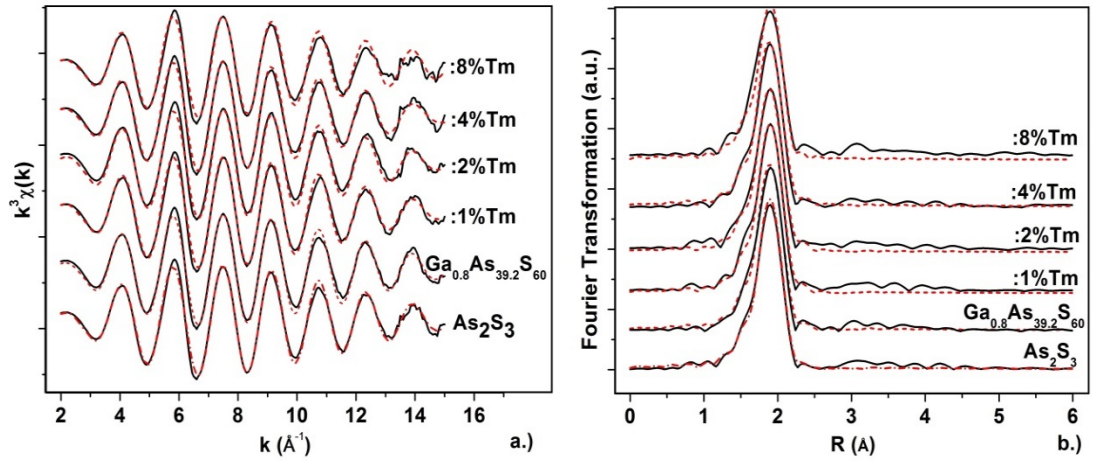

Fig. 5.4. k^3-weighted As K-edge EXAFS spectra (a) and the magnitudes of Fourier transformation (b). Black solid lines represent experimental data, red dash lines correspond to fit

	N_{As-S} (±0.2)	r_{As-S}(Å) (±0.005)	σ^2 (Å^2) ±0.001	R-factor
As_2S_3	3.0	2.280	0.003	0.004
$Ga_{0.8}As_{39.2}S_{60}$	2.9	2.279	0.003	0.005
$Ga_{0.8}As_{39.2}S_{60}$: 1%Tm	3.0	2.279	0.003	0.006
$Ga_{0.8}As_{39.2}S_{60}$: 2%Tm	2.9	2.279	0.003	0.006
$Ga_{0.8}As_{39.2}S_{60}$: 4%Tm	2.9	2.279	0.003	0.005
$Ga_{0.8}As_{39.2}S_{60}$: 8%Tm	2.8	2.281	0.004	0.005

Table 5.1: As K-edge EXAFS structural parameters (the coordination number N, the bond length r and Debye-Waller factor σ) for Tm doped $Ga_{0.8}As_{39.2}S_{60}$ glasses

The fitting of EXAFS spectra showed that the first neighbour of As is sulphur and yields the first-shell coordination numbers of N~3 at r=2.28Å, which reflects the As–S bonding distance. This value of As-S distance (2.28 Å) is close to the mean As–S distance in crystalline As_2S_3 [155]. The present results are consistent with those reported by other authors [156], where the local atomic structure is formed of [$AsS_{3/2}$] units, and each arsenic atom is bound to three sulphur atoms with As-S bond lengths of 2.2701 Å, 2.2894 Å and 2.2919 Å [157].

The insertion of gallium (or thulium) in the As_2S_3 matrix did not show any modification in the pyramidal units [$AsS_{3/2}$], i.e. neither the average distance between As and S nor the coordination number of As were changed (table 5.1). Despite de fact that Raman spectra showed a formation of As-As bonds, no As-As bond was observed in the present EXAFS analysis. This could be related with the fact that these bonds are quite disordered in the glass and therefore the bands are overlapped in the spectra. So the contribution of As-As is not significant and only a single large peak is always obtained in spectra.

It must be noted that the disorder inherent in a glass and the similar electronic structures of Ga and As backscattering atoms do not allow to distinguish at least the nature of the second neighbour of As (or Ga) directly by EXAFS.

Ga K-edge

Fig. 5.5 shows the k^3-weighted $\chi(k)$ spectra and Fourier transformed spectra of the Ga K-edge. The resulting fitting of the first coordination shell of Ga are summarized in Table 5.2. It revealed that the Ga atoms in these glasses are surrounded by 4 sulphurs, like in the crystalline compound Ga_2S_3 which is in accordance with Goodyear et al. [158], where the structure of the Ga_2S_3 crystal is composed of [GaS_4] tetrahedral units. The interatomic distance Ga-S in the $Ga_{0.8}As_{39.2}S_{60}$ matrix is 2.27Å, which is almost the same as in the crystalline Ga_2S_3 (2.29Å) [159]. The estimated standard deviation is about 0.01. Benazeth et al. [160] also studied the structure of bulk gallium lanthanum sulphide (GLS) glasses using EXAFS at the Ga K-edge and lanthanum L_3-edge. Their results showed as well that in the glass the gallium atoms exist in tetrahedral networks of GaS_4 and the Ga–S distances are identical to those existing in the crystalline form of Ga_2S_3. Upon the addition of Tm, the coordination number of Ga stays constant andfurther changes in the Tm concentration do not lead to any additional changes in the coordination of Ga. However, at higher concentrations of Tm the bond distance of Ga-S becomes slightly shorter. Hence, increasing of the Tm concentration in the glass matrix leads to slight contraction of [GaS_4] tetrahedral.

The results are presented only for 1 and 2% of Tm. For the compositions with higher concentration of Tm aberrations appear in the spectra, due the fact that bonding energies of Ga K-edge and Tm L_1-edge are very close.

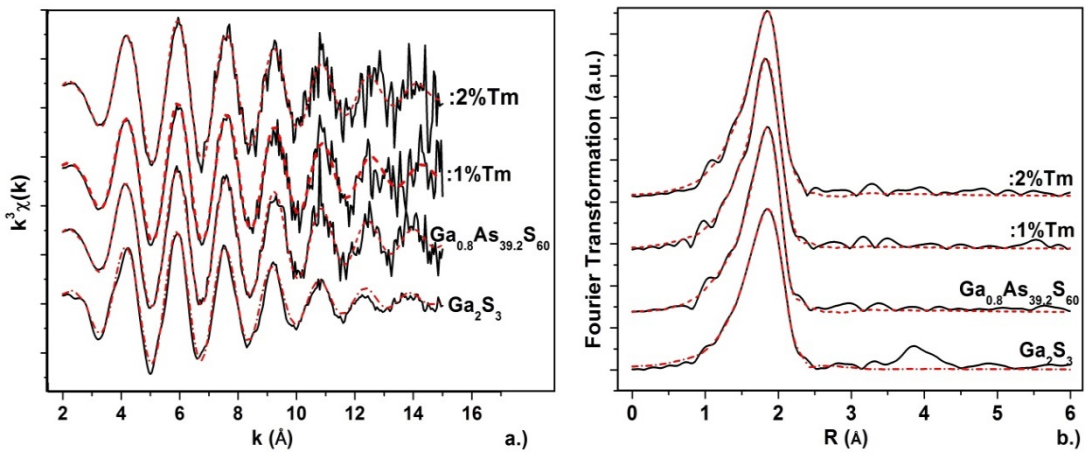

Fig. 5.5. k^3-weighted Ga K-edge EXAFS spectra and the magnitudes of Fourier transformation. Black solid lines represent experimental data, red dash lines correspond to fit

	N_{Ga-S} (±0.3)	r_{Ga-S} (Å) (±0.01)	σ^2 (Å^2) (±0.001)	R-factor
c-Ga_2S_3	3.9	2.29	0.005	0.02
$Ga_{0.8}As_{39.2}S_{60}$	3.9	2.27	0.004	0.02
$Ga_{0.8}As_{39.2}S_{60}$: 1%Tm	4.0	2.27	0.005	0.02
$Ga_{0.8}As_{39.2}S_{60}$: 2%Tm	4.0	2.26	0.005	0.02

Table 5.2: Ga K-edge EXAFS structural parameters (the coordination number N, the bond length R and Debye-Waller factor σ) for Tm doped $Ga_{0.8}As_{39.2}S_{60}$ glasses

Tm L_3-edge

Figs. 5.6 shows the k^3-weighted χ(k) spectra and Fourier transformed spectra of Tm^{3+} ions in $Ga_{0.8}As_{39.2}S_{60}$ glasses. The increase of Tm concentration resulted in significant changes in the shape of k^3-weighted χ(k) and Fourier transformed R-space spectra, indicating modifications of local structure around Tm^{3+} ions. The two peaks between 3-5Å are more prominent in the Tm spectra than in the As and Ga spectra

which indicates that the Tm is in a more well-ordered environment at all concentrations.

Table 5.3 shows results of the fitting on the first coordination shell around Tm^{3+} ions. Current EXAFS analysis at Tm L_3-edge indicates that Tm ions are coordinated with sulphur ions, in accordance with the previous reports [126]. It can be observed that for small content of Tm^{3+} ions the coordination number is about 7.

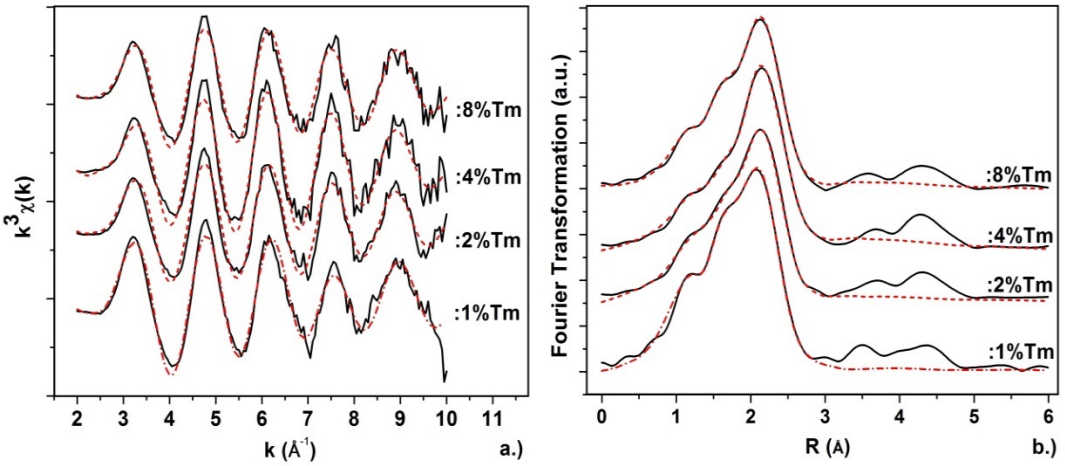

Fig. 5.6. k^3-weighted Tm L_3-edge EXAFS spectra and the magnitudes of Fourier transformation. Black solid lines represent experimental data, red dash lines correspond to fit

	N_{Tm-S} (±0.5)	r_{Tm-S} (Å) (±0.008)	σ^2 (Å^2) (±0.001)	R-factor
$Ga_{0.8}As_{39.2}S_{60}$: 1%Tm	6.5	2.666	0.016	0.003
$Ga_{0.8}As_{39.2}S_{60}$: 2%Tm	5.4	2.695	0.011	0.001
$Ga_{0.8}As_{39.2}S_{60}$: 4%Tm	4.9	2.716	0.011	0.005
$Ga_{0.8}As_{39.2}S_{60}$: 8%Tm	4.2	2.713	0.011	0.003

Table 5.3: Tm K-edge EXAFS structural parameters (the coordination number N, the bond length R and Debye-Waller factor σ) for Tm doped $Ga_{0.8}As_{39.2}S_{60}$ glasses

However, upon the addition of Tm, the coordination environment of Tm^{3+} shows gradual changes, i.e. with the increase of the concentration of Tm^{3+} from 1% to 8%, the coordination number decreases from 7 to 4 and the Debye-Waller factor decreases from 0.016 to 0.011. Simultaneously, the distance between Tm and S becomes larger (from 2.66Å to 2.71Å). According to ref. [126] in the crystalline Tm_2S_3 the Tm-S distance is about 2.74Å, so the increase of Tm-S bond length in the

glass and the decreasing of Debye-Waller factor could means that crystalline units of Tm_2S_3 began to form in the glass matrix, when the concentration of Tm increases. This is in good agreement with X-ray diffraction spectra of Tm^{3+} doped $Ga_{0.8}As_{39.2}S_{60}$ glasses already reported in our previous work [16]. Meanwhile, the diminution of coordination number could be explained by the fact that at high concentrations the atoms of Tm become closer, leading to inhomogeneous distribution or clustering of Tm atoms. The Tm-Tm bond distance is known to be about 3.2-3.4 Å [161], but no Tm atom was observed in the first coordination shell of Tm. These bonds are significantly disordered in a glass and they could be simply not visible in the spectra.

In summary, the EXAFS analysis did not show any changes in the local environment of As with the incorporation of Tm. However, introduction of Tm^{3+} ions in the glass matrix leads to the contraction of Ga-S distance in the GaS_4 tetrahedra. Meanwhile, the formation of Tm_2S_3 crystalline units in the glass matrix is observed when the concentration of Tm became relatively high, which is reflected by the decrease of Debye-Waller factor, and the increase of Tm-S bond length.

As it was already mentioned above the maximum intensity of luminescence of Tm-ions in $Ga_{0.8}As_{39.2}S_{60}$ glass matrix was observed at 2at% of Tm [136], and it decreases with the further increase of Tm content. Thus we can conclude that at 2at%, despite the coordination number of Tm decreases from 7 to 6, the concentration of homogenously distributed luminescent centers increases in the glass matrix, which promotes the increase of luminescence. However, starting from 4at% the coordination number of Tm decreases up to 5 and the environment of Tm becomes less favourable for the solubility of ions. Moreover, from 4at% the concentration of Tm ions is so high that the mean distance between ions could become small enough for spatial migration of the excitation energy, from one Tm-ion to a neighbouring ion, becomes possible. This leads to depopulation of excited states and decrease of the luminescence.

5.4. CONCLUSION

The combination of the analyses of Raman spectra of Tm^{3+} doped $Ga_xAs_{40-x}S_{60}$ glasses and EXAFS spectra at As K-edge, Ga K-edge and Tm L_3-edge revealed that

the atomic structure of initial As_2S_3 glasses matrix consists of pyramidal units of [$AsS_{3/2}$] interconnected through As-S-S-As bridges. The As atoms are three fold coordinated with two fold-coordinated S atoms with the distance about 2.28Å. The incorporation of Ga_2S_3 leads to the formation of [GaS_4] tetrahedra, by means of breaking both the As–S bond in AsS_3 of pyramidal units and the interconnecting S–S chains. The deficiency of sulphur is compensated by the formation of As_4S_4 realgar units, as the amount of Ga_2S_3 increases. Successively, the incorporation of Tm gradually breaks the [$AsS_{3/2}$] pyramids and takes the role of charge compensators for non-bridging S ions forming Tm-S bonds. No dissociation of [GaS_4] tetrahedra occurred with the incorporation of Tm. However, Ga-S bond length decreases from 2.29Å to 2.26Å with the increase of Tm concentration. The local environment of Tm undergoes significant changes upon the variation of its content in the glass. With the increasing of Tm content from 1% to 8% the coordination number gradually decreases from 7 to 4, and simultaneously the Tm-S bond distance increases from 2.66Å to 2.71Å approaching that of crystalline Tm_2S_3, which indicates the formation of crystalline units and Tm clusters in the glass at higher Tm concentration.

ACKNOWLEDGEMENTS

The authors would like to thank the Canadian Excellence Research Chair program (CERC) on Enabling Photonic Innovations for Information and Communication for their financial support. The supports of Natural Sciences and Engineering Research Council of Canada (NSERC) and of the Canada Foundation for Innovation (CFI) agencies are also acknowledged. MRCAT operations are supported by the Department of Energy and the MRCAT member institutions. This research used resources of the Advanced Photon Source, a U.S. Department of Energy (DOE) Office of Science User Facility operated for the DOE Office of Science by Argonne National Laboratory under Contract No. DE-AC02-06CH11357.

CHAPTER 6

TAILORING OF PROCESSING PARAMETERS FOR PURIFYING Tm DOPED As-S -BASED GLASSES

As discussed in the introduction, the impurities present a major concern for any optical glass and represent a particular problem when exploring new glass compositions. In this sense, one of the most important advantages of As_2S_3 glasses is that the impurities can be decreased notably in these glasses, due to the purification of starting elements. The technique of the purification of As_2S_3 glasses, via chemical distillation of sulphur and sublimation of arsenic, is already well developed in our research group at COPL.

This chapter first discusses the steps and processes of chemical distillation, that were used for the purification of Tm doped As-S-Ga glasses, followed by discussion of strategies, applied on the optimization of thermal parameters of As-S-Ga glass matrix, that leads to the diminution of the melting temperature of the system and facilitation of distillation process of these glasses.

6.1. PURIFICATION OF Tm^{3+} DOPED As-S-Ga GLASS

The next step, after obtaining of Tm^{3+} doped As-S-Ga luminescent fiber, was the purification of this glass preform in order to remove the impurities, which had led to appearance of strong absorption bands in the NIR transmission spectra (Fig. 4.3). For this purpose a standard chemical distillation technique was used. Normally, the method of thermal distillation is more efficient for systems with lower melting temperature, so using this method for Tm doped As-S-Ga glassy system we expected to implement a partial distillation of the glass preform, because of higher melting points of Tm (1545°C) and Ga_2S_3 (1090°C) compounds.

The scheme for the chemical distillation is presented in the Fig. 6.1. The system consists of three interconnected ampoules, the two of which were placed in special

furnaces. The open edge of the system is attached to a high vacuum pump (10^{-5} Torr). The purification procedure included melting of the glass, followed by vacuum distillation of the melt. The doped glass was loaded into the first ampoule (reactor) and slowly heated up to 600°C. Distilled elements were condensed in the second ampoule (receiver), which was maintained at 150°C. Extracted impurities condensed in the third ampoule (trap) left at room temperature. After the distillation process was finished the receiver was sealed from both sides and placed in the rocking furnace at 900°C for the homogenisation of the purified melt.

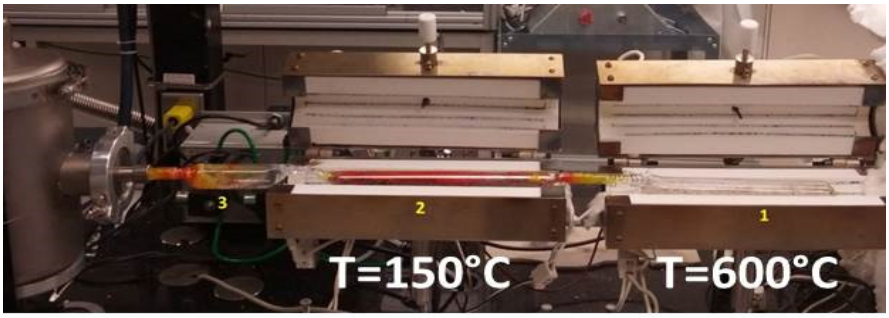

Fig. 6.1. Scheme of purification of Tm doped As-S-Ga glass via chemical distillation 1) Ampoule loaded with Tm doped As-S-Ga glass, 2) Condensed elements after distillation, 3) Trap for extracted impurities

After the distillation was completed, a yellow powdered compound was formed in the reactor, indicating that this composition was not distilled completely. In order to find the content of the powdered compound, a XRD analysis was done and the results are presented in Fig. 6.2. As it was found out, this substance represents a mixture of two crystalline compounds: Ga_2S_3 and Tm_2S_3. The distillation of these compounds was failed, because of their low volatility.

An elemental analysis was performed for the glass before and after the purification, using Energy Dispersive X-ray (EDX) spectroscopy to find the concentration changes of elements in the glass after the distillation. The same elemental analysis was done for the non-distilled compound as well. The results are shown in Table 6.1. Usually, this technique is not very effective for the analysis of RE ions, since a small amount of RE ions is not detectable by EDX, because of the lower power and resolution of the device, but it gave a general idea on the concentration of components in the glass.

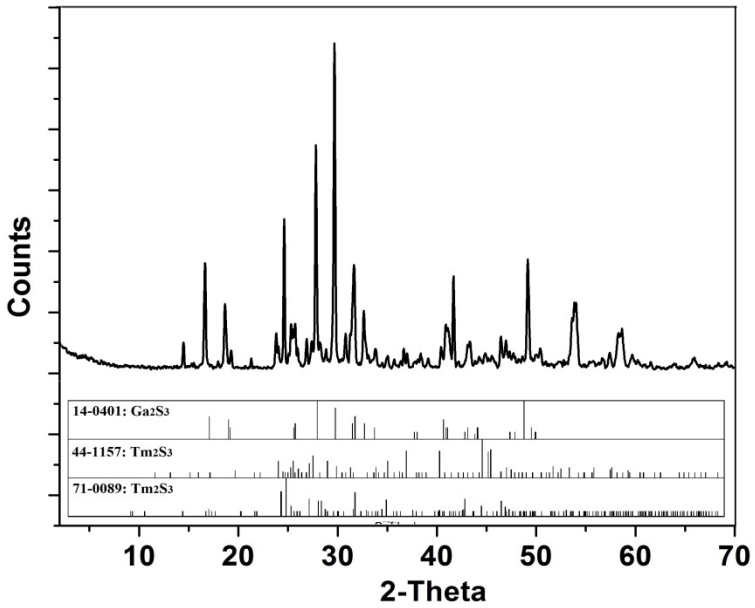

Fig. 6.2. XRD spectra of non-distilled substance after the purification of Tm doped As-S-Ga glass

	Expected	Obtained		
		Before purification	After purification	Non-distilled powder
As	38.81	41.05	42.66	0.00
S	59.40	57.96	57.28	55.48
Ga	0.79	0.99	0.06	44.52
Tm	1.00	-	-	-

Table 6.1. EDX of As-S-Ga:Tm glass before and after purification

As we can see, all of As_2S_3 was distilled and almost all of the Ga and the Tm stayed in the reactor. No luminescence was observed in the purified glass. Therefore, in order to be able to purify this system we needed to decrease the melting temperature of the glass matrix.

6.2. DIMINUTION OF THE MELTING POINT OF As-S-GA GLASS MATRIX

In order to make possible a complete distillation of Tm doped As-S-Ga glasses a reduced melting temperature of this system is needed. For this purpose, we replaced the gallium sulphide (Ga_2S_3) with melting point of 1090°C with the gallium iodide (GaI_3) with the melting point of 212°C.

Ga-I-As-S glass was fabricated trough the pre-purified As_2S_3 glass and GaI_3 crystalline compound (99.999%). Because of high hydrophobic nature of GaI_3 compound, the elements were weighted and loaded in the ampoule in a glove box filled with ultra-high purity grade argon gas. The parameters of synthesis for this system were the same as those for As-S-Ga (at 900°C during 12 hours and quenching in the water). Since the system Ga-I-As-S is prepared through GaI_3 compound, thus 4mol% of GaI_3 was incorporated into the As_2S_3 glass to maintain the same atomic percentage of Ga (0.8 at.%) as in the $Ga_{0.8}As_{39.2}S_{60}$ (the best composition for the doping of Tm).

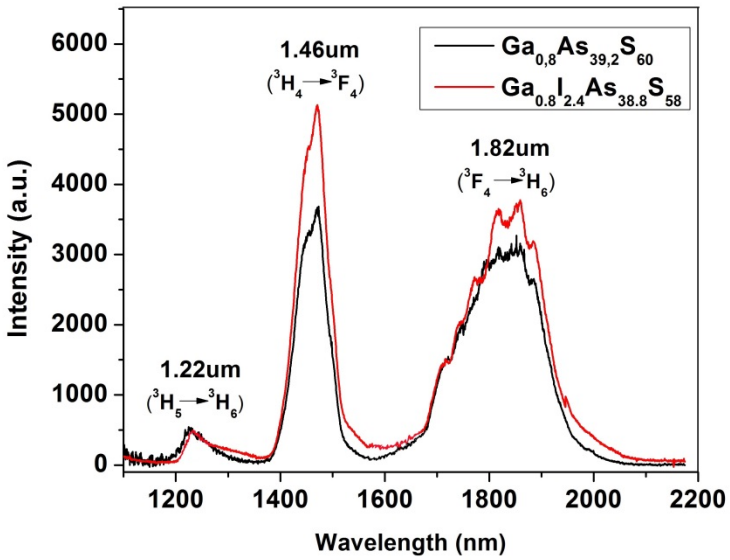

Fig.6.3. Emission spectra of 2%Tm doped chalcogenide glasses based on Ga_2S_3 and GaI_3 (excitation at 800nm)

The concentration of Tm^{3+} was fixed to 2 at%. The fluorescence spectrum was measured for excitation wavelength of 800 nm. The results are presented in Fig. 6.3, comparing with $Ga_{0.8}As_{39.2}S_{60}$ glass.

We observed the same emission bands centered at 1.22 μm, 1.46 μm and 1.82 μm in the spectrum; however the incorporation of iodine in the Ga-As-S system increased the intensity of the band at 1.46 μm about 1.5 times, while maintaining almost constant the intensities of the emission bands at 1.22 μm and 1.82 μm.

Table 6.2 shows the thermal and optical properties of Ga(I)-As-S glasses doped with 2%Tm^{3+}. As it is seen, the addition of iodine in the $Ga_{0.8}As_{39.2}S_{60}$ matrix decreased its T_g and the density, as well as the refractive index.

	Tg (°C) (±2°C)	**Density (g/cm³) (±0.05)**	**Refractive index (±0.003)**	
			1308nm	**1538nm**
As_2S_3	200	3.43	2.400	2.390
$Ga_{0.8}As_{39.2}S_{60}$	193	3.22	2.455	2.445
$Ga_{0.8}I_{2.4}As_{38.8}S_{58}$	173	3.25	2.435	2.425

Table 6.2. Characteristics of 2%Tm^{3+} doped chalcogenide glasses based on Ga_2S_3 and GaI_3

6.3. PURIFICATION OF Tm^{3+} DOPED I-Ga-As-S GLASS

For the purification of this new glassy system based on GaI_3 the same distillation scheme was used, as shown in Fig. 6.1, except that the matrix with desired composition was prepared separately and loaded in the reactor. The metallic Tm was loaded in the receiver to avoid the formation of lower volatile compound of Tm_2S_3 in the reactor. Prior the distillation, the receiver was heated at 500°C during 30 minutes to extract the impurities of oxygen, hydrogen and carbon from the ampoule, after what the receiver was maintained at room temperature to avoid the evaporation of iodine. The temperature of the reactor increased slowly up to 600°C. Unfortunately, after the distillation was completed the same yellow powdered substance was again formed in the reactor.

An analysis of XRD was performed for the powdered settling to find the content of this substance. The result is shown in Fig. 6.4. As it is seen, despite the fact that the Ga_2S_3 had been replaced with GaI_3, during the synthesis of the matrix a lower volatile compound of Ga_2S_3 was formed in the glass and prevented the complete distillation of this system.

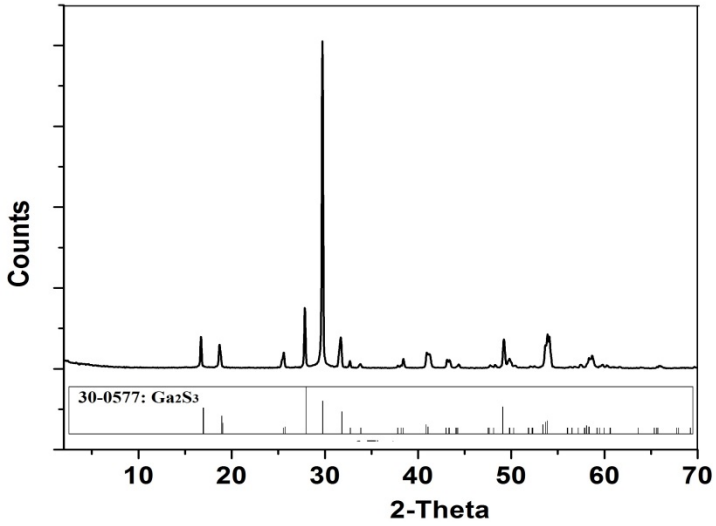

Fig. 6.4. XRD spectra of non-distilled substance after the purification of I-Ga-As-S glass matrix

The results of EDX analysis for the I-Ga-As-S glass before and after the purification, as well as, for the non-distilled compound are presented in Table 6.3. As it is observed, all of the arsenic and iodine were distilled, while the substantial part of the formed Ga_2S_3 compound stayed in the reactor. As always, the small amount of the Tm is related with the fact that RE ions were not detectable by EDX.

The luminescence spectrum of 2%Tm doped I-Ga-As-S purified glass was measured at the excitation wavelength of 800 nm (Fig. 7.2c) and all of three emission bands were observed in the spectrum, despite the fact that almost no Ga stayed in the glass after the purification. This revealed that the iodine has its own contribution in the emission properties of Tm in the matrix of As_2S_3. Besides, low melting temperature of iodine made the purification of the raw materials (pre-processing) and the glass purification (post-processing) easier compared to the Ga based glasses.

	$Ga_{0.8}I_{2.4}As_{38.8}S_{58}$: 2%Tm purified glass		Non-distilled powder
	Expected	**Obtained**	**Obtained**
Ga	0.8	0.28	42.00
I	2.35	2.49	0
As	38.02	40.17	0
S	56.83	57.06	49.71
Tm	2	-	-
O	0	0	8.29

Table 6.3. EDX of I-Ga-As-S:Tm glass before and after purification

Further investigations of I-As-S system will allow finding the best ratio of element concentration in the glass to produce optimal physical and optical properties for achieving a high purity glass with high luminescence efficiency.

CHAPTER 7

THE ROLE OF IODINE IN THE SOLUBILITY OF Tm^{3+} IONS IN As_2S_3 GLASSES

As it was revealed in chapter 6 despite the fact that Ga notably increased the solubility of Tm ions in the As_2S_3 glass matrix, it can limit the use of Tm doped Ga-As-S glasses in several active applications, since the glass formation region is very small in this system, leading to fast crystallisation of the glass. Besides, the low volatility of Ga_2S_3 compound prevented the purification of these glasses and therefore made unavailable the use of some wavelengths in NIR spectrum, because of strong absorption bands.

As we saw, t iodine had its own contribution in the solubility of Tm^{3+} ions in the glass matrix. Moreover, the low melting point of this element can promote the purification of the glass via chemical distillation. So this chapter is dedicated to the detailed investigation of the importance of iodine in the solubility of Tm^{3+} ions As_2S_3 glasses.

This chapter is based on an article manuscript that discusses the role of iodine in the luminescence properties of Tm^{3+} ions in the As_2S_3 matrix, as well as, the changes of optical and thermal properties of the glass depending on the concentration of iodine and Tm. Structural studies were performed as well to explain the mechanisms responsible for the increase of solubility of Tm in the glass with the addition of iodine.

RÉSUMÉ DE L'ARTICLE INSÉRÉ

Le rôle d'iode dans la solubilité des ions de Tm^{3+} dans le verre As_2S_3

Ce travail étudie l'effet d'iode sur les propriétés de photoluminescence des ions de Tm^{3+} dans la matrice d'As_2S_3. Le rapport des concentrations de Tm et d'iode a été optimisé afin d'obtenir les meilleurs paramètres convenables pour le fibrage de ce système. L'effet de l'iode sur les propriétés fondamentales de verre dopé au Tm, y compris les caractéristiques optiques et thermiques, ont été explorées aussi. Les changements structuraux du système en fonction des concentrations d'iode et de Tm ont été explorés et corrélés avec caractéristiques de luminescence. En plus, on a été réussi à purifier la matrice hôte, par la méthode de distillation chimique, et à obtenir une fibre de haute pureté dopé aux ions de Tm^{3+}.

OPTICAL MATERIALS EXPRESS Vol. 6, No. 1 (2016) pp. 230-243

Article history:
Received 29 Oct 2015
Revised 18 Nov 2015
Accepted 26 Nov 2015
Published 21 Dec 2015

The Role of Iodine in the Solubility of Tm^{3+} Ions in As_2S_3 Glasses

A. Galstyan1,[1,*] S.H. Messaddeq,[1] I Skripachev,[2] T. Galstian[1] and Y. Messaddeq[1]

1. The Center for Optics, Photonics and Lasers (COPL), Laval University, 2375 rue de la Terrasse, Quebec, QC G1V 0A6, Canada
2. Institute of Chemistry of High Purity Substances of the Russian Academy of Sciences,49 Tropinin Str., Nizhniy Novgorod, 603950, Russia
**ani.galstyan.1@ulaval.ca*

Abstract: The effect of iodine (I_2) on the photoluminescence properties of Tm^{3+} ions in the As_2S_3 matrix was investigated. Results showed three strong emission bands at 1.22 µm ($^3H_5 \rightarrow {}^3H_6$), 1.46 µm ($^3H_4 \rightarrow {}^3F_4$) and 1.82 µm ($^3F_4 \rightarrow {}^3H_6$) under the excitation wavelength of 800 nm, indicating that I_2 enables the solubility of Tm^{3+} ions in As_2S_3 glasses. The concentration ratio of I_2 and Tm^{3+} were optimized and it revealed that increasing of the concentration of I_2 by 4 times in the glass increases the solubility of Tm ions three times. The effects of I_2 on the fundamental glass properties, including optical, thermal and structural characteristics, were explored as well.

OCIS codes: (160.0160) Materials; (160.5690) Rare-earth-doped materials

7.1. INTRODUCTION

One of the most interesting promises of chalcogenide glasses (ChG) is related to their capacity to be doped by rare-earth (RE) ions, with the aim to create new infrared (IR) radiation sources, lasers and amplifiers. The main advantage of ChG as a host matrix for RE ions is the low phonon energy (360–400 cm^{-1}) comparing with fluoride (580 cm^{-1}) or oxide (1100 cm^{-1}) glasses [162]. This enables many RE transitions in the near and middle IR regions, which are normally quenched in silica or fluoride glasses.

The primary criteria in the search of an appropriate ChG host for the above-mentioned applications are the transparency in the visible and near IR regions, small optical losses at the pump and emission wavelengths, good thermal stability allowing fiber drawing and sufficient solubility for the RE ions, which is an important factor for ensuring the efficiency of an amplifier or laser. The difficulties to combine all of the required properties in a single ChG restrain their use in practical devices. A variety of chalcogenide systems, based on arsenic [36,134], germanium [112,117,163], gallium [33,120-122] and their combinations [41,42,91,113,114,116,118,119,164,165] were considered as host glasses for RE ions. Some of them have poor thermal stability (Ge–Ga–S [3,164,165] and Ge–La–S [166]), others exhibit insufficient solubility for RE ions (As–S [36] and Ge-S [112]).

Among all ChG systems, As_2S_3 glasses were most extensively studied because of their high thermal stability, broad transparency window (up to 7 μm) and ease of fiber fabrication [60]. Several demonstrations of RE doped As_2S_3 glasses have been made [36,134], however, it was established that only very small amount of REs can be incorporated in this glass matrix before the microscopic clustering and appearance of ion-ion interaction. RE ions require a large coordination number and the insufficient quantity of non-bridging sulphur, needed to coordinate the isolated REs in the network of As_2S_3, causes the clustering of ions.

According to previous reports, there are some glass modifiers, namely some metals (Ga, In) [38,39,123,136,167], which enhance the solubility of RE ions in ChG. The increased solubility of RE is related to the fact that the incorporation of Ga (In)

provides compensation for the negative charge of free S^{2-} ions by forming chemical bonds with RE ions. The effect of Ga in the solubility of Tm^{3+} ions in the glass matrix of As_2S_3 is reported in ref [136]. As it was shown three strong emission bands at wavelengths of 1.22 μm ($^3H_5 \rightarrow {}^3H_6$), 1.46 μm ($^3H_4 \rightarrow {}^3F_4$) and 1.82 μm ($^3F_4 \rightarrow {}^3H_6$) were obtained in the infrared emission spectra of Tm with the addition of Ga into the host. However, the glass formation region is very small in Ga-As-S system and only up to 3.5at% of Ga can be incorporated into the matrix [127] without crystallisation, which on its turn limits the solubility of higher concentrations of RE ions. Besides, optical losses in the metal (Ga/In) based chalcogenides are enhanced due to the multiphonon absorption of metal-chalcogen bonds.

Some reports indicated that halides (I_2) [6,43,168,169] also can prevent the clustering of RE ions in ChG. Halide and chalcogenide glasses differ significantly in most aspects, including their methods of fabrication, basic glass and spectral properties. So, the incorporation of halogen elements into ChG (so-called chalcohalides) can reduce undesirable losses in the glass by mean of decreasing the number of metal-chalcogen bonds. This should lead to compromise between the improvement of optical properties and thermochemical instability incurred by the formation of weak metal-halogen bonds. Glass formation in I-As-S system was first reported by Flaschen et al. in 1960 [74]. The glass formation region is large, and glasses containing up to 33at% of I_2 were successfully prepared.

The goal of this work is the study of the role of I_2 in the solubility of RE ions in the As_2S_3 glass matrix and to obtain purified glass preform doped with RE ions. Different compositions of I-As-S glasses were used as host matrices for Tm^{3+} ions in order to find the optimal concentration ration of I_2 and Tm for obtaining the highest possible luminescence efficiency. The effects of I_2 and Tm on the optical, thermal, structural and photoluminescence properties of the glass are also investigated. In order to improve the optical quality of the glass matrix, a distillation of the glass matrix, with the optimal concentration of constituents, was performed under high vacuum and a Tm^{3+} doped high purity glass was produced.

7.2. EXPERIMENT

Glass synthesis: Tm^{3+} doped I-As-S bulk glasses were fabricated using the pre-purified As_2S_3 glass, solid iodine and metallic Tm^{3+}. Traditional melt quenching method was applied. Glasses were synthesized in quartz ampoules sealed under high vacuum (10^{-5} Torr). The synthesis was carried out at the temperature of 750°C for 12 hours, and the glasses were cooled down with air. Samples were annealed at 130-160°C (depending on glass transition temperature) for 6 hours to remove the thermal stress. The glass rods were then cut into disks and polished with an abrasive silicon carbide disc to obtain flat and transparent bulk glasses.

Purification of glass matrix: ChG purification is performed in special furnace in a series of dynamic distillations under high vacuum. Our purification system consisted of three interconnected ampoules: reactor, receiver and trap (Fig.7.1).

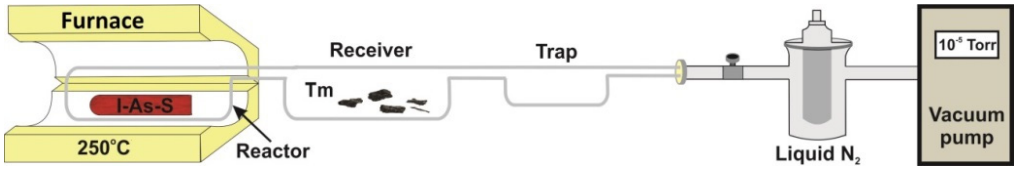

Fig. 7.1. Setup of glass purification

First, the glass matrix (without Tm) with desired chemical composition was prepared separately (at 600°C), loaded into the reactor and placed in the furnace. The Tm^{3+} was loaded in the receiver ampoule and maintained at room temperature. The system was attached to the high vacuum pump. The purification procedure included melting the I-As-S matrix at 250°C, followed by vacuum distillation of the melt. Extracted impurities condensed in the trap. Afterwards the receiver ampoule was sealed from both sides. Then the purified glass melt with Tm was homogenized in a rocking furnace at 750°C.

Characterisation: The emission spectra of Tm^{3+} doped I-As-S glasses were collected with a Horiba Jobin Yvon NanoLog 3-22-TRIAX spectrofluorometer. The samples were excited at 800 nm wavelength with a 450 W continuous xenon lamp connected to a computer controlled monochromator. The luminescence spectra were measured with a Symphony II CCD detector operating in the infrared spectral region

ranging from 1000 nm to 2200 nm. Fluorescence lifetime measurements were also performed with a NIR PMT single channel detector with 1000 - 1700 nm wavelength range. The fluorescence decay curves were fitted with a first-order exponential decay to extract the emission lifetimes.

The IR transmission spectra from 1 to 20 μm were measured with a Perkin Elmer Frontier FT-IR/FIR Spectrometer using the factory-supplied MIR source and MIR TGS detector combination.

The refractive index was measured with a Metricon 2010/M prism coupler for different wavelengths (633 nm, 972 nm, 1308 nm and 1538 nm). The prisms 200-P-5 and 200-P-6 were used for these measurements. The measurement error was about ±0.003.

The glass transition temperature (T_g) was measured with a Netzsch 404 F3 Pegasus differential scanning calorimeter (DSC). A 20 mg glass sample was placed in the aluminium crucible and heated up to 300 °C (10°C/min ramp) and the heat flow was compared with that of an empty crucible. The measurement error was ±2°C.

The coefficient of linear thermal expansion of the samples was measured with Netzsch 402 F1 Hyperion thermomechanical analyser. The samples (with the diameter of 10 mm and height of 6mm) were brought into contact with push rod of fused silica, inserted in the furnace and heated up to 200°C with controlled temperature program. The length change in the sample was measured as a function of temperature by a highly sensitive inductive displacement transducer via a push rod. The measurement error was $\pm 0.05 \cdot 10^{-6}$ 1/°C.

The viscosity of glasses in the softening range was measured with Bansbach Easylift Theta US parallel plate high temperature viscometer. The disk of glass (with about 10 mm diameter and 6 mm height) is sandwiched between two parallel silica plates inside a well-insulated furnace. The samples were heated up to 300°C at a heating rate of 5°C/min, under the compressive load of 300 mg. By means of recording the rate of the thickness change of the sample as a function of time (using a linearly variable differential transformer (LVDT)), the logarithm of viscosity is calculated by DilaSoft I program. The estimated error was about ±3°C on the temperature values and $\sim 10^{\pm 0.2}$ Poise on the viscosity values.

The X-ray diffraction (XRD) spectra of the glass samples were obtained with a Siemens D5000 X-ray diffractometer. The X-ray source was made of a Cu anode and emitted at a wavelength of 1.54 Å. XRD data were collected in reflection mode with Theta-Theta configuration (2Theta step = 0.02°, time step = 1.2 s) using a NaI scintillation counter detector. It was processed with the JADE 2.1 software based on the JCPDS database of International Centre for Diffraction Data (ICDD).

The Raman spectra were collected with a Renishaw inVia spectrometer coupled a Leica DM2700 microscope. A back-scattering geometry was used in the frequency range of 100-600 cm^{-1}. The excitation light source was vertically polarized He-Ne laser with 633 nm wavelength and 17 mW power. The laser beam was focused with a 50X long working distance objective, generating a sub-micron spot size containing a total power at the sample of approximately 5-10mW. The frequency uncertainty was estimated to be ± 2 cm^{-1}. The deconvolution of Raman spectra were performed using curve fit function of Wire 4.1 software.

7.3. RESULTS

7.3.1. PHOTOLUMINESCENCE OF Tm^{3+} IN I-As-S MATRIX

As it is known from our previous work [136], no emission of Tm^{3+} ions was observed in the As_2S_3 glass matrix. The luminescence spectra of Tm^{3+} doped I-As-S glasses for excitation wavelength of 800 nm are presented in Fig. 7.2. As it can be seen, the presence of I_2 enables the solubility of Tm^{3+} ions in the As_2S_3 matrix. Three emission bands centered at 1.22 μm, 1.46 μm and 1.82 μm were observed in the spectra, corresponding to the optical transitions $^3H_5 \rightarrow {}^3H_6$, $^3H_4 \rightarrow {}^3F_4$ and $^3F_4 \rightarrow {}^3H_6$, respectively (Fig. 7.2b) [37,170].

In order to find the maximal content of I_2 that can be incorporated in the glass matrix of As_2S_3 to improve the Tm^{3+} emission properties, the concentration of I_2 was gradually increased up to 15 at%, maintaining the S/As ratio equal to 1.5 (as in As_2S_3). The content of Tm^{3+} ions was fixed to 1 at% (presented atomic percentages are calculated). The emission properties of I-As-S glasses depending on the I_2 concentration are presented in fig. 7.2a. With the increasing of I_2 concentration from

2.5 to 10%, the intensity of luminescence gradually increased for all three emission bands. At 15% the intensity decreased. It was thus concluded that ratio I_2/Tm^{3+} equal to 10:1 corresponds to the maximum ratio to improve the solubility of Tm ions in the glass.

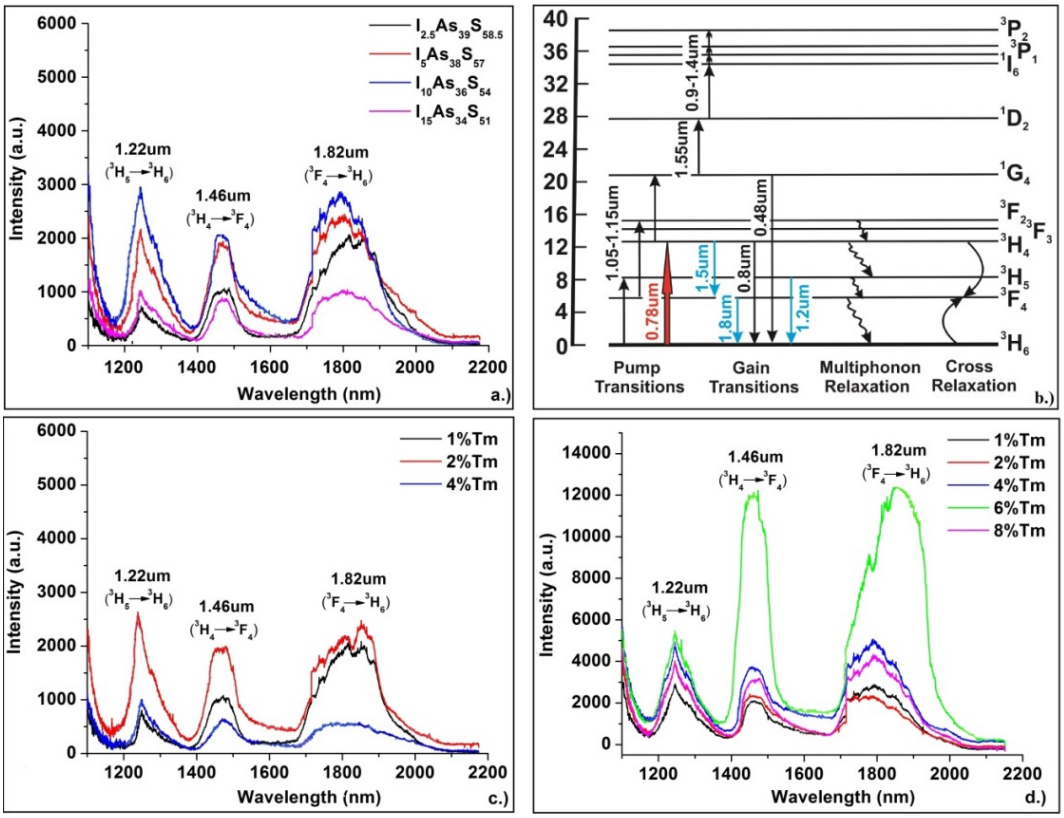

Fig. 7.2. Emission spectra of Tm^{3+} doped I-As-S glasses a.) 1%Tm doped I-As-S glasses; b.)Tm^{3+} energy levels diagram c.) Tm doped $I_{2.5}As_{39}S_{58.5}$ glasses; d.) Tm doped $I_{10}As_{36}S_{54}$ glasses (excitation at 800 nm)

To find the limit of solubility of Tm ions in the I-As-S system (depending on the content of I_2 in the glass), two glass compositions with low and high content of I_2, namely $I_{2.5}As_{39}S_{58.5}$ and $I_{10}As_{36}S_{54}$, were chosen as host matrices for Tm ions. The luminescence spectra of Tm^{3+} doped $I_{2.5}As_{39}S_{58.5}$ and $I_{10}As_{36}S_{54}$ glasses depending on Tm concentration are presented in the figures 7.2c and 7.2d, respectively. As we can see in $I_{2.5}As_{39}S_{58.5}$ glass matrix the maximum intensity is observed for 2at%Tm, so we can suppose that the solubility of Tm is limited to 2 at.% since above the 4%Tm

the intensity of luminescence decreased. Contrariwise, in the $I_{10}As_{36}S_{54}$ matrix the highest photoluminescence efficiency reached at 6 at% of Tm.

With increasing the amount of Tm up to 8% we can note that the intensity of emission decreased, indicating that the limit of solubility of Tm ions in this matrix is about 6%. From these results, we can conclude that the increasing of the concentration of I_2 by a factor of 4 in the As_2S_3 glass matrix increases the solubility of Tm ions three times.

The fluorescence lifetimes of Tm^{3+} doped I-As-S glasses for excitation wavelength of 800 nm were measured, and no substantial changes have been obtained depending on the concentration of I_2 and Tm. The lifetime of emission band at 1.22μm band is about $1{,}8 \cdot 10^{-5}$ sec. and at 1.46μm it is about $7{,}9 \cdot 10^{-5}$ sec. The measurement error was about $\pm 0.1 \cdot 10^{-5}$ sec.

As the glass matrix $I_{10}As_{36}S_{54}$ has enhanced RE ions solubility, preserving good optical properties, further characterisations (optical, thermal and structural) are presented hereafter for this glass matrix as a function of Tm concentration.

7.3.2. OPTICAL PROPERTIES

The infrared transmission spectra of Tm^{3+} doped I-As-S glasses as a function of the concentration of I_2 and Tm are shown in Fig. 7.3a and 7.3b, respectively. The spectrum of un-doped and purified As_2S_3 glass is presented for comparison. The maximum transmission of I-As-S glasses is lower than that of As_2S_3, but the increase of I_2 concentration in I-As-S leads to the increase of maximum transmission of glass and broadens the transmission range up to 9 μm (Fig. 7.3a).

As it can be seen from Fig. 7.3b the increase of Tm concentration in the $I_{10}As_{36}S_{54}$ glass leads to the decrease of maximum transmission of the glass. The absorption bands observed in the spectra of the doped glasses are attributed to impurities coming from traces of oxygen and hydrogen and they are assigned to S-H (3.96 um), O-H (3.06um), H_2O (6.62um) and As-O (10.1um) [92]. This is due to the fact that the doped glasses were synthesized using commercial chemical products and have not been additionally purified during the preparation.

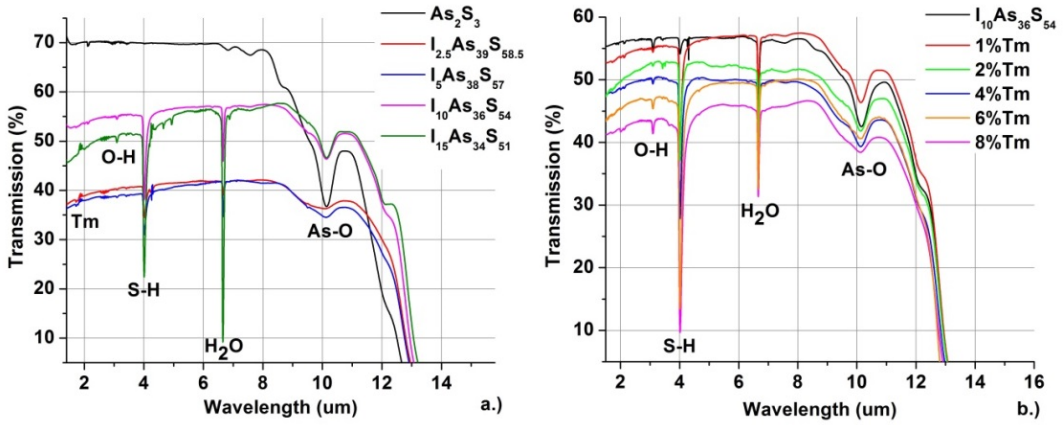

Fig. 7.3. IR transmission spectra of Tm doped I-As-S glasses a.) 1%Tm doped I-As-S glasses; b.) Tm doped $I_{10}As_{36}S_{54}$ glasses (thickness is 2mm)

Dependence of the refractive indices of Tm doped I-As-S glass on the concentration of I_2 and Tm are presented in Fig. 7.4a and 7.4b, respectively. The incorporation of I_2 in the As_2S_3 glass matrix and the increase of its content up to 15% gradually decreased the refractive index (fig. 7.4a). Contrariwise, the increase of the concentration of Tm increased the refractive index (fig. 7.4b). For 8%Tm the refractive index increased by ~0.1 compared with the host matrix $I_{10}As_{36}S_{54}$.

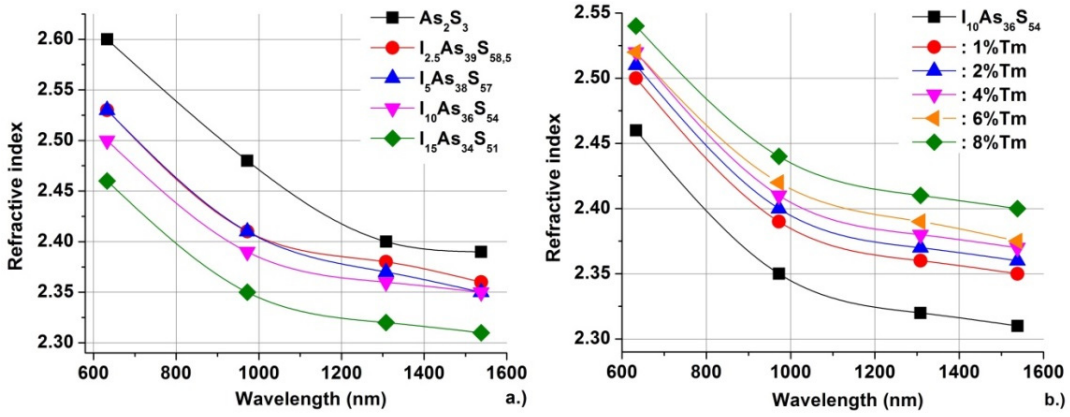

Fig. 7.4. Refractive index of Tm doped I-As-S glasses a.) 1%Tm doped I-As-S glasses; b.) Tm doped $I_{10}As_{36}S_{54}$ glasses (error ±0.003)

7.3.3. THERMAL PROPERTIES

Figures 7.5a and 7.5b show the glass transition temperature (T_g), and the coefficient of thermal expansion (α) of Tm^{3+} doped I-As-S glasses versus the content of I_2 and Tm, respectively. The addition of I_2 in the As_2S_3 matrix and the increasing

of its concentration gradually decreased the T_g of glass from 200°C to 114°C. Simultaneously, the coefficient of thermal expansion increased from $21.4 \cdot 10^{-6}$ to $39.5 \cdot 10^{-6}$. On the other hand with the increase of Tm content up to 8% in the matrix $I_{10}As_{36}S_{54}$ the T_g gradually increases (Fig. 7.5b) from 133°C to 150°C. Meanwhile, the coefficient of thermal expansion decreased from $33.9 \cdot 10^{-6}$ to $28.8 \cdot 10^{-6}$.

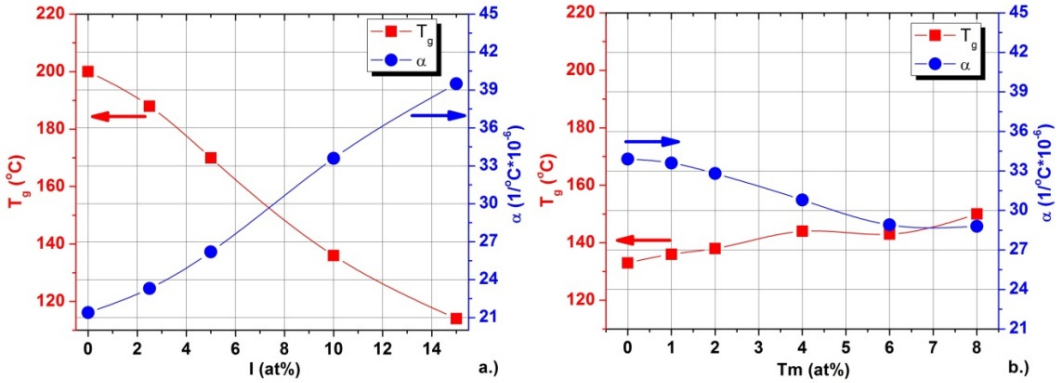

Fig. 7.5. Glass transition temperature and coefficient of thermal expansion of Tm doped I-As-S glasses a.) 1%Tm doped I-As-S glasses; b.) Tm doped $I_{10}As_{36}S_{54}$ glasses (T_g error is ±2°C, α error is $\pm 0.005 \cdot 10^{-6}$ 1/°C)

Figure 7.6 presents the viscosity-temperature curves of Tm^{3+} doped I-As-S glasses in the glass softening range depending on the concentration of I_2 and Tm. It may be seen that the extrusion viscosity of As_2S_3 is about $10^{10.3}$ Poise at 234°C. With the increase of the content of I_2 in the glass the viscosity-temperature curves have tended to shift gradually to a lower temperature and at 15%I_2 the temperature of extrusion viscosity decreases up to 139°C (Fig. 7.6a). From these data it follows that at equal temperatures the viscosity of I_2 based glasses is considerably less than that of As_2S_3. In a similar way, the addition of Tm began to increase the temperature of extrusion viscosity and for 8%Tm it reached to 190°C, compared with $I_{10}As_{36}S_{54}$ matrix (152°C) (fig. 7.6b).

Generally it is established that the suitable viscosity at which the fiber can be drawn is in the range of $10^{6.5}$-$10^{5.5}$ Poises, so to find the temperature of fiber drawing for this system, the viscosity data were extrapolated into the range up to 10^5 Poise, as shown in Fig. 7.6. It revealed that the addition of up to 15%I_2 in the As_2S_3 glass decreases the fiber drawing temperature by nearly 90°C. In contrast, the incorporation

of up to 8%Tm increased the fiber drawing temperature of $I_{10}As_{36}S_{54}$ glass matrix by 35°C.

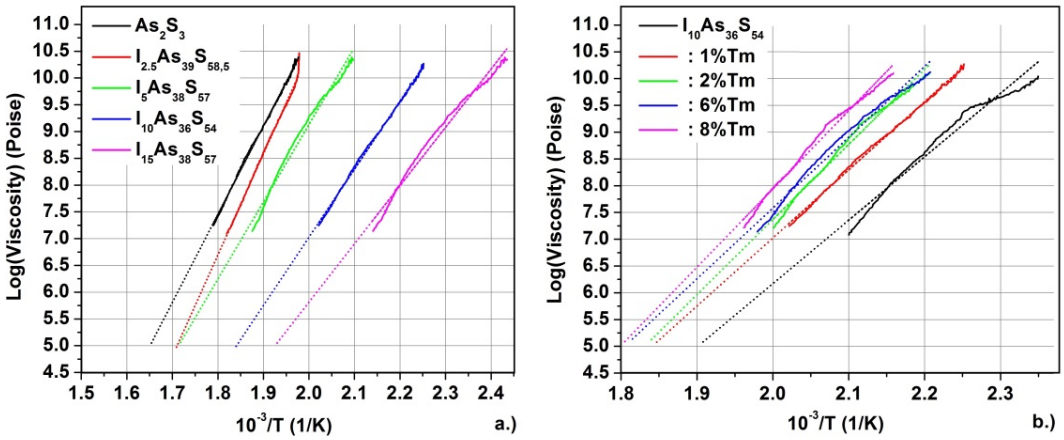

Fig. 7.6. Viscosity vs. inverse of absolute temperature for Tm doped I-As-S glasses in the softening range a.) 1%Tm doped I-As-S glasses; b.) Tm doped $I_{10}As_{36}S_{54}$ glasses

Considering the linear relation between the log(η) and temperature (1/T), the activation energy was calculated by the following equation [171]:

$$\Delta E = Rd(\log \eta) / d(1/T) \qquad (1)$$

where R is the gas constant. The results are presented in Table 7.1. The obtained activation energy of As_2S_3 glass is equal to 32.72kcal/mole and with the addition of 2.5%I_2 and 1%Tm in As_2S_3 it increases up to 37.59kcal/mole. However, the further increase of the content of I_2 decreases the activation energy up to 21.6kcal/mole (at 15%I). Similarly, the activation energy of $I_{10}As_{36}S_{54}$ matrix (M) is equal to 23.53kcal/mole and upon the addition of Tm (up to 8%) it increased gradually up to 29.04kcal/mole. This may indicate that at 2.5%I_2 the contribution of 1%Tm on the properties of As_2S_3 is more significant compared to I_2, which lead to the increase of activation energy.

Composition	Activation energy (kcal/mole)	Composition	Activation energy (kcal/mole)
As_2S_3	32.72	$I_{10}As_{36}S_{54}$ (M)	23.53
$I_{2.5}As_{39}S_{58.5}$ (:1%Tm)	37.59	(M) :1%Tm	25.27
$I_5As_{38}S_{57}$ (:1%Tm)	28.65	(M) :2%Tm	27.86
$I_{10}As_{36}S_{54}$ (:1%Tm)	25.27	(M) :6%Tm	28.48
$I_{15}As_{34}S_{51}$ (:1%Tm)	21.63	(M) :8%Tm	29.04

Table 7.1: Activation energy of Tm doped I-As-S glasses vs content of I_2 and Tm^{3+}

7.3.4. STRUCTURAL PROPERTIES

To understand which kind of structural changes occur in the As_2S_3 glass matrix by the incorporation of I_2 and which mechanisms are responsible for the luminescence of Tm^{3+} ions, structural studies were done on I-As-S system using X-ray diffraction (XRD) and Raman spectroscopy.

The XRD patterns recorded for Tm^{3+} doped I-As-S glasses are presented in Fig. 7.7. The patterns associated to 1%Tm doped I-As-S samples reveal broad diffraction lines indicating an amorphous character (Fig. 7.7a). Figure 7.7b shows the XRD spectra of Tm^{3+} doped $I_{10}As_{36}S_{54}$ glasses depending on Tm concentration. As it can be seen the samples having ≤6at%Tm are completely amorphous (no apparent crystallization). However, for the concentration of Tm =8at% small diffraction peaks, assigned to Tm_2S_3 crystalline phase (JCPDS card No. 44-1157), arise from the broad vitreous profile, which provide evidence in the favour of partial crystallisation of the glass at higher Tm concentrations.

Raman spectra (normalized at 342 cm^{-1}) of 1%Tm^{3+} doped I-As-S glasses depending on I_2 concentration are presented in Fig. 7.8. From the Raman spectra of As_2S_3 glass (Fig. 7.8a) we can observe 2 main bands centered at 342 cm^{-1} and 495 cm^{-1}. The most intense broad band, centered at 342 cm^{-1}, is assigned to the symmetric stretching vibrational modes of [$AsS_{3/2}$] regular pyramids [140-143]. The band at 495 cm^{-1} is associated to vibrational mode of S-S bridges in S_2As-S-S-AsS_2 fragment [140,143,144].

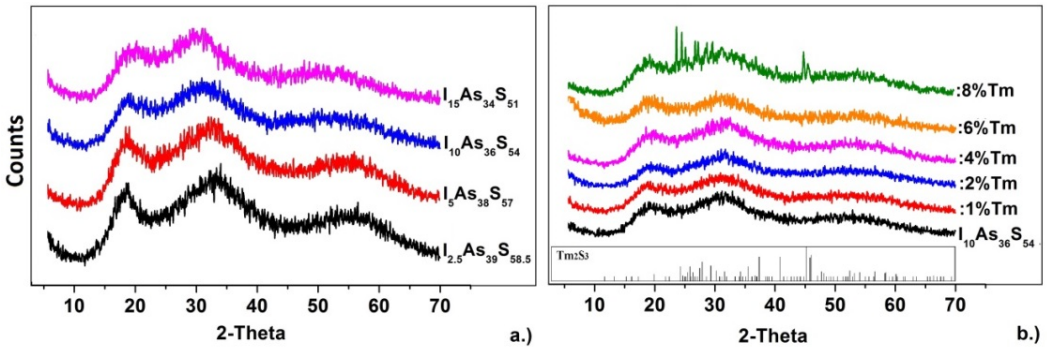

Fig. 7.7. X-ray diffraction spectra of Tm doped I-As-S glasses
a.)1%Tm doped I-As-S glasses; b.) Tm doped $I_{10}As_{36}S_{54}$ glasses

The addition of I_2 to As_2S_3 gives rise to two bands centered at 188 cm^{-1} and 211 cm^{-1}, (fig.7.8a). Besides, with the incorporation of I_2 the band at 495 cm^{-1} increases. The band centered at 188 cm^{-1} is attributed to the Tm-S bond (inset in Fig. 7.8a). According to Khiminets et al. the band at 210 cm^{-1} is assigned to stretching vibration of $IAsS_{2/2}$ groups [172]. They investigated the Raman spectra of quasibinary join AsI_3-As_2S_3 of the ternary As-S-I system and suggested that the incorporation of AsI_3 in the matrix of As_2S_3 leads to the formation of $IAsS_{2/2}$-$S_{2/2}AsI$ type of molecules, so called twisted chain structure. Whereas, Koudelka et al. propose that the band at 208cm^{-1} in the Raman spectra of $As_{40-x}S_{60}I_x$ glasses is assigned to symmetrical stretching vibration of discrete AsI_3 pyramidal molecules [173], claiming that the formation of discrete molecules is more favourable due to the low total energy of the system with symmetric groups (AsI_3, As_2S_3 and S_8 rings). They assumed that the structure is composed of $AsS_{3/2}$ pyramidal units mixed with dissolved units of AsI_3 and S_8. In these Raman data no S_8 ring (band at 475 cm^{-1}) was observed. With the addition of I_2 we observed only an increase of 495 cm^{-1} band (S-S bridges) accompanied by a decrease of the band at 342 cm^{-1} (showing a dissociation of $AsS_{3/2}$ pyramidal units). Hence, we associate the band at 211 cm^{-1} to $IAsS_{2/2}$ units. The same twisted chain structure has been proposed by Hopkins et al. [174] when studying the structure of the I-As-S system by X-ray diffraction, showing that arsenic is coordinated to two sulphur atoms and one iodine atom on average.

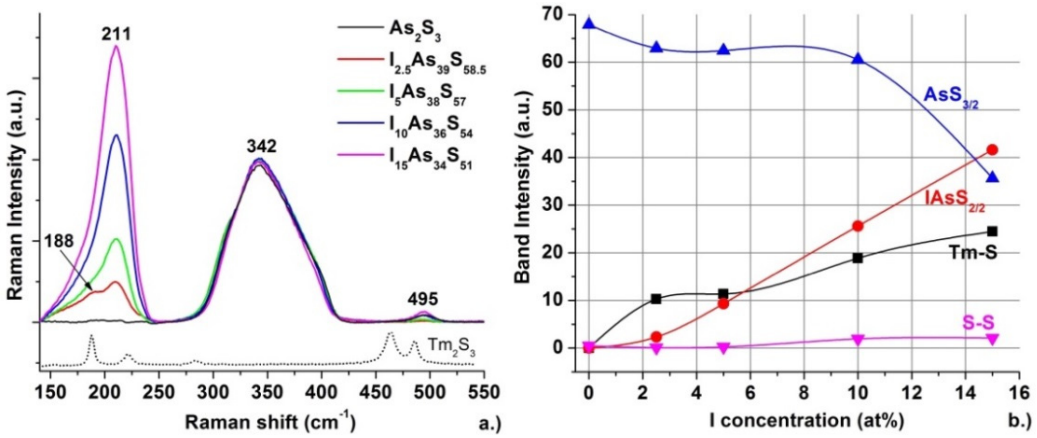

Fig. 7.8. a.) Raman spectra of 1%Tm^{3+} doped I-As-S glasses, b.) Raman bands intensities vs concentration of I_2

In order to understand the role of the addition of I_2 on the solubility of RE into the matrix of arsenic sulphide, the Raman spectra of studied glasses were deconvoluted with Gaussian peaks using least squares approach. The intensity of each band was calculated by integrating the surface of the corresponding peak for all Raman modes present in the spectra. The resulting structural trends for each assigned structural units depending on I_2 contents are presented in Fig. 7.8b. It can be seen that the band corresponding to the symmetric stretching of [$AsS_{3/2}$] pyramids (342cm^{-1}) decreases with the addition of I_2 in the matrix, whereas the band assigned to $AsIS_{2/2}$ structural units (211 cm^{-1}) significantly increases in amplitude. Simultaneously, the bands at 188 cm^{-1} (Tm-S) and at 495 cm^{-1} (S-S) increase with the increase of the I_2 concentration.

Figure 7.9a and 7.9b show Raman spectra (normalized at 342 cm^{-1}) of Tm doped $I_{10}As_{36}S_{54}$ glasses and intensities of observed bands depending on Tm concentration (1-8 at.%). As we can see AsS_3 pyramids stay almost intact upon the increase of Tm concentration up to 4%, whereas the band 188 cm^{-1} (Tm-S) continues to increase slightly, simultaneously leading to a decrease of 495 cm^{-1} (S-S). At higher concentration of Tm (>4 at.%) it seems that the intensity of Tm-S band reaches saturation. However the band $IAsS_{2/2}$ begins to decrease, and meanwhile an increase of AsS_3 bands is observed.

We expected that the dissociation of $IAsS_{2/2}$ units and the reformation of AsS_3 pyramids should lead to the formation of Tm-I linkages. The formation energy of

TmI_3 (0.477eV/atom (OQMD ID: 347708)) is much lower comparing to the formation energy of Tm_2S_3 (2.262eV/atom (OQMD ID: 23780)), so the formation of Tm-I bonds should be more advantageous. However no band associated to Tm-I (168 cm^{-1}, inset in Fig 7.9a) was detected in the Raman spectra by deconvolution. Probably this band is small and just overlapped with the stronger bands at 188cm^{-1} and 211 cm^{-1}. This can be explained with the fact that the formation of Tm-S bonds is more favourable in these glasses because of the much smaller atomic masse of S compared to I_2. Additionally, we may note that the higher noises obtained in Raman spectra of TmI_3 are related to the lower melting temperature of this compounds. The bands at 310 cm^{-1} and 380 cm^{-1} (Fig. 7.9a) included in the deconvolution of spectra correspond to interactions among the $AsS_{3/2}$ pyramids [140].

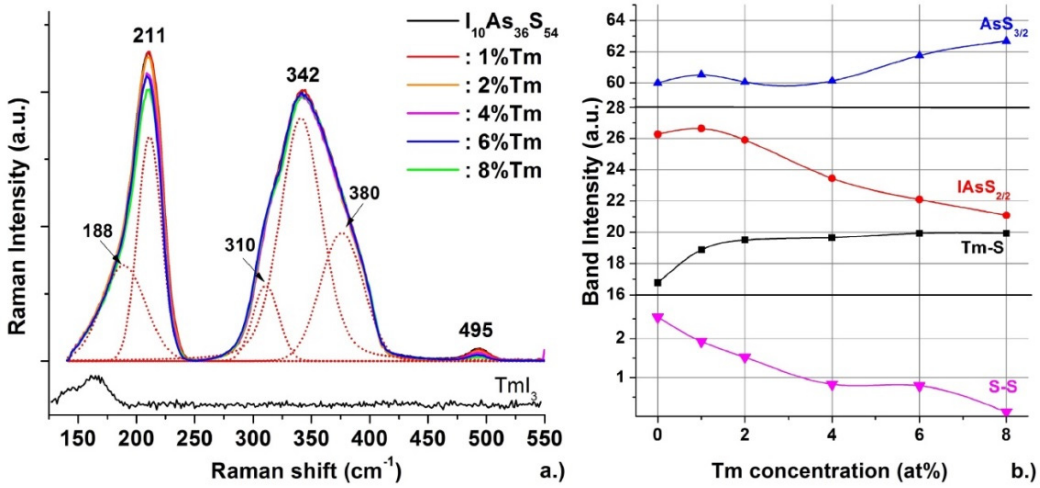

Fig. 7.9. a.) Raman spectra of Tm^{3+} doped $I_{10}As_{36}S_{54}$ glasses (dash lines represent deconvoluted curves) b.) Raman band intensities vs concentration of Tm

7.3.5. PURIFICATION OF Tm^{3+} DOPED I-As-S GLASS

One of the key requirements of chalcogenide materials is purity, because it has decisive effect on their application. Hydrogen, oxygen, carbon and other impurities considerably reduce the transmission of chalcogenide glasses especially in middle infrared spectral region, which prevent their applications. Besides, the presence of OH^- complex in the glass has an important implication in the luminescence efficiency of RE ions [175]. At high OH^- concentrations, a direct energy transfer occurs from

the excited ion to OH^-, which has adverse effect on luminescence properties of the glass. So the purification of glass matrix is one of the most important steps in the procedure of fabrication of doped glasses.

Based on above shown results, the 2%Tm^{3+} doped $I_{10}As_{36}S_{54}$ glass composition was chosen for performing an additional purification to improve the quality of the glass matrix. Figure 7.10 shows the infrared transmission spectra of above mentioned bulk glass synthesized with as-received chemicals and with purified matrix. As it can be seen with only one distillation cycle the impurity losses, attributed to the fundamental S-H vibrational (3.96 μm), S-H combinational (3.78 μm) [176] and H_2O vibrational (6.62 μm) bands, are dramatically decreased in the glass. Additionally, the transparency of the purified glass is improved comparing to the non-purified.

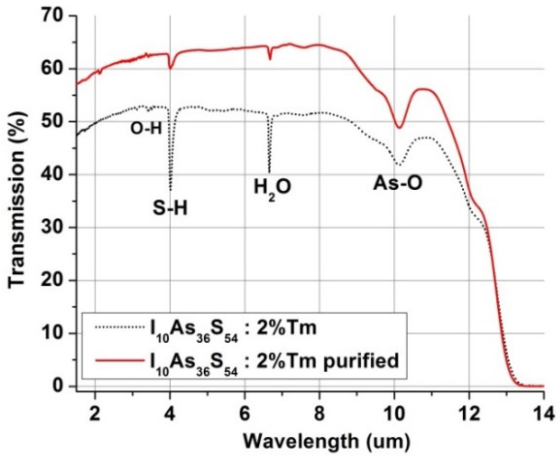

Fig. 7.10. Infrared transmission spectra of 2%Tm^{3+} doped $I_{10}As_{36}S_{54}$ glass before and after purification

It is known that the luminescence efficiency and the emission lifetime of RE ions in the glass strongly depend on the concentration of OH-groups in the matrix [175,177]. Since initially the concentration of OH-group was small in the matrix (Fig. 7.10), the additional purification did not change luminescence properties of this glass. The same intensity and the lifetime of emission of Tm^{3+} have been obtained for non-purified glass and the glass with purified matrix (not presented).

Previous study presented by our group [136] indicates that Ga can dissolve Tm^{3+} ions in the matrix of As_2S_3 as well. However, the drawback of the Ga based chalcogenide glasses is the required high reaction temperature and long synthesis procedure, due to the low reactivity of Ga with sulphur. Also, Ga_2S_3 compound

cannot be distillated during the glass purification, because of its high melting point (1090°C) and therefore it leads to the contamination of the sulphide with impurities originating from the walls of the ampoule. In contrast, the low melting temperature of I_2 (113.7°) makes the purification of the raw materials (pre-processing) and the glass purification (post-processing) easier with less consuming time.

So we can conclude that I_2 can completely replace Ga because of its sufficient solubility for the RE ions, larger transparency region in IR, sufficient thermal stability for fiber drawing and promising way to decrease optical loses in these glass matrices.

7.3.6. EMISSION PROPERTIES OF Tm^{3+} DOPED I-As-S GLASS FIBER

The chalcogenide glass fiber was drawn using the pull from preform method. 2%Tm^{3+} doped $I_{2.5}As_{39}S_{58.5}$ composition was chosen for the fiber fabrication, since we did not succeed to obtain a fiber with a good quality using preforms with higher concentrations of iodine. A fiber with ~250um diameter was obtained.

We measured the amplified spontaneous emission (ASE) spectrum generated by this fiber. The setup used for this experiment is shown in Fig. 4.2. The emission spectrum of the fiber is presented in Fig. 7.11. It was recorded at a spectral resolution of 2 nm and was averaged over 5 independent measurements. Three emission bands are clearly seen ($^3H_5 \rightarrow {}^3H_6$ around 1.2 μm, $^3H_4 \rightarrow {}^3F_4$ around 1.4 μm and $^3F_4 \rightarrow {}^3H_6$ around 1.8 μm) which is consistent with the fluorescence observed in the bulk samples with an excitation wavelength near 800 nm.

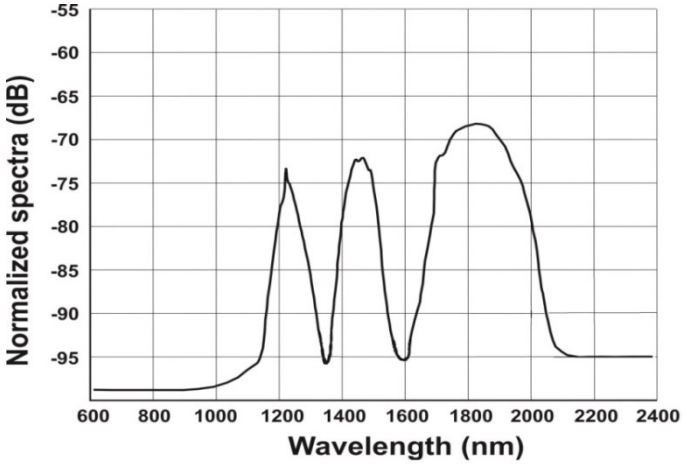

Fig. 7.11. Emission (ASE) spectra of 2%Tm^{3+} doped $I_{2.5}As_{39}S_{58.5}$ fiber (excitation at 789 nm)

7.4. DISCUSSION

First we will discuss the structure of Tm doped I-As-S glasses. Based on the Raman spectra of As_2S_3 glass the three-dimensional network of As_2S_3 glass can be interpreted using trigonal pyramidal units [$AsS_{3/2}$], which are interconnected through As-S-S-As bridges. With the incorporation of I_2 the $AsS_{3/2}$ pyramidal units are disassociated by means of the formation of As-I bonds, which lead to the formation of $AsIS_{2/2}$ structural units. Hence, we can suppose that our system mostly consists of the AsS_3 pyramids mixed with $AsIS_{2/2}$ twisted chains as it is schematically presented in Fig. 7.12. This network configuration provides sufficient number of non-bridging sulphur for coordinating Tm ions in the rigid network of As_2S_3, which leads to the increase of the solubility of Tm ions in the glass. As we can see from Fig. 7.8b, the S-S bonds increase more slowly compared with $AsIS_{2/2}$ and Tm-S bonds, showing that the large part of non-bridging sulphur was bonded with Tm.

When the content of I_2 reaches 15% the intensity of $AsIS_{2/2}$ band become higher than that of $AsS_{3/2}$ (Fig. 7.8b), showing that the structure consists of more twisted chains than polymeric pyramids. This probably leads to the degradation of some fundamental properties of As_2S_3 glass, incurred by the formation weak metal-halogen bonds, which may cause the decrease of the luminescence of the Tm at 15at% of I_2.

With the increase of Tm up to 6% the intensity of Tm-S band continues to increase (see Fig. 7.9b), showing that more Tm-S bonds are formed in the glass leading to an increase of luminescence. At higher concentrations of Tm (>6 at.%) the formation of Tm-S bonds seems to reach saturation and luminescence intensity decreases (Fig. 7.1d). So we can assume that at 8at% of Tm^{3+} the ions begin to cluster because of the insufficient quantity of non-bridging sulphur atoms. Therefore, the mean distance between Tm^{3+} ions in the lattice becomes small enough so the transfer of excitation energy to neighbouring ions becomes possible, which depopulates the excited states, leading to the decrease of the emission intensity.

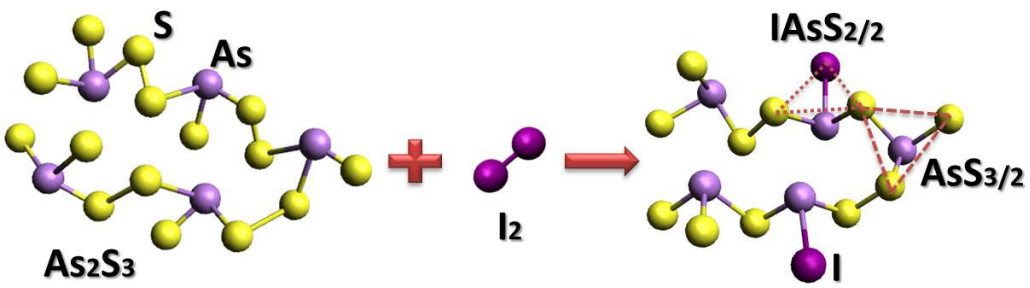

Fig. 7.12. Schematic representation of structural units formed in As_2S_3 glass with incorporation of I_2

According to Hooke's law, the frequency of bond vibration is inversely proportional to the atomic mass of elements in the glass. The incorporation of I_2 and Tm (with much higher atomic masses comparing to As and S) results in a decrease in the frequency of bond vibration and therefore, the long-wavelength cut-off edge of transmission increases (Fig. 7.3a). Usually, the lower transmission is caused by the presence of inhomogeneities or the formation of structural defects (for example As-As or Tm-Tm homo-polar bonds) in the glass. We can suppose that the incorporation of 1%Tm in the $I_{2.5}As_{39}S_{58.5}$ matrix has created some structural defects in the glass leading to the decrease of transmission (Fig. 7.3a). This could be explained by the fact that the contribution of Tm clusters in the properties of this composition is more significant comparing to I_2, since the 2.5at%I is not enough to provide sufficient content of non-bridging sulphur for the dissolution of Tm ions. The higher activation energy of 1%Tm doped $I_{2.5}As_{39}S_{58.5}$ glass is due to the same reason (Table 7.1). However, the increase of I_2 content reduces the number of As-S bonds (responsible for higher absorption coefficient), by forming As-I bonds, and simultaneously supplies the sulphur necessary to form Tm-S hetero-bonds, leading to the formation of more homogeneous glass with less structural defects. This leads to the increase of the maximum transmission of the glass. The decrease of transmission of $I_{10}As_{36}S_{54}$ with the further increasing of Tm concentration (Fig. 7.3b) in the glass is related to the formation of Tm_2S_3 crystals in the glass, as it is shown in Fig. 7.7b.

The introduction of halogen promotes the dissociation of the As-S structure favouring the destruction of the compact character of the glass network of As_2S_3, which may result in the decrease of its density [178], despite the higher atomic mass

of I_2 compared with sulphur and arsenic. This leads to the decrease of refractive index of the glass (as well as the viscosity) with the increase of I_2 concentration (Fig. 7.4a). In agreement with the classical dielectric theory, the refractive index depends on the density and the polarizability of atoms in a given material. According to the Lorenz-Lorenz relation [179] larger is the atomic radius of the atom, larger will be its polarizability and consequently larger will be the refractive index (Fig. 7.4b). So in our case the increase of Tm concentration probably increases the polarizability [180] of the glass matrix, due to its much larger atomic radius leading to the increase of the refractive index.

It is known that in As_2S_3 glasses As-S bond strength is about 90.7 kcal/mole [181], and the incorporation of I_2 in the glass eliminates the As from S-As-S bonds through the formation of As-I (70.9 kcal/mole) [181] and S-S (33 kcal/mole) lower strength bonds [60], which leads to the decrease of bonding strength of the glass and therefore of the T_g. The atomic distance As-S is about 2.28Å [157], whereas the As-I distance is about 2.45Å [178] so the formation of As-I bonds in the glass network causes a deformation of the layer structure and an expansion of interlayer distance. Consequently, it becomes easy for the glass to expand thermally.

7.5. SUMMARY

The incorporation of I_2 in the network of As_2S_3 glasses increase the solubility of Tm^{3+} ions, through the dissociation of $AsS_{3/2}$ pyramidal units and the formation of As-I bonds, which provides non-bridging sulphur for RE ions. Three strong emission bands of Tm^{3+} ions at wavelengths around 1.2 μm ($^3H_5 \rightarrow {}^3H_6$), 1.4 μm ($^3H_4 \rightarrow {}^3F_4$) and 1.8 μm ($^3F_4 \rightarrow {}^3H_6$) were observed under the excitation by a lamp at 800 nm. The increase of the concentration of I_2 by a factor of 4 in the glass increases the solubility of Tm ions three times. We have determined the best concentration ratio of elements in the glass to produce optimal physical, optical and thermal properties of the glass for achieving high stability, high luminescence efficiency and low losses.

We think that for the fabrication of efficient and compact sources of laser radiation operating in near infrared region, the RE doped I-As-S glass fiber can be considered as a serious contender.

ACKNOWLEDGEMENTS

The authors would like to thank the Canadian Excellence Research Chair program (CERC) on Enabling Photonic Innovations for Information and Communication for their financial support. The Natural Sciences and Engineering Research Council of Canada (NSERC) and the Canada Foundation for Innovation (CFI) agencies are also acknowledged. The work was performed according to collaboration in the frame of project of Russian Scientific Foundation RSF No. 15-12-200400.

CHAPTER 8
CONLUSION AND FUTURE WORKS

The results obtained in this thesis can be divided into two parts. The first part is devoted to the investigation of the influence of Ga on the solubility of Tm ions in As_2S_3 glass. One of the main achievements is the production of Tm^{3+} doped Ga-A-S glasses with different concentration of Ga and Tm^{3+}. The Ga/Tm concentration ratio is established to achieve the best composition in this system appropriate for fiber drawing. It was experimentally shown that the incorporation of Ga enabled the solubility of Tm^{3+} ions in the matrix of As_2S_3, and the increase of Ga concentration gradually increased the intensity of luminescence for the same quantity of Tm in the glass. The first Tm^{3+} doped Ga-As-S optical glass fiber was fabricated as well and the three emission bands of Tm^{3+} in NIR were obtained. Moreover, the modification of molecular structure of the glass, with the incorporation of Ga that leads to the increase of the solubility of Tm is revealed, using Raman and EXAFS spectroscopy. A molecular structure of Tm^{3+} doped Ga-As-S glass was proposed and it was correlated with the fluorescent features of the system.

The second part refers to study of the role of iodine in the emission properties of Tm^{3+} in As_2S_3 glasses. Matrices with different content of I_2 were fabricated to find the limit of solubility of Tm^{3+} ions in the glass depending on the concentration of I_2. It was revealed that the increasing of the concentration of I_2 by a factor of 4 in the As_2S_3 glass matrix increases the solubility of Tm ions three times. Besides, the variation of the content of I_2 and Tm allowed the effective modification of optical (transmission, refractive index, photoluminescence) and thermal (glass transition temperature, viscosity, coefficient of thermal expansion) properties of this glassy system. Structural studies of Tm^{3+} doped I-As-S glasses were carried out as well and some mechanisms responsible for the solubility of Tm^{3+} in this system were proposed. In addition, it was shown that the replacement of Ga with I_2 decreased the melting point of the system and promoted the chemical distillation of the glass matrix, leading to obtaining the first high purity chalcogenide glass doped with Tm^{3+}

ions. Tm^{3+} doped I-As-S glass fiber was fabricated as well, showing all three emission bands of Tm in NIR spectral region.

Although a lot of effort had been devoted to the fabrication and characterization of the glasses discussed in this thesis, a lot of efforts are still necessary to produce high optical fiber with lower optical losses in the MIR and considerable improvements are still required for optimization of wave guiding parameters of the fiber for practical use.

The obtained results can serve for other academic investigations and can be used in different applications, as well. For example, the high solubility of RE ions in this glassy system can enable the co-doping of the matrix with several RE ions (Er^{3+}, Dy^{3+}, Pr^{3+} etc.) to obtain continuous luminescence spectrum in NIR region. Further optimisation of reported structure (especially the optimisation of limiting optical conditions) can lead to the development of optical devices operating the wavelengths above 2 μm where silica fiber is not operating.

BIBLIOGRAPHY

[1] P. P. Sorokin and M. J. Stevenson, "Solid-State Optical Maser Using Divalent Samarium in Calcium Fluoride," *IBM J. Res. Dev.*, vol. 5, no. 1, pp. 56–58, Jan. 1961.

[2] E. Snitzer, "Optical Maser Action of Nd^{+3} in a Barium Crown Glass," *Phys. Rev. Lett.*, vol. 7, no. 12, pp. 444–446, Dec. 1961.

[3] E. Snitzer, "Proposed Fiber Cavities for Optical Masers," *J. Appl. Phys.*, vol. 32, no. 1, p. 36, Feb. 1961.

[4] F. P. Kapron, "Radiation losses in glass optical waveguides," *Appl. Phys. Lett.*, vol. 17, no. 10, p. 423, Dec. 1970.

[5] O. Humbach, H. Fabian, U. Grzesik, U. Haken, and W. Heitmann, "Analysis of OH absorption bands in synthetic silica," *J. Non. Cryst. Solids*, vol. 203, pp. 19–26, Aug. 1996.

[6] R. J. Mears, L. Reekie, I. M. Jauncey, and D. N. Payne, "Low-noise erbium-doped fibre amplifier operating at 1.54μm," *Electronics Letters*, vol. 23, no. 19. IET Digital Library, pp. 1026–1028, 10-Sep-1987.

[7] M. Petrovich, "Gallium lanthanum sulphide glasses for near-infrared photonic applications'' PhD Thesis, University of Southampton, 16-May-2003.

[8] A. Mairaj, "Optical waveguides and lasers in improved gallium lanthanum sulphide glass, PhD Thesis Chapter 1, University of Southampton." 31-May-2003.

[9] M. A. Hughes, "Modified chalcogenide glasses for optical device applications," PhD Thesis, University of Southampton, May-2007.

[10] J. Lucas, "Fluoride glasses," *Curr. Opin. Solid State Mater. Sci.*, vol. 2, no. 4, pp. 405–411, Aug. 1997.

[11] L. B. Shaw, B. Cole, P. A. Thielen, J. S. Sanghera, and I. D. Aggarwal, "Mid-wave IR and long-wave IR laser potential of rare-earth doped chalcogenide glass fiber," *IEEE J. Quantum Electron.*, vol. 37, no. 9, pp. 1127–1137, 2001.

[12] M. Poulain, M. Poulain, and J. Lucas, "Les fluorozirconates de terres rares LnZrF7," *Mater. Res. Bull.*, vol. 7, no. 4, pp. 319–325, Apr. 1972.

[13] M. Yamada, M. Shimizu, T. Kanamori, Y. Ohishi, Y. Terunuma, K. Oikawa, H. Yoshinaga, K. Kikushima, Y. Miyamoto, and S. Sudo, "Low-noise and high-power Pr/sup 3+/-doped fluoride fiber amplifier," *IEEE Photonics Technol. Lett.*, vol. 7, no. 8, pp. 869–871, Aug. 1995.

[14] T. Komukai, T. Yamamoto, T. Sugawa, and Y. Miyajima, "Upconversion pumped thulium-doped fluoride fiber amplifier and laser operating at 1.47 μm," *IEEE J. Quantum Electron.*, vol. 31, no. 11, pp. 1880–1889, 1995.

[15] T. Sakamoto, M. Shimizu, M. Yamada, T. Kanamori, Y. Ohishi, Y. Terunuma, and S. Sudo, "35-dB gain Tm-doped ZBLYAN fiber amplifier operating at 1.65 μm," *IEEE Photonics Technol. Lett.*, vol. 8, no. 3, pp. 349–351, Mar. 1996.

[16] F. Huang, Y. Guo, Y. Ma, L. Zhang, and J. Zhang, "Highly Er^{3+}-doped ZrF_4-based fluoride glasses for 2.7 μm laser materials.," *Appl. Opt.*, vol. 52, no. 7, pp. 1399–403, Mar. 2013.

[17] D. Faucher, M. Bernier, G. Androz, N. Caron, and R. Vallée, "20 W passively cooled single-mode all-fiber laser at 2.8 μm.," *Opt. Lett.*, vol. 36, no. 7, pp. 1104–6, Apr. 2011.
[18] D. Faucher, M. Bernier, N. Caron, and R. Vallée, "Erbium-doped all-fiber laser at 2.94 microm.," *Opt. Lett.*, vol. 34, no. 21, pp. 3313–5, Nov. 2009.
[19] R. Paschotta, N. Moore, W. A. Clarkson, A. C. Tropper, D. C. Hanna, and G. Maze, "230 mW of blue light from a thulium-doped upconversion fiber laser," *IEEE J. Sel. Top. Quantum Electron.*, vol. 3, no. 4, pp. 1100–1102, 1997.
[20] J. Schneider, C. Carbonnier, and U. B. Unrau, "Characterization of a Ho^{3+}-doped fluoride fiber laser with a 3.9-μm emission wavelength" *Appl. Opt.*, vol. 36, no. 33, p. 8595, Nov. 1997.
[21] J.S. Sanghera, I.D. Aggarwal, L.B. Shaw, L.E. Busse, P. Thielen, V. Nguyen, P. Pureza, S. Bayya, and F. Kung, "Applications of chalcogenide glass optical fibers at NRL. Journal of Optoelectronics and Advanced Materials" 3(2), p. 627- 640, 2001.
[22] B. J. Eggleton, B. Luther-Davies, and K. Richardson, "Chalcogenide Photonics," *Nat. Photonics*, vol. 5, Jan. 2011.
[23] J.-L. Adam, "Non-oxide glasses and their applications in optics," *J. Non. Cryst. Solids*, vol. 287, no. 1–3, pp. 401–404, Jul. 2001.
[24] H. Fritzsche, "Photo-induced fluidity of chalcogenide glasses," *Solid State Commun.*, vol. 99, no. 3, pp. 153–155, Jul. 1996.
[25] A. K. Mairaj, A. Fu, H. N. Rutt, and D. W. Hewak, "Optical channel waveguide in chalcogenide (Ga:La:S) glass," *Electronics Letters*. 03-Jan-2001.
[26] O. . Efimov, L. . Glebov, K. . Richardson, E. Van Stryland, T. Cardinal, S. . Park, M. Couzi, and J. . Brunéel, "Waveguide writing in chalcogenide glasses by a train of femtosecond laser pulses," *Opt. Mater. (Amst).*, vol. 17, no. 3, pp. 379–386, Aug. 2001.
[27] G. Beadie, W. . Rabinovich, J. Sanghera, and I. Aggarwal, "Fabrication of microlenses in bulk chalcogenide glass," *Opt. Commun.*, vol. 152, no. 4–6, pp. 215–220, Jul. 1998.
[28] J. S. Wang, E. M. Vogel, E. Snitzer, J. L. Jackel, V. L. da Silva, and Y. Silberberg, "1.3 μm emission of neodymium and praseodymium in tellurite-based glasses," *J. Non. Cryst. Solids*, vol. 178, pp. 109–113, Nov. 1994.
[29] J. . Hector, J. Wang, D. Brady, M. Kluth, D. . Hewak, W. . Brocklesby, and D. . Payne, "Spectroscopy and quantum efficiency of halide-modified gallium–lanthanum sulfide glasses doped with praseodymium," *J. Non. Cryst. Solids*, vol. 239, no. 1–3, pp. 176–180, Oct. 1998.
[30] T. Schweizer, D. W. Hewak, B. N. Samson, and D. N. Payne, "Spectroscopy of potential mid-infrared laser transitions in gallium lanthanum sulphide glass," *J. Lumin.*, vol. 72–74, pp. 419–421, Jun. 1997.
[31] T. Schweizer, B. N. Samson, R. C. Moore, D. W. Hewak, and D. N. Payne, "Rare-earth doped chalcogenide glass fibre laser," *Electron. Lett.*, vol. 33, no. 5, p. 414, 1997.
[32] A.-M. Loireau-Lozac'h, M. Guittard, and J. Flahaut, "Verres formes par les sulfures L2S3 des terres rares avec le sulfure de gallium Ga2S3," *Mater. Res. Bull.*, vol. 11, no. 12, pp. 1489–1496, Dec. 1976.
[33] Y. D. West, T. Schweizer, D. J. Brady, D. W. Hewak "Gallium Lanthanum

Sulphide Fibers for Infrared Transmission," *Fiber Integr. Opt.*, vol. 19, no. 3, pp. 229–250, Jul. 2000.
[34] D. J. Brady, "Gallium lanthanum sulphide based glasses for mid-infrared optical fibres," *Journal of Non-Crystalline Solids*. 01-Sep-1999.
[35] N. S. Kapany and R. J. Simms, "Recent developments in infrared fiber optics∗," *Infrared Phys.*, vol. 5, no. 2, pp. 69–80, Jun. 1965.
[36] J. Heo, "Optical characteristics of rare-earth-doped sulphide glasses," *J. Mater. Sci. Lett.*, vol. 14, no. 14, pp. 1014–1016, 1995.
[37] T. Schweizer, B. N. Samson, J. R. Hector, W. S. Brocklesby, D. W. Hewak, and D. N. Payne, "Infrared emission and ion–ion interactions in thulium- and terbium-doped gallium lanthanum sulfide glass," *J. Opt. Soc. Am. B*, vol. 16, no. 2, p. 308, Feb. 1999.
[38] C. Lin, S. Dai, C. Liu, B. Song, Y. Xu, F. Chen, and J. Heo, "Mechanism of the enhancement of mid-infrared emission from GeS_2-Ga_2S_3 chalcogenide glass-ceramics doped with Tm3+," *Appl. Phys. Lett.*, vol. 100, no. 23, p. 231910, Jun. 2012.
[39] A. B. Seddon, Z. Tang, D. Furniss, S. Sujecki, and T. M. Benson, "Progress in rare-earth-doped mid-infrared fiber lasers.," *Opt. Express*, vol. 18, no. 25, pp. 26704–19, Dec. 2010.
[40] B. Aitken, M. A. Newhouse, "Ga- and/or In-containing AsGe sulfide glasses", U.S. Patent 5,389,584, 1995.
[41] Y. S. Han, J. Heo, and Y. B. Shin, "Cross relaxation mechanism among Tm3+ ions in $Ge_{30}Ga_2As_6S_{62}$ glass," *J. Non. Cryst. Solids*, vol. 316, no. 2–3, pp. 302–308, Feb. 2003.
[42] Z. Yang, L. Luo, and W. Chen, "The 1.23 and 1.47 μm emissions from Tm^{3+} in chalcogenide glasses," *J. Appl. Phys.*, vol. 99, no. 7, p. 076107, Apr. 2006.
[43] D. Shixun, P. Bo, Z. Pengjun, X. Tiefeng, X. Wang, N. Qiuhua, and Z. Xianghua, "The near- and mid-infrared emission properties of Tm^{3+}-doped GeGaS–CsI chalcogenide glasses," *J. Non. Cryst. Solids*, vol. 356, no. 44–49, pp. 2424–2428, Oct. 2010.
[44] S. J. Breiner, "The discoverers of glass.," *Science*, vol. 307, no. 5715, p. 1563, Mar. 2005.
[45] Jerzy Zarzycki. "Glasses and the Vitreous State". Cambridge University Press, (1991).
[46] P. K. Gupta, "Non-crystalline solids: glasses and amorphous solids," *J. Non. Cryst. Solids*, vol. 195, no. 1–2, pp. 158–164, Feb. 1996.
[47] C. Schultz-Sellack, "Annalen der Physik und Chemie 139 (1870) 182."
[48] Z. U. Borisova, "Glassy Semiconductors," *Plenum, New York, NY*, Sep. 1981.
[49] *Kolomiets, B.T.:* The role of adsorption layers in exo-electron emission from oxide surfaces. *Phys. Status Solidi 7, 359–363 (1964a)*. New York, NY: Springer New York.
[50] Kokorina, V.F. "Glasses for Infrared Optics". CRC Press, Boca Raton, FL (1996)."
[51] R. FRERICHS, "New Optical Glasses with Good Transparency in the Infrared," *J. Opt. Soc. Am.*, vol. 43, no. 12, p. 1153, Dec. 1953.
[52] M. A. Popescu, *Non-Crystalline Chalcogenicides Kluwer, Dordrecht (2000)*. .
[53] W. C. Zingaro, R.A., Cooper, "Selenium. Van Nostrand Reinhold Company,

New York, NY." 29-Mar-1974.
[54] M. Stolz, R. Winter, W. S. Howells, R. L. McGreevy, and P. A. Egelstaff, "The structural properties of liquid and quenched sulphur II," *J. Phys. Condens. Matter*, vol. 6, no. 20, pp. 3619–3628, May 1994.
[55] B. Bureau, C. Boussard-Pledel, P. Lucas, X. Zhang, and J. Lucas, "Forming glasses from Se and Te.," *Molecules*, vol. 14, no. 11, pp. 4337–50, Jan. 2009.
[56] T. Miyashita and Y. Terunuma, "Optical Transmission Loss of As-S Glass Fiber in 1.0-5.5 μm Wavelength Region," *Jpn. J. Appl. Phys.*, vol. 21, no. Part 2, No. 2, pp. L75–L76, Feb. 1982.
[57] T. Kanamori, Y. Terunuma, and T. Miyashita, "Preparation of chalcogenide optical fiber," *Rev. Electr. Commun. Lab.*, vol. 32, no. 3, pp. 469–477, 1984.
[58] M. Saito and M. Takizawa, "Teflon-clad As-S glass infrared fiber with low-absorption loss," *J. Appl. Phys.*, vol. 59, no. 5, p. 1450, 1986.
[59] G. . Devyatykh, M. . Churbanov, I. . Scripachev, G. . Snopatin, E. . Dianov, and V. . Plotnichenko, "Recent developments in As–S glass fibres," *J. Non. Cryst. Solids*, vol. 256–257, pp. 318–322, Oct. 1999.
[60] S. Tsuchihashi and Y. Kawamoto, "Properties and structure of glasses in the system As-S," *J. Non. Cryst. Solids*, vol. 5, no. 4, pp. 286–305, Mar. 1971.
[61] K. S. Tanaka, "Amorphous Chalcogenide Semiconductors and Related Materials" *Springer USA*, 2011.
[62] S. R. Elliott, "A unified model for reversible photostructural effects in chalcogenide glasses," *J. Non. Cryst. Solids*, vol. 81, no. 1–2, pp. 71–98, Apr. 1986.
[63] J. Nishii, S. Morimoto, I. Inagawa, R. Iizuka, T. Yamashita, and T. Yamagishi, "Recent advances and trends in chalcogenide glass fiber technology: a review," *J. Non. Cryst. Solids*, vol. 140, pp. 199–208, Jan. 1992.
[64] M. Poulain, M. Poulain, and J. Lucas, "Verres fluores au tetrafluorure de zirconium proprietes optiques d'un verre dope au Nd^{3+}," *Mater. Res. Bull.*, vol. 10, no. 4, pp. 243–246, Apr. 1975.
[65] P. W. France, *Fluoride glass optical fibres*. Blackie, 1990.
[66] I. Aggarwal, "Fluoride Glass Fiber Optics," *Academic Press, New York*, 1991.
[67] M. Poulain, "New trends in halide glass compositions," *J. Non. Cryst. Solids*, vol. 184, pp. 103–108, May 1995.
[68] A. Akella, E. A. Downing, and L. Hesselink, "New fluoroindate glass compositions," *J. Non. Cryst. Solids*, vol. 213–214, pp. 1–5, May 1997.
[69] J. A. Harrington, *Infrared Fibers and Their Applications*. SPIE Press, 2004.
[70] C. J. Simmons, H. Sutter, J. H. Simmons, and D. C. Tran, "Chemical durability of Zr-Ba-La-AI-Li fluoride glass," *Mater. Res. Bull.*, vol. 17, p. 1203, Oct. 1982.
[71] A. D. Pearson "Modern Aspects of the Vitreous State'' Vol. 3, Butterworths, Washington, 1964."
[72] D. S. Ma, P. S. Danielson, and C. T. Moynihan, "Multiphonon absorption in xAs_2S_3-$(1-x)GeS_2$ glasses," *J. Non. Cryst. Solids*, vol. 81, no. 1–2, pp. 61–70, Apr. 1986.
[73] J. HEO, "1.3-μm-emission properties and local structure of Dy^{3+} in chalcohalide glasses," *Comptes rendus. Chim.*, vol. 5, no. 11, pp. 739–749.
[74] S. S. Flaschen, A. D. Pearson, and W. R. Northover, "Low Melting Sulfide-

Halogen Inorganic Glasses," *J. Appl. Phys.*, vol. 31, no. 1, p. 219, Jan. 1960.
[75] J. S. Sanghera, J. Heo, and J. D. Mackenzie, "Chalcohalide glasses," *J. Non. Cryst. Solids*, vol. 103, no. 2–3, pp. 155–178, Jul. 1988.
[76] J. Lucas, X.H. Zhang, Mater. Res. Bull 21 (1986) 371.
[77] J. Heo and J. D. Mackenzie, "Chalcohalide glasses," *J. Non. Cryst. Solids*, vol. 111, no. 1, pp. 29–35, Sep. 1989.
[78] X. H. Zhang, G. Fonteneau, and J. Lucas, "Tellurium halide glasses. New materials for transmission in the 8–12 μm range," *J. Non. Cryst. Solids*, vol. 104, no. 1, pp. 38–44, Aug. 1988.
[79] S. Sudo, *Optical fiber amplifiers : materials, devices, and applications*. Boston Mass.: Artech House, 1997.
[80] B. C. G. G. Blasse, "Luminescent Materials," *Springer. Berlin Germany*, 1994.
[81] M. J. F. Digonnet, "Rare-Earth-Doped Fiber Lasers and Amplifiers," *Chapter 2, CRC Press, USA*, 2001. .
[82] S. Hufner and B. R. Judd, "Optical Spectra of Transparent Rare Earth Compounds," *Phys. Today*, vol. 32, no. 3, p. 76, Jan. 1979.
[83] B. R. Judd, "Optical Absorption Intensities of Rare-Earth Ions," *Phys. Rev.*, vol. 127, no. 3, pp. 750–761, Aug. 1962.
[84] G. S. Ofelt, "Intensities of Crystal Spectra of Rare-Earth Ions," *J. Chem. Phys.*, vol. 37, no. 3, p. 511, Jul. 1962.
[85] L. A. Riseberg, M. J. Weber. "Relaxation phenomena in rare earth luminescence. In: Progress in Optics. E. Wolf, ed. North-Holland, Amsterdam, 1976, pp 90–159."
[86] W. T. Carnall, H. Crosswhite, and H. M. Crosswhite, "Energy level structure and transition probabilities in the spectra of the trivalent lanthanides in LaF_3," *Argonne Natl. Lab. Rep.*, 1978.
[87] A. Kiel, "Multi Phonon Spontaneous Emission in Paramagnetic Crystals," *Quantum Electron. Proc. third Int. Congr. Ed. by P. Grivet N. Bloembergen. Publ. by Dunod Éditeur*, 1964.
[88] L. A. Riseberg and H. W. Moos, "Multiphonon Orbit-Lattice Relaxation of Excited States of Rare-Earth Ions in Crystals," *Phys. Rev.*, vol. 174, no. 2, pp. 429–438, Oct. 1968.
[89] C. B. Layne, W. H. Lowdermilk, and M. J. Weber, "Multiphonon relaxation of rare-earth ions in oxide glasses," *Phys. Rev. B*, vol. 16, no. 1, pp. 10–20, Jul. 1977.
[90] *S. Hufner. Optical Spectroscopy Of Transparent Rare Earth Materials. Academic Press, New York, 1978.* .
[91] V. G. Truong, A. M. Jurdyc, B. Jacquier, B. S. Ham, A. Q. Le Quang, J. Leperson, V. Nazabal, and J. L. Adam, "Optical properties of thulium-doped chalcogenide glasses and the uncertainty of the calculated radiative lifetimes using the Judd-Ofelt approach," *J. Opt. Soc. Am. B*, vol. 23, no. 12, p. 2588, Dec. 2006.
[92] G. E. Snopatin, V. S. Shiryaev, V. G. Plotnichenko, E. M. Dianov, and M. F. Churbanov, "High-purity chalcogenide glasses for fiber optics," *Inorg. Mater.*, vol. 45, no. 13, pp. 1439–1460, Nov. 2009.
[93] G. G. Devyatykh, E. M. Dianov, V. G. Plotnichenko, I. V. Scripachev, and M. F. Churbanov, *Fiber waveguides based on high-purity chalcogenide glasses*,

vol. 5. Elsevier, 1991.
[94] J. L. Adam, *Chalcogenide Glasses: Preparation, Properties and Applications*. Elsevier Science, 2014.
[95] M. F. Churbanov, V. S. Shiryaev, V. V. Gerasimenko, A. A. Pushkin, I. V. Skripachev, G. E. Snopatin, and V. G. Plotnichenko, "Stability of the Optical and Mechanical Properties of Chalcogenide Fibers," *Inorg. Mater.*, vol. 38, no. 10, pp. 1063–1068.
[96] A. K. Varshneya, *Fundamentals of Inorganic Glasses*. Waltam, MA, Academic Press, 1993.
[97] G. J. Dienes and H. F. Klemm, "Theory and Application of the Parallel Plate Plastometer," *J. Appl. Phys.*, vol. 17, no. 6, p. 458, Jul. 1946.
[98] A. N. Gent, "Theory of the parallel plate viscometer," *Br. J. Appl. Phys.*, vol. 11, no. 2, pp. 85–87, Feb. 1960.
[99] A. K. Varshneya, N. H. Burlingame, W. H. Schkultze, "Parallel plate viscometry to study deformation induced viscosity changes in glass," *Glastechn. Ber. 63K (1990), 447-459*. .
[100] Standard Test Method for Measurement of Viscosity of Glass Between 10 4 Pa·s and 10 8 Pa·s by Viscous Compression of a Solid Right Cylinder [Metric], 1996.
[101] A. Fluegel, "Viscosity measurement techniques for glass," *November 2005*. .
[102] ThermoNicolet, "Introduction to Fourier Transform Infrared Spectoscopy".
[103] J. R. Verkouteren, E. B. Steel, E. S. Windsor, and J. M. Phelps, "Accuracy of the double variation technique of refractive index measurement," *J. Res. Natl. Inst. Stand. Technol.*, vol. 97, no. 6, p. 693, Nov. 1992.
[104] F. M. E. Bailey, J. Duran, "Theory, Setup,& Operation of a Metricon 2010 Prism Coupler." .
[105] Metricon 2010/M prism coupler Overview — Brochure.
[106] Horiba Jobin Yvon NanoLog spectrofluorometer — Brochure.
[107] N. F. Mott, "Electrons in disordered structures," *Adv. Phys.*, vol. 16, no. 61, pp. 49–144, Jan. 1967.
[108] G. Vlaica and L. Olivi, "EXAFS Spectroscopy: a Brief Introduction," *Croat. Chem. Acta*, vol. 77, no. 3, pp. 427–433, Oct. 2004.
[109] M. Newville, "Fundamentals of XAFS," *Rev. Mineral. Geochemistry*, vol. 78, no. 1, pp. 33–74, Feb. 2014.
[110] James A. Harrington 'Infrared Fibers and Their Applications' chapter 1, SPIE press (2004).
[111] A. B. Seddon, Z. Tang, D. Furniss, S. Sujecki, and T. M. Benson, "Progress in rare-earth-doped mid-infrared fiber lasers.," *Opt. Express*, vol. 18, no. 25, pp. 26704–26719, 2010.
[112] D. R. Simons, A. J. Faber, and H. de Waal, "GeSx glass for Pr3+-doped fiber amplifiers at 1.3 μm," *J. Non. Cryst. Solids*, vol. 185, no. 3, pp. 283–288, Jun. 1995.
[113] K. Abe, H. Takebe, and K. Morinaga, "Preparation and properties of Ge-Ga-S glasses for laser hosts," *J. Non. Cryst. Solids*, vol. 212, no. 2–3, pp. 143–150, Jun. 1997.
[114] J. Heo, W. Y. Cho, and W. J. Chung, "Sensitizing effect of Tm^{3+} on 2.9 μm emission from Dy^{3+}-doped $Ge_{25}Ga_5S_{70}$ glass," *J. Non. Cryst. Solids*, vol. 212,

no. 2–3, pp. 151–156, Jun. 1997.
[115] K. Wei, D. P. Machewirth, J. Wenzel, E. Snitzer, and G. H. Sigel, "Spectroscopy of Dy^{3+} in Ge-Ga-S glass and its suitability for 1.3-microm fiber-optical amplifier applications.," *Opt. Lett.*, vol. 19, no. 12, pp. 904–906, 1994.
[116] J. Heo and Y. B. Shin, "Absorption and mid-infrared emission spectroscopy of Dy^{3+} in Ge-As(or Ga)-S glasses," *J. Non. Cryst. Solids*, vol. 196, pp. 162–167, Mar. 1996.
[117] B. Frumarová, P. Němec, M. Frumar, J. Oswald, and M. Vlček, "Synthesis and optical properties of the Ge–Sb–S:$PrCl_3$ glass system," *J. Non. Cryst. Solids*, vol. 256–257, pp. 266–270, Oct. 1999.
[118] V. Moizan, V. Nazabal, J. Troles, P. Houizot, J.-L. Adam, J.-L. Doualan, R. Moncorgé, F. Smektala, G. Gadret, S. Pitois, and G. Canat, "Er^{3+}-doped GeGaSbS glasses for mid-IR fibre laser application: Synthesis and rare earth spectroscopy," *Opt. Mater. (Amst).*, vol. 31, no. 1, pp. 39–46, Sep. 2008.
[119] F. Prudenzano, L. Mescia, L. Allegretti, M. De Sario, F. Smektala, V. Moizan, V. Nazabal, J. Troles, J. L. Doualan, G. Canat, J. L. Adam, and B. Boulard, "Simulation of mid-IR amplification in Er^{3+}-doped chalcogenide microstructured optical fiber," *Opt. Mater. (Amst).*, vol. 31, no. 9, pp. 1292–1295, Jul. 2009.
[120] D. N. Payne, J. A. Medeiros Neto, D. W. Hewak, R. I. Laming, and B. N. Samson, "Emission at 1.3 μm from dysprosium-doped Ga:La:S glass," *Electron. Lett.*, vol. 30, no. 12, pp. 968–970, Jun. 1994.
[121] K. Kadono, H. Higuchi, M. Takahashi, Y. Kawamoto, and H. Tanaka, "Upconversion luminescence of Ga_2S_3-based sulfide glasses containing Er^{3+} ions," *J. Non. Cryst. Solids*, vol. 184, pp. 309–313, May 1995.
[122] R. Reisfeld and A. Bornstein, "Absorption and emission spectra in chalcogenide glass of the composition 0.7Ga2S3-0.27La2S3-0.03Nd_2S_3," *Chem. Phys. Lett.*, vol. 47, no. 1, pp. 194–196, Apr. 1977.
[123] T. H. Lee, S. I. Simdyankin, J. Hegedus, J. Heo, and S. R. Elliott, "Spatial distribution of rare-earth ions and GaS_4 tetrahedra in chalcogenide glasses studied via laser spectroscopy and ab initio molecular dynamics simulation," *Phys. Rev. B*, vol. 81, no. 10, p. 104204, Mar. 2010.
[124] J. Heo, J. Min Yoon, and S.-Y. Ryou, "Raman spectroscopic analysis on the solubility mechanism of La^{3+} in GeS_2–Ga_2S_3 glasses," *J. Non. Cryst. Solids*, vol. 238, no. 1–2, pp. 115–123, Sep. 1998.
[125] S. Sen, C. W. Ponader, and B. G. Aitken, "Ge and As x-ray absorption fine structure spectroscopic study of homopolar bonding, chemical order, and topology in Ge-As-S chalcogenide glasses," *Phys. Rev. B*, vol. 64, no. 10, p. 104202, Aug. 2001.
[126] J. H. Song, Y. G. Choi, K. Kadono, K. Fukumi, H. Kageyama, and J. Heo, "EXAFS investigation on the structural environment of Tm^{3+} in Ge–Ga–S–CsBr glasses," *J. Non. Cryst. Solids*, vol. 353, no. 13–15, pp. 1251–1254, May 2007.
[127] B. Kolimiets, N. Goryunova, V. Shilo "Glassy state in chalcogenides" Publishing House of the USSR Academy of Sciences pp. 456-460m, 1960.
[128] H. Tichá, L. Tichý, N. Ryšavá, and A. Tříska, "Some physical properties of the

glassy $(GeS_2)_x(Sb_2S_3)_{1-x}$ system," *J. Non. Cryst. Solids*, vol. 74, no. 1, pp. 37–46, Sep. 1985.
[129] M. Ichikawa, T. Wakasugi, and K. Kadono, "Glass formation, physico-chemical properties, and structure of glasses based on Ga_2S_3–GeS_2–Sb_2S_3 system," *J. Non. Cryst. Solids*, vol. 356, no. 43, pp. 2235–2240, Sep. 2010.
[130] K. Kadono, T. Yazawa, M. Shojiya, and Y. Kawamoto, "Judd–Ofelt analysis and luminescence property of Tm^{3+} in Ga_2S_3–GeS_2–La_2S_3 glasses," *J. Non. Cryst. Solids*, vol. 274, no. 1–3, pp. 75–80, Sep. 2000.
[131] Y. B. Shin, W. Y. Cho, and J. Heo, "Multiphonon and cross relaxation phenomena in Ge-As(or Ga)-S glasses doped with Tm^{3+}," *J. Non. Cryst. Solids*, vol. 208, no. 1–2, pp. 29–35, Nov. 1996.
[132] B. Cole, L. Shaw, P. Pureza, R. Mossadegh, J. Sanghera, and I. Aggarwal, "Rare-earth doped selenide glasses and fibers for active applications in the near and mid-IR," *J. Non. Cryst. Solids*, vol. 256–257, pp. 253–259, Oct. 1999.
[133] Y. D. West, T. Schweizer, D. J. Brady, D. W. Hewak, "Gallium Lanthanum Sulphide Fibers for Infrared Transmission," *Fiber Integr. Opt.*, vol. 19, no. 3, pp. 229–250, Jul. 2000.
[134] Y. Ohishi, A. Mori, T. Kanamori, K. Fujiura, and S. Sudo, "Fabrication of praseodymium-doped arsenic sulfide chalcogenide fiber for 1.3-??m fiber amplifiers," *Appl. Phys. Lett.*, vol. 65, no. 1, pp. 13–15, 1994.
[135] A. Mori, Y. Ohishi, T. Kanamori, and S. Sudo, "Optical amplification with neodymium-doped chalcogenide glass fiber," *Appl. Phys. Lett.*, vol. 70, no. 10, p. 1230, Mar. 1997.
[136] A. Galstyan, S. H. Messaddeq, V. Fortin, I. Skripachev, R. Vallée, T. Galstian, and Y. Messaddeq, "Tm3+ doped Ga–As–S chalcogenide glasses and fibers," *Opt. Mater. (Amst).*, vol. 47, pp. 518–523, Sep. 2015.
[137] A. J. Kropf, J. Katsoudas, S. Chattopadhyay, T. Shibata, E. A. Lang, V. N. Zyryanov, B. Ravel, K. McIvor, K. M. Kemner, K. G. Scheckel, S. R. Bare, J. Terry, S. D. Kelly, B. A. Bunker, C. U. Segre, R. Garrett, I. Gentle, K. Nugent, and S. Wilkins, "The New MRCAT (Sector 10) Bending Magnet Beamline at the Advanced Photon Source," in *Journal of Synchrotron Radiation*, 2010, vol. 1234, pp. 299–302.
[138] M. Newville, "IFEFFIT : interactive XAFS analysis and FEFF fitting," *J. Synchrotron Radiat.*, vol. 8, no. 2, pp. 322–324, Mar. 2001.
[139] B. Ravel and M. Newville, "ATHENA, ARTEMIS, HEPHAESTUS: data analysis for X-ray absorption spectroscopy using IFEFFIT.," *J. Synchrotron Radiat.*, vol. 12, no. Pt 4, pp. 537–41, Jul. 2005.
[140] T. Wagner, S. O. Kasap, M. Vlcek, A. Sklenár, and A. Stronski, "Modulated-temperature differential scanning calorimetry and Raman spectroscopy studies of As_xS_{100-x} glasses," *J. Mater. Sci.*, vol. 33, no. 23, pp. 5581–5588.
[141] R. Golovchak, O. Shpotyuk, J. S. Mccloy, B. J. Riley, C. F. Windisch, S. K. Sundaram, A. Kovalskiy, and H. Jain, "Structural model of homogeneous As–S glasses derived from Raman spectroscopy and high-resolution XPS," *Philos. Mag.*, vol. 90, no. 34, pp. 4489–4501, Nov. 2010.
[142] M. S. Iovu, S. D. Shutov, A. M. Andriesh, E. I. Kamitsos, C. P. E. Varsamis, D. Furniss, A. B. Seddon, and M. Popescu, "Spectroscopic study of As_2S_3 glasses doped with Dy, Sm and Mn," *J. Non. Cryst. Solids*, vol. 326–327, pp.

306–310, Oct. 2003.
[143] E. Bychkov, M. Miloshova, D. L. Price, C. J. Benmore, and A. Lorriaux, "Short, intermediate and mesoscopic range order in sulfur-rich binary glasses," *J. Non. Cryst. Solids*, vol. 352, no. 1, pp. 63–70, Jan. 2006.
[144] F. Kyriazis, A. Chrissanthopoulos, V. Dracopoulos, M. Krbal, T. Wagner, M. Frumar, and S. N. Yannopoulos, "Effect of silver doping on the structure and phase separation of sulfur-rich As–S glasses: Raman and SEM studies," *J. Non. Cryst. Solids*, vol. 355, no. 37–42, pp. 2010–2014, Oct. 2009.
[145] S. A. Solin and G. N. Papatheodorou, "Irreversible thermostructural transformations in amorphous As_2S_3 films: A light-scattering study," *Phys. Rev. B*, vol. 15, no. 4, pp. 2084–2090, Feb. 1977.
[146] S. H. Santagneli, J. Schneider, I. Skripachev, S. J. L. Ribeiro, and Y. Messaddeq, "Preparation and characterization of new glassy system $As_2P_2S_8$-Ga_2S_3.," *J. Phys. Chem. B*, vol. 112, no. 16, pp. 4943–7, May 2008.
[147] R. Holomb, M. Veres, and V. Mitsa, "Ring-, branchy-, and cage-like AsnSm nanoclusters in the structure of amorphous semiconductors: ab initio and Raman study," *J. Optoelectron. Adv. Mater.*, vol. 11, no. 7, pp. 917–923.
[148] C. Julien, S. Barnier, M. Massot, N. Chbani, X. Cai, A. M. Loireau-Lozac'h, and M. Guittard, "Raman and infrared spectroscopic studies of Ge-Ga-Ag sulphide glasses," *Mater. Sci. Eng. B*, vol. 22, no. 2–3, pp. 191–200, Jan. 1994.
[149] X. F. Wang, S. X. Gu, J. G. Yu, X. J. Zhao, and H. Z. Tao, "Structural investigations of GeS_2–Ga_2S_3–CdS chalcogenide glasses using Raman spectroscopy," *Solid State Commun.*, vol. 130, no. 7, pp. 459–464, May 2004.
[150] T. H. Lee, S. I. Simdyankin, L. Su, and S. R. Elliott, "Evidence of formation of tightly bound rare-earth clusters in chalcogenide glasses and their evolution with glass composition," *Phys. Rev. B*, vol. 79, no. 18, p. 180202, May 2009.
[151] B. . Aitken and C. . Ponader, "Physical properties and Raman spectroscopy of GeAs sulphide glasses," *J. Non. Cryst. Solids*, vol. 256–257, pp. 143–148, Oct. 1999.
[152] K. Arai, H. Namikawa, K. Kumata, T. Honda, Y. Ishii, and T. Handa, "Aluminum or phosphorus co-doping effects on the fluorescence and structural properties of neodymium-doped silica glass," *J. Appl. Phys.*, vol. 59, no. 10, p. 3430, May 1986.
[153] S. Yang, X. Wang, H. Guo, G. Dong, B. Peng, J. Qiu, R. Zhang, and Y. Shi, "Broadband near-infrared emission in Tm^{3+}-Dy^{3+} codoped amorphous chalcohalide films fabricated by pulsed laser deposition.," *Opt. Express*, vol. 19, no. 27, pp. 26529–35, Dec. 2011.
[154] W. A. Pisarski, J. Pisarska, G. Dominiak-Dzik, and W. Ryba-Romanowski, "Visible and infrared spectroscopy of Pr^{3+} and Tm^{3+} ions in lead borate glasses," *J. Phys. Condens. Matter*, vol. 16, no. 34, pp. 6171–6184, Sep. 2004.
[155] D. J. E. Mullen and W. Nowacki, "Sulfides and sulfo salts. 65. Refinement of the crystal structures of realgar, AsS, and orpiment, As_2S_3' Z. Kristallogr., , 136, 48, 1972.
[156] S. Sen, C. W. Ponader, and B. G. Aitken, "Ge and As x-ray absorption fine structure spectroscopic study of homopolar bonding, chemical order, and topology in Ge-As-S chalcogenide glasses," *Phys. Rev. B*, vol. 64, no. 10, p. 104202, Aug. 2001.

[157] Donghui Zhao 'Atomistic Mechanisms and Kinetics of Photoinduced Changes in Chalcogenide Glasses' Thesis, Lehigh University 2011.
[158] J. Goodyear and G. A. Steigmann, "The crystal structure of α-Ga_2S_3," *Acta Crystallogr.*, vol. 16, no. 10, pp. 946–949, Oct. 1963.
[159] A. M. Loireau-Lozac'h, F. Keller-Besrest, and S. Bénazeth, "Short and Medium Range Order in Ga–Ge–S Glasses: An X-Ray Absorption Spectroscopy Study at Room and Low Temperatures," *J. Solid State Chem.*, vol. 123, no. 1, pp. 60–67, Apr. 1996.
[160] S. Benazeth, M. . Tuilier, A. . Loireau-Lozac'h, H. Dexpert, P. Lagarde, and J. Flahaut, "An EXAFS structural approach of the lanthanum-gallium-sulfur glasses," *J. Non. Cryst. Solids*, vol. 110, no. 1, pp. 89–100, Jul. 1989.
[161] V. Katchkanov, J. F. W. Mosselmans, S. Dalmasso, K. P. O'Donnell, S. Hernandez, K. Wang, R. W. Martin, O. Briot, N. Rousseau, G. Halambalakis, K. Lorenz, and E. Alves, "Extended X-ray absorption fine structure studies of thulium doped GaN epilayers," *Superlattices Microstruct.*, vol. 36, no. 4–6, pp. 729–736, Oct. 2004.
[162] A. K. Mairaj 'Optical waveguides and lasers in improved gallium Lanthanum sulphide glass' Thesis, chapter1, University of Southampton, June 2003.
[163] V. Krasteva, D. Machewirth, and G. . Sigel, "Pr^{3+}-doped Ge–S–I glasses as candidate materials for 1.3 μm optical fiber amplifiers," *J. Non. Cryst. Solids*, vol. 213–214, pp. 304–310, May 1997.
[164] K. Wei, D. P. Machewirth, J. Wenzel, E. Snitzer, and G. H. Sigel, Jr., "Spectroscopy of Dy^{3+} in Ge-Ga-S glass and its suitability for 13-μm fiber-optical amplifier applications," *Opt. Lett.*, vol. 19, no. 12, p. 904, Jun. 1994.
[165] K. Wei, D. P. Machewirth, J. Wenzel, E. Snitzer, and G. H. Sigel, "Pr^{3+}-doped Ge-Ga-S glasses for 1.3 μm optical fiber amplifiers," *J. Non. Cryst. Solids*, vol. 182, no. 3, pp. 257–261, Mar. 1995.
[166] C. C. Ye, D. W. Hewak, M. Hempstead, B. N. Samson, and D. N. Payne, "Spectral properties of Er^{3+}-doped gallium lanthanum sulphide glass," *J. Non. Cryst. Solids*, vol. 208, no. 1–2, pp. 56–63, Nov. 1996.
[167] H. Sakr, D. Furniss, Z. Tang, L. Sojka, N. A. Moneim, E. Barney, S. Sujecki, T. M. Benson, and A. B. Seddon, "Superior photoluminescence (PL) of Pr^{3+}-In, compared to Pr^{3+}-Ga, selenide-chalcogenide bulk glasses and PL of optically-clad fiber.," *Opt. Express*, vol. 22, no. 18, pp. 21236–52, Sep. 2014.
[168] D. . Machewirth, K. Wei, V. Krasteva, R. Datta, E. Snitzer, and G. . Sigel, "Optical characterization of Pr3+ and Dy3+ doped chalcogenide glasses," *J. Non. Cryst. Solids*, vol. 213–214, pp. 295–303, May 1997.
[169] M. F. Churbanov, I. V. Scripachev, V. S. Shiryaev, V. G. Plotnichenko, S. V. Smetanin, E. B. Kryukova, Y. N. Pyrkov, and B. I. Galagan, "Chalcogenide glasses doped with Tb, Dy and Pr ions," *J. Non. Cryst. Solids*, vol. 326–327, pp. 301–305, Oct. 2003.
[170] Cole et al, "Heavy metal modified silica glass fibers doped with thulium, holmium, and thulium-sensitized-holmium high quantum efficiencies." United States Patent 23-Dec-2003.
[171] S. Suzuki, Y. Kamiya,Y. Suzuki, and T. Kobayashi, "Viscosity of Glass in the Transition Region in the Systems As-S, As-S-I and As-S-Tl," *J. Soc. Mater. Sci. Japan*, vol. 21, no. 221, pp. 143–147, Feb. 1972.

[172] O. V. Khiminets, P. P. Puga, V. V. Khiminets, I. I. Rosola, and G. D. Puga, “Raman spectra of the As-S-I system of glasses,” *J. Appl. Spectrosc.*, vol. 28, no. 4, pp. 477–479, Apr. 1978.
[173] L. Koudelka and M. Pisárčik, “Raman spectra and structure of As□S□I system glasses,” *J. Non. Cryst. Solids*, vol. 64, no. 1–2, pp. 87–94, Apr. 1984.
[174] T. E. Hopkins, R. A. Pasternak, E. S. Gould, and J. R. Herndon, “x-ray diffraction study of arsenic trisulfide-iodine glasses,” *J. Phys. Chem.*, vol. 66, no. 4, pp. 733–736, Apr. 1962.
[175] V. P. Gapontsev, S. M. Matitsin, A. A. Isineev, and V. B. Kravchenko, “Erbium glass lasers and their applications,” *Opt. Laser Technol.*, vol. 14, no. 4, pp. 189–196, Aug. 1982.
[176] M. Zhu, X. Wang, C. Jiang, H. Xu, Q. Nie, P. Zhang, S. Dai, X. Shen, T. Xu, G. Tao, and X. Zhang, “Freely adjusted properties in Ge–S based chalcogenide glasses with iodine incorporation,” *Infrared Phys. Technol.*, vol. 69, pp. 118–122, Mar. 2015.
[177] V. P. Gapontsev, Y. E. Sverchkov, A. K. Gromov, A. A. Izyneev, and V. B. Kravchenko, “Parameters and mechanism of elementary interaction of the electronic excitation of rare-earth ions with the local impurity oscillations,” vol. 29, Jan. 1979.
[178] J. Heo, “Chalcohalide glasses for infrared fiber optics,” *Opt. Eng.*, vol. 30, no. 4, p. 470, Apr. 1991.
[179] Y. Y. Huang, A. Sarkar, and P. C. Schultz, “Relationship between composition, density and refractive index for germania silica glasses,” *J. Non. Cryst. Solids*, vol. 27, no. 1, pp. 29–37, Jan. 1978.
[180] E. R. Shaaban, Y. A. M. Ismail, and H. S. Hassan, “Compositional dependence of the optical properties of amorphous Se80−xTe20Bix thin films using transmittance and reflectance measurements,” *J. Non. Cryst. Solids*, vol. 376, pp. 61–67, Sep. 2013.
[181] Y.-R. Luo, *Comprehensive Handbook of Chemical Bond Energies*. CRC Press, 2007.